X-ray Spectroscopy Application on Energy Materials

林彥谷 副研究員
國家同步輻射研究中心
科學研究組 材料小組
lin.yg@nsrrc.org.tw

國家同步輻射研究中心
National Synchrotron Radiation Research Center

溫度及能量指標
Temperature and Energy

大氣指標
Atmospheric Composition

海洋及水文指標
Ocean and Water

永凍圈指標
Cryosphere

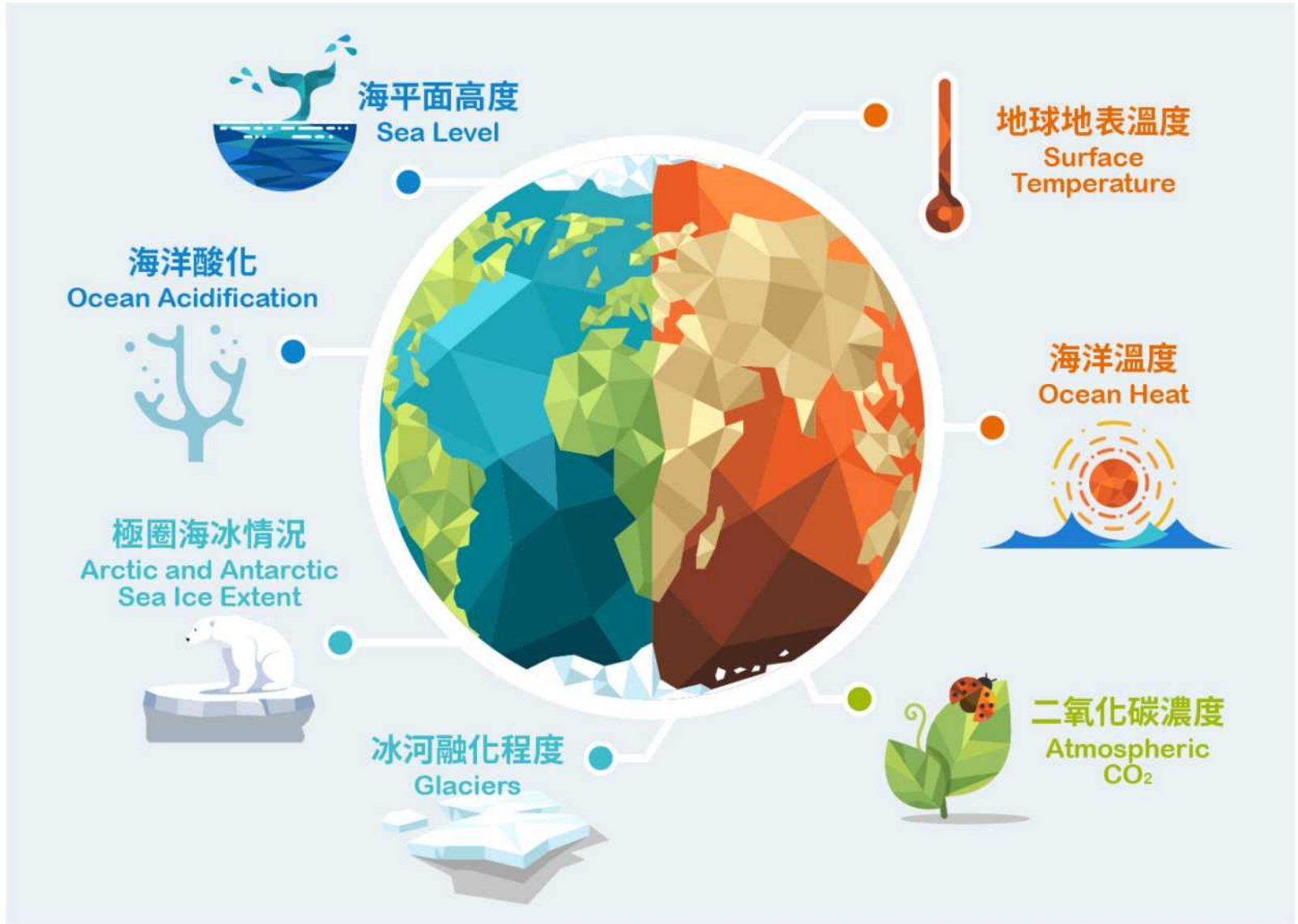

世界氣候正在暖化

1850至2021年間，陸地及海洋年均溫度與歷年平均值的對比

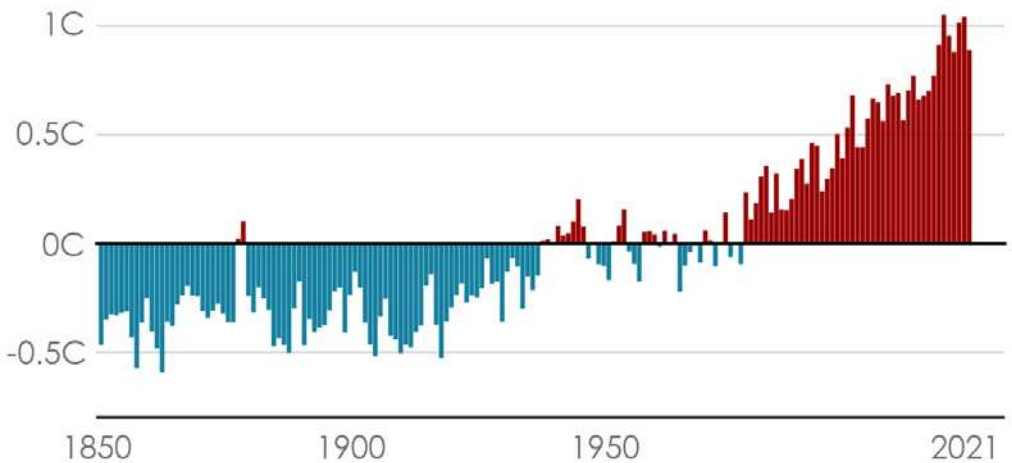

注：歷年平均值根據1951年1月至1980年12月數據計算

資料來源：加州大學伯克利分校

BBC

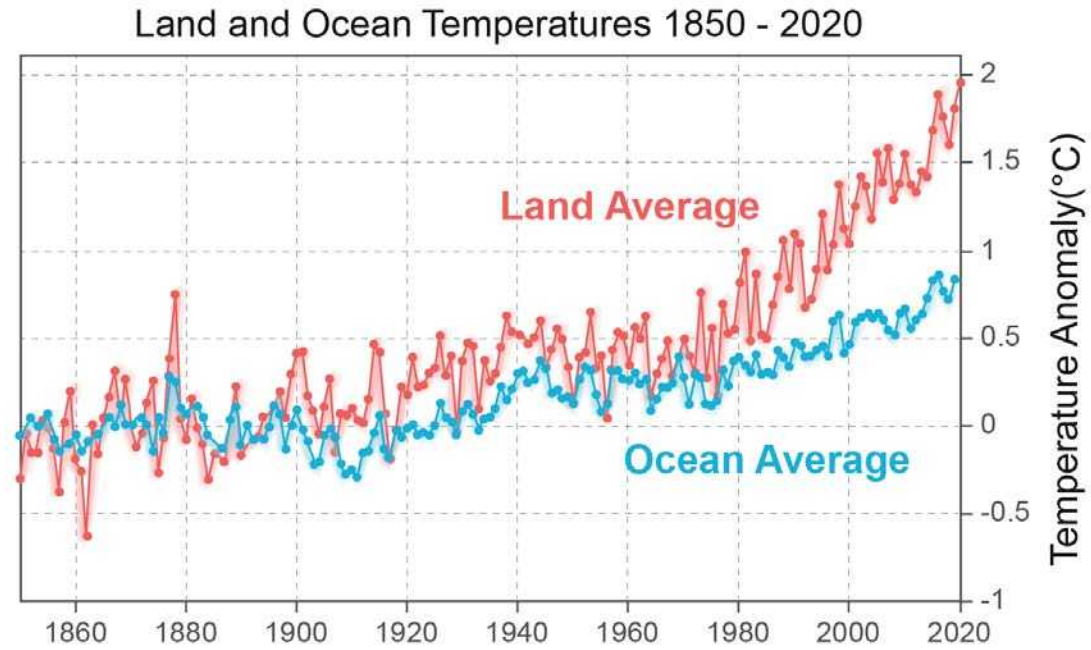

資料來源：Berkeley Earth

Sea level rise

地球的海平面，每年上升3.3公釐(3.3mm)

A rise at an average of 3.3 mm per year

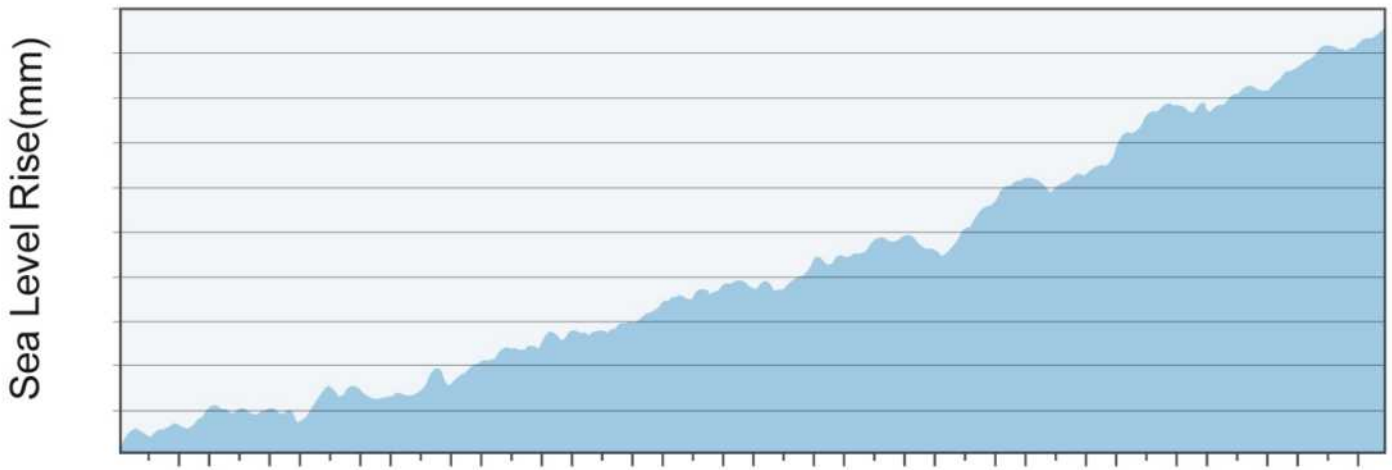

資料來源：GCOS

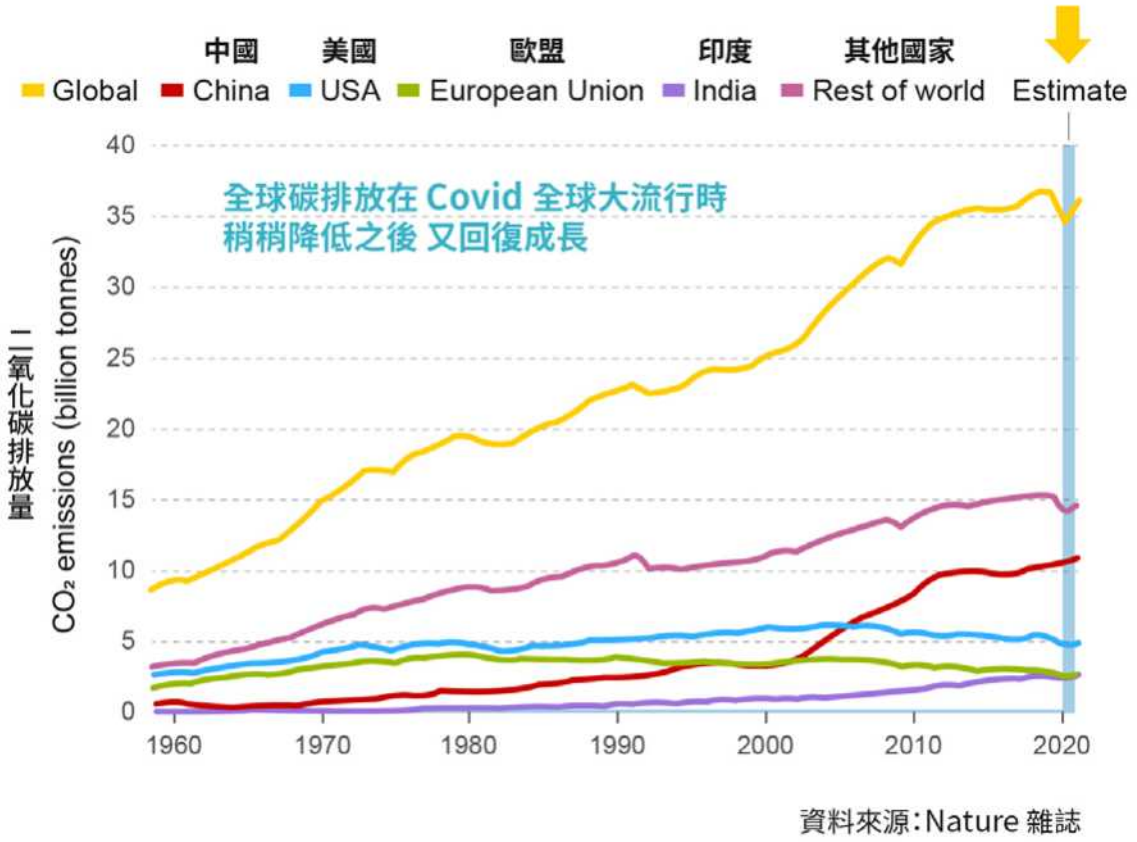
中國
美國
歐盟
印度
其他國家
Global
China
USA
European Union
India
Rest of world
Estimate
全球碳排放在 Covid 全球大流行時
稍稍降低之後 又回復成長
二氧化碳排放量
CO₂ emissions (billion tonnes)
40
35
30
25
20
15
10
5
0
1960
1970
1980
1990
2000
2010
2020
資料來源：Nature 雜誌

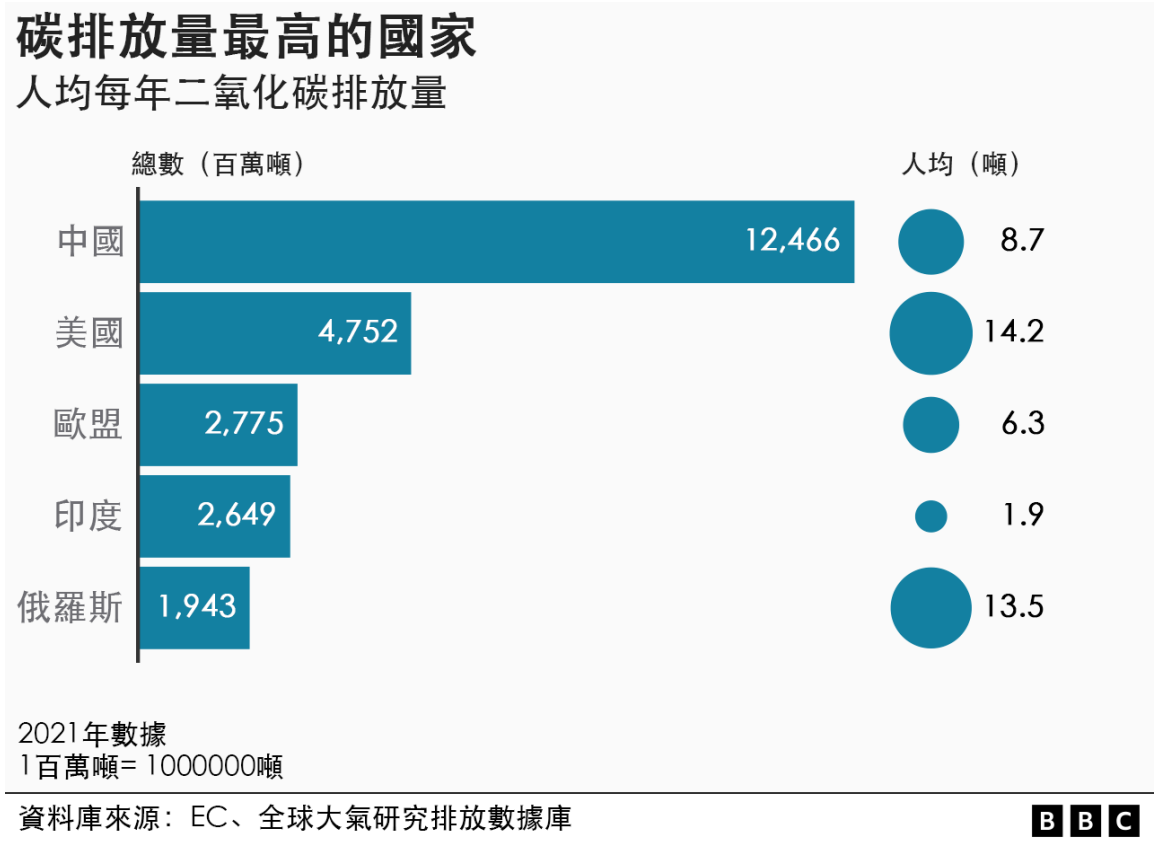
碳排放量最高的國家
人均每年二氧化碳排放量
總數（百萬噸）
人均（噸）
中國
12,466
8.7
美國
4,752
14.2
歐盟
2,775
6.3
印度
2,649
1.9
俄羅斯
1,943
13.5
2021年數據
1百萬噸= 1000000噸
資料庫來源：EC、全球大氣研究排放數據庫
BBC

COP27的七大關鍵議題

議題	COP26	COP27	是否有進展
損失與損害（Loss and Damage）	停留在格拉斯哥對話，無明確目標	首次通過決議，成立損失與損害基金	✔
1000億美元氣候融資	工業國家2009年承諾每年提供，遲遲未達標	今年仍未兌現承諾	×
巴黎協定第六條（國際碳市場）	拍板規則書，確立國際碳交易原則，禁止各國重複計算減碳貢獻	定義雙軌制（two-tier）碳市場，企業向其他國家購買碳權，若用在非強制性減碳目的，雙方皆可計算減碳貢獻，有助國際自願性碳市場的發展	✔
全球甲烷承諾	105國簽署，目標在2030年前減少30%甲烷排放	增加約50國簽署	✔
化石燃料限制	宣示逐步減少（phase down）燃煤	無進展，今年決議文鼓勵各國使用「低排放能源」（low-emission energy），遭批仍然允許使用天然氣、搭配碳捕捉技術的燃煤。	×
升溫目標	宣示以「地球升溫控制在1.5°C內」為首要目標	維持既有目標，但各國減碳野心無進展，按照目前步調難以達標	×
2030減碳目標	全球應在2030年減少45%溫室氣體排放	重申既有目標。今年僅28國更新國家自定貢獻（NDCs），計算後與去年相比無進展	×

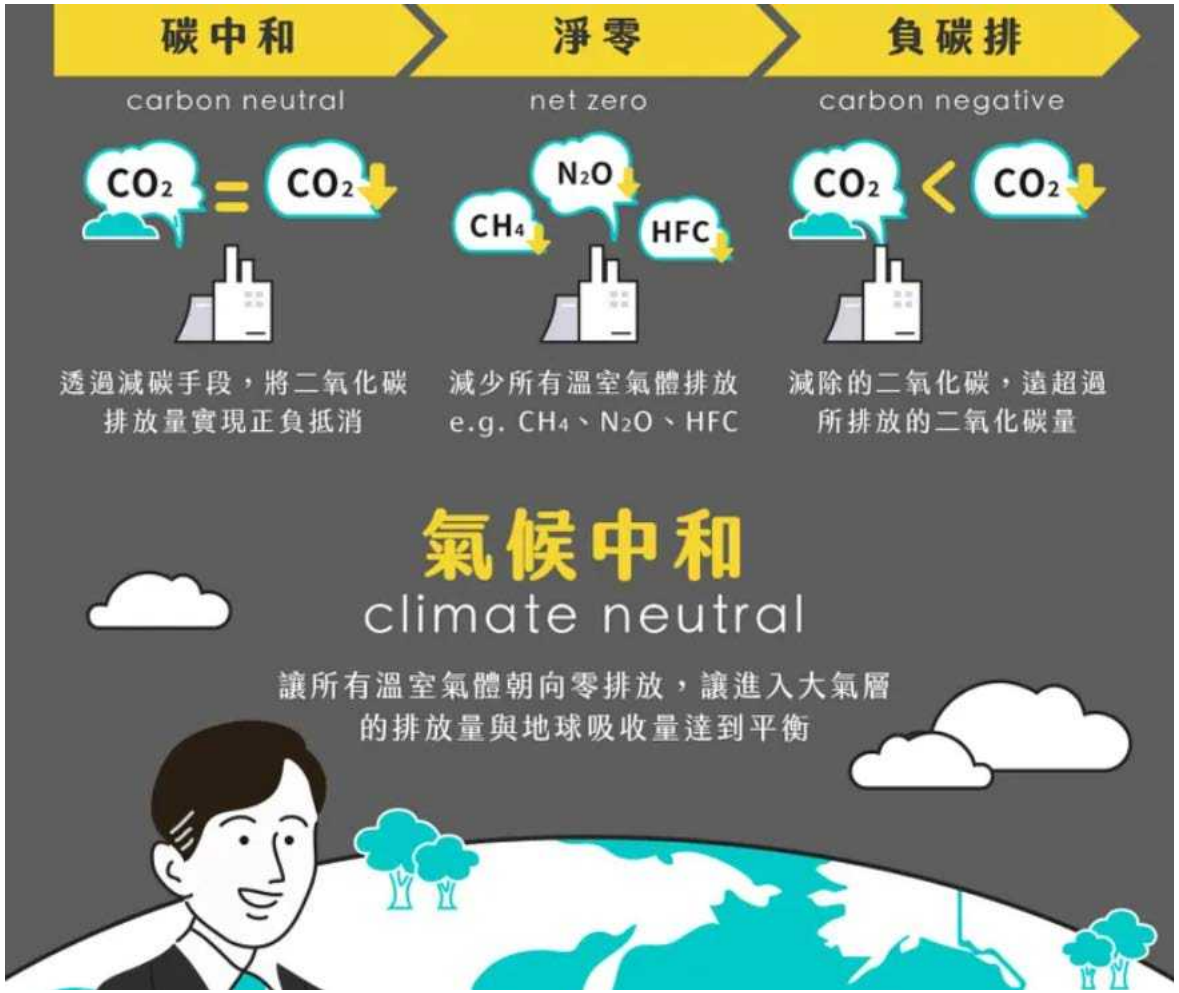
碳中和
carbon neutral
淨零
net zero
負碳排
carbon negative
CO_2 = CO_2
N_2O
CH_4
HFC
CO_2 < CO_2
透過減碳手段，將二氧化碳排放量實現正負抵消
減少所有溫室氣體排放 e.g. CH_4、N_2O、HFC
減除的二氧化碳，遠超過所排放的二氧化碳量
氣候中和
climate neutral
讓所有溫室氣體朝向零排放，讓進入大氣層的排放量與地球吸收量達到平衡

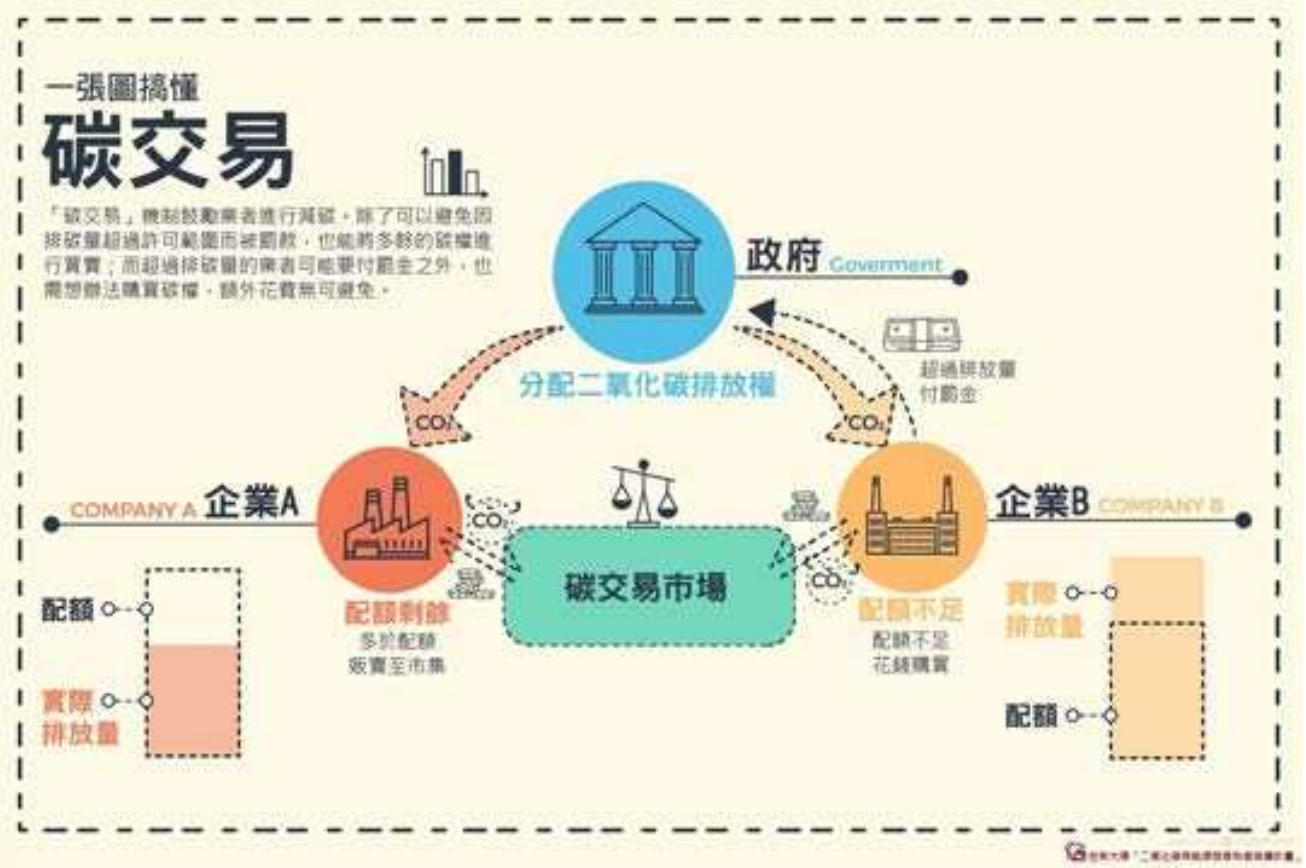
一張圖搞懂
碳交易
「碳交易」機制鼓勵廠商進行減碳，除了可以避免因排放量超過許可範圍而被罰款，也能將多餘的碳權進行買賣；而超過排碳量的廠商可能要付罰金之外，也需想辦法購買碳權，額外花費無可避免。
政府 Goverment
分配二氧化碳排放權
超過排放量付罰金
COMPANY A 企業A
企業B COMPANY B
碳交易市場
配額剩餘
多於配額販賣至市集
配額不足
配額不足花錢購買
配額
實際排放量
實際排放量
配額

台灣氣候變遷績效指標（CCPI 2023）

指　　標	等　級	排　名
溫室氣體排放（40%）	**非常差**	**58**
人均溫室氣體排放當前水準	非常差	-
人均溫室氣體排放目前趨勢	中　等	-
人均溫室氣體排放 以升溫 2°C 以下為基準	非常差	-
2030年溫室氣體排放目標 以升溫 2°C 以下為基準	非常差	-
再生能源（20%）	**非常差**	**57**
再生能源占比（TPES）	非常差	-
再生能源目前趨勢	佳	-
再生能源占比（TPES） 以升溫 2°C 以下為基準	非常差	-
2030年再生能源目標 以升溫 2°C 以下為基準	非常差	-
能源使用（20%）	**非常差**	**54**
人均能源使用（TPES）當前水準	差	-
人均能源使用（TPES）目前趨勢	中　等	-
人均能源使用（TPES）當前水準 以升溫 2°C 以下為基準	非常差	-
2030年能源使用目標 以升溫 2°C 以下為基準	非常差	-
氣候政策（20%）	**差**	**42**
國家氣候政策	差	-
國際氣候政策	中　等	-

譯　　註｜非常好（Very High）、佳（High）、中等（Medium）、差（Low）、非常差（Very Low）
資料來源｜CCPI 2023　整理｜陳文姿　製圖｜劉紀岑

環境資訊中心 Environmental Information Center

氣候變遷績效指標排名（CCPI 2023）

非常好　佳　中等　差　非常差

排名	國家
1	從缺
2	從缺
3	從缺
4	丹麥
5	瑞典
6	智利
7	摩洛哥

排名	國家
8	印度
11	英國
16	德國
19	歐盟
20	埃及
23	西班牙
28	法國

排名	國家
38	巴西
40	越南
42	泰國
50	日本
51	中國
52	美國
55	澳洲

排名	國家
57	中華台北
58	加拿大
59	俄羅斯
60	韓國
61	哈薩克
62	沙烏地阿拉伯
63	伊朗

譯　註｜報告以 *Chinese Taipei*（中華台北）稱呼我國，本文於圖表忠實呈現報告用語。
資料來源｜CCPI 2023　整理｜陳文姿　製圖｜劉紀岑

環境資訊中心 Environmental Information Center

歷年發購電量及結構

台電系統歷年發購電量

單位：億度

各能源別

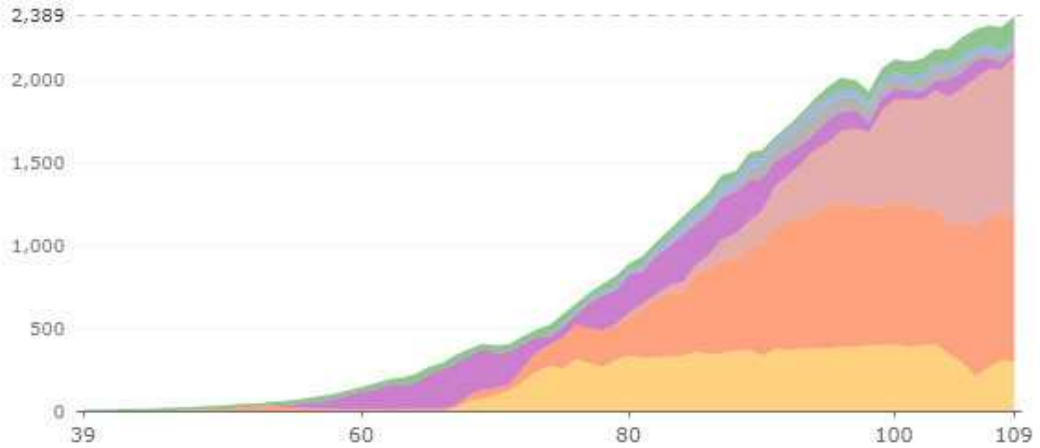

109 年發購電量結構

台電系統歷年發購電量

單位：億度

各能源別

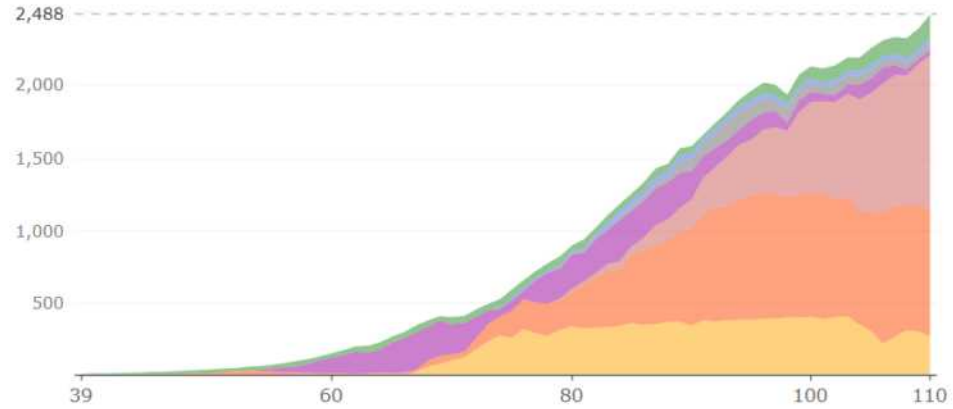

110 年發購電量結構

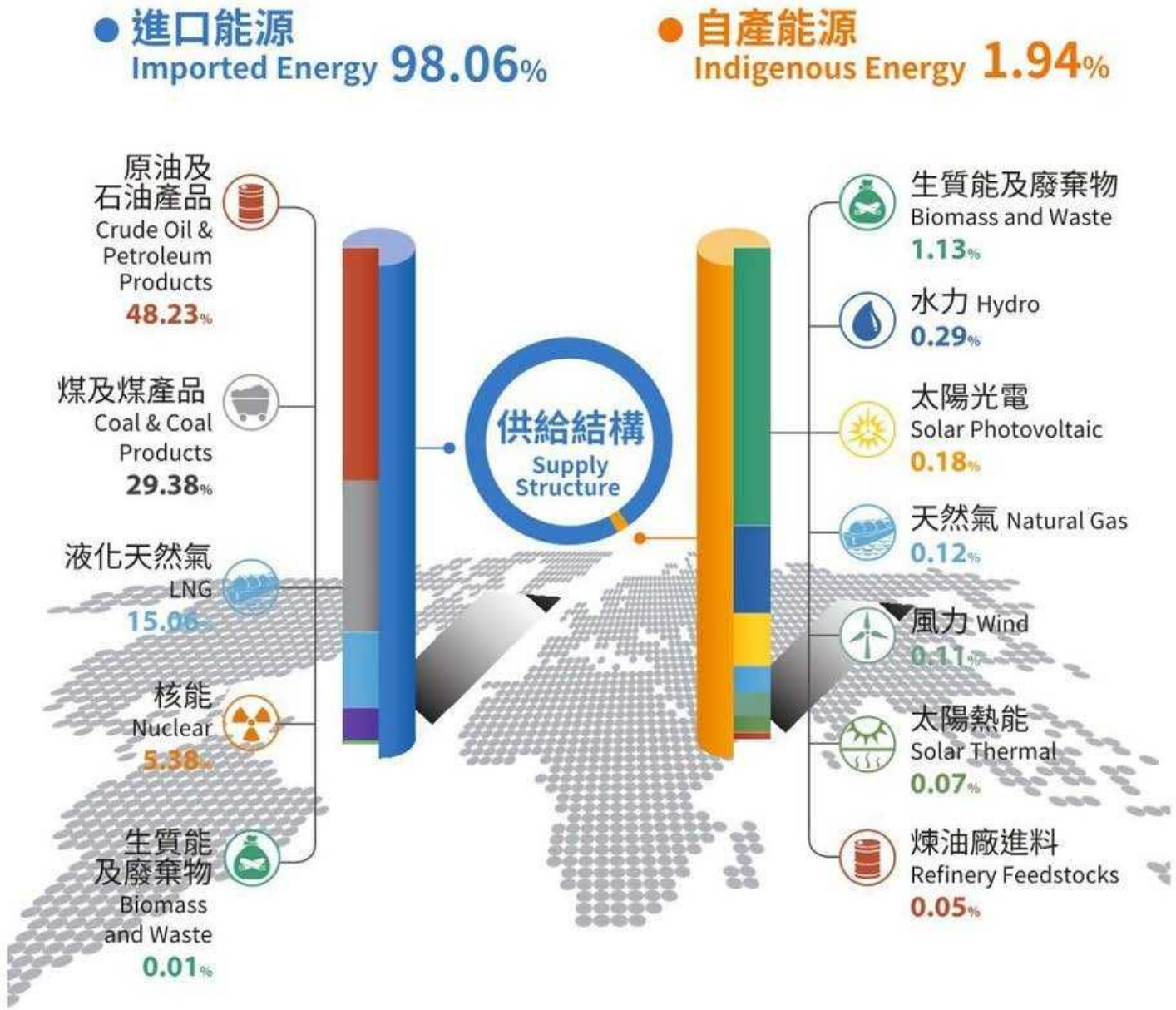
● 進口能源
Imported Energy 98.06%
● 自產能源
Indigenous Energy 1.94%
原油及石油產品
Crude Oil & Petroleum Products
48.23%
煤及煤產品
Coal & Coal Products
29.38%
液化天然氣
LNG
15.06%
核能
Nuclear
5.38%
生質能及廢棄物
Biomass and Waste
0.01%
供給結構
Supply Structure
生質能及廢棄物
Biomass and Waste
1.13%
水力 Hydro
0.29%
太陽光電
Solar Photovoltaic
0.18%
天然氣 Natural Gas
0.12%
風力 Wind
0.11%
太陽熱能
Solar Thermal
0.07%
煉油廠進料
Refinery Feedstocks
0.05%

經濟部

一、台灣能源轉型目標與願景

■ 於2025年達成20-30-50潔淨能源發電結構與非核家園願景

再生能源發電量占比達20%

燃煤發電量占比降至30%

低碳天然氣發電量占比達50%

既有核電廠不延役核四廢止

註：因核三廠2號機於2025年5月17日除役，憂燃煤及其它中核能占比仍有1.1%。

2

能源配比發展路徑與近年能源結構占比走勢

2016年（起始年）	2025年
燃氣 31.5%	燃氣 ?%（原規畫50%）
燃煤 45.9%	燃煤 ?%（原規畫30%）
再生能源 4.82%	再生能源 ?%（原規畫20%）
核能 12.0%	核能 0%

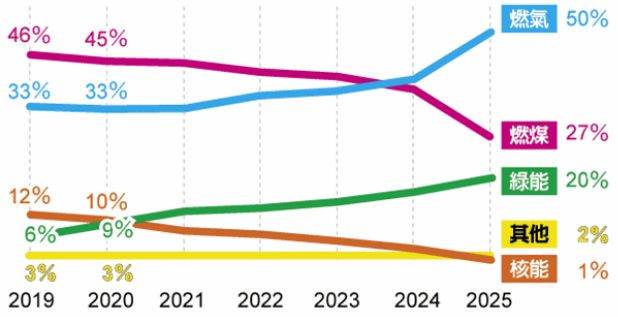

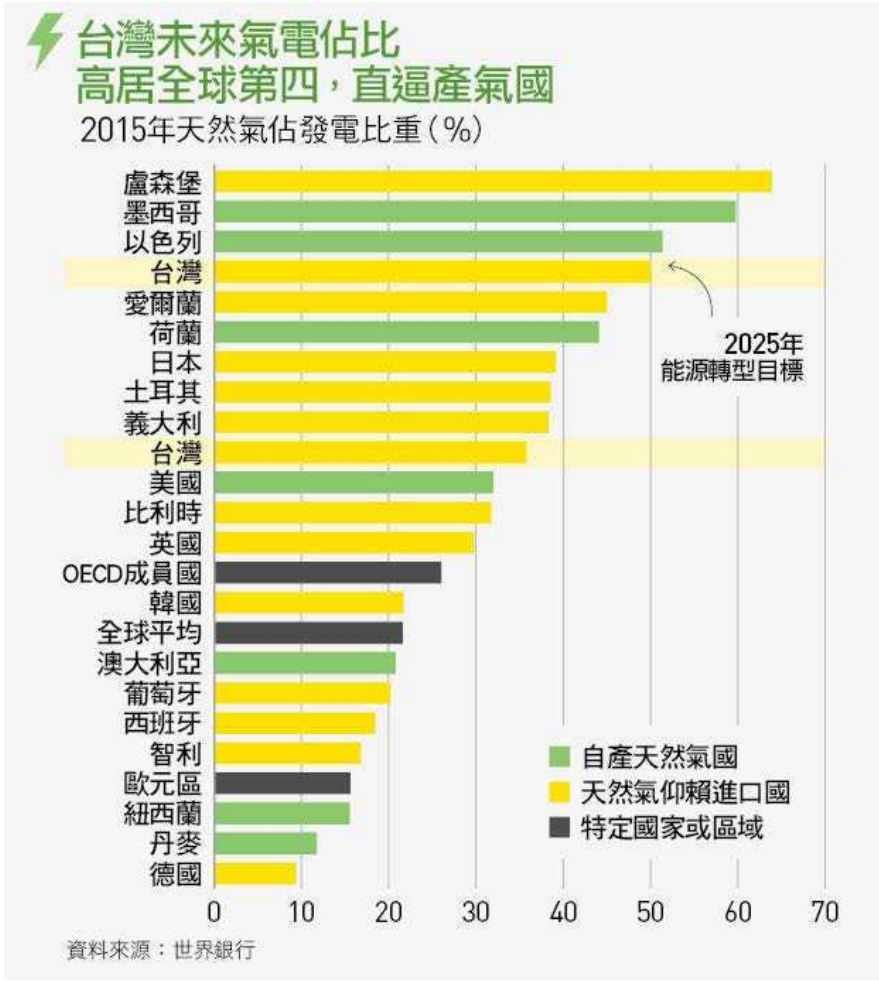

淺談同步輻射光源應用

「同步輻射」是什麼？跟核能電廠一樣有輻射的問題嗎？

圖 1　位於新竹科學園區的臺灣光源與臺灣光子源設施。（圖片來源：國家同步輻射研究中心）

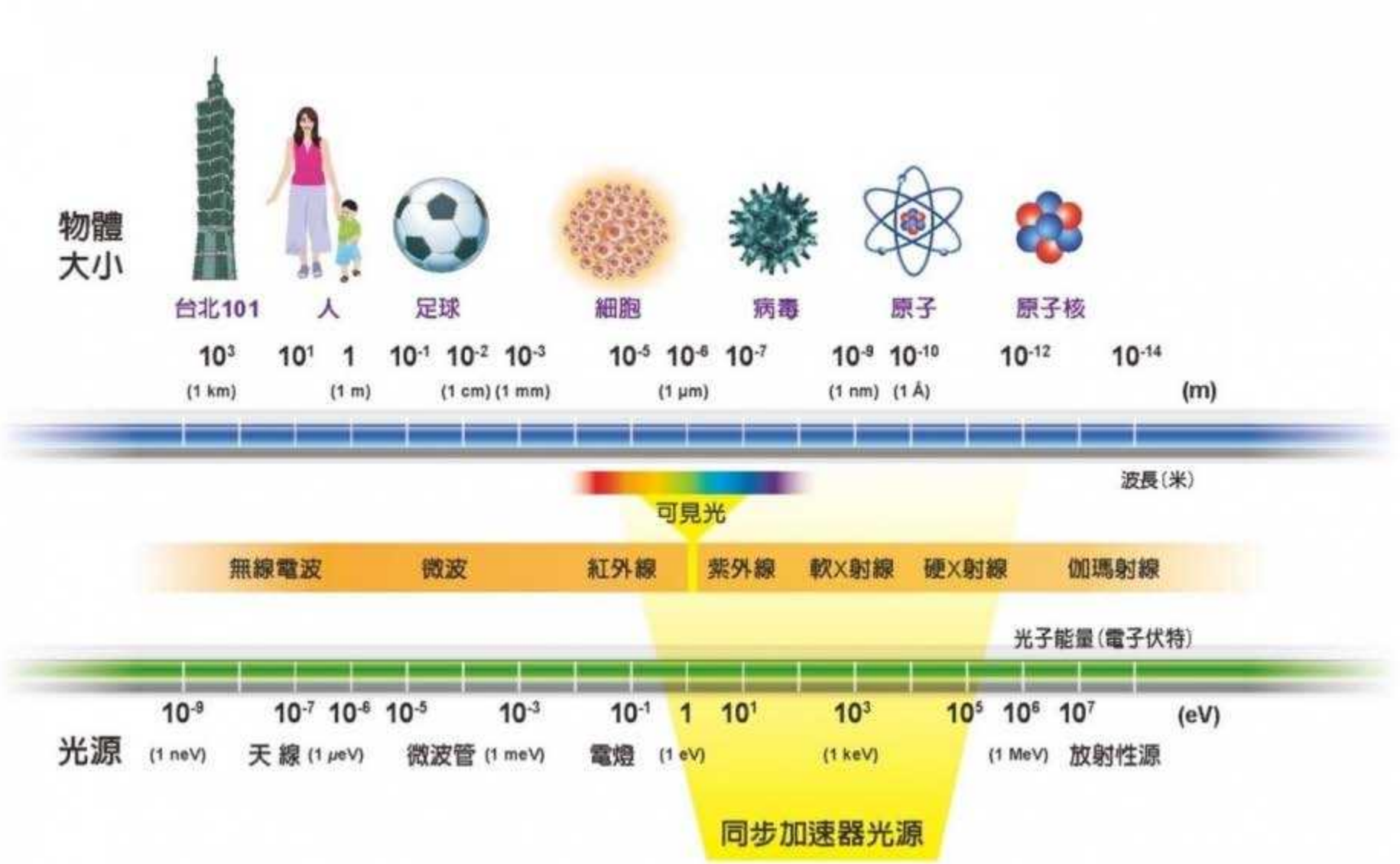
物體
大小
台北101
人
足球
細胞
病毒
原子
原子核
10^3 (1 km)
10^1
1 (1 m)
10^-1
10^-2 (1 cm)
10^-3 (1 mm)
10^-5
10^-6 (1 μm)
10^-7
10^-9 (1 nm)
10^-10 (1 Å)
10^-12
10^-14
(m)
波長(米)
可見光
無線電波
微波
紅外線
紫外線
軟X射線
硬X射線
伽瑪射線
光子能量(電子伏特)
10^-9 (1 neV)
10^-7
10^-6 (1 μeV)
10^-5
10^-3 (1 meV)
10^-1
1 (1 eV)
10^1
10^3 (1 keV)
10^5
10^6 (1 MeV)
10^7
(eV)
光源
天線
微波管
電燈
放射性源
同步加速器光源

同步輻射產生之光源和一般X光機產生之光源原因不同。不同之處為X光機是用高速電子撞擊金屬靶，將內層電子游離出來後，外層電子躍遷回 去放出的光；同步輻射是用電磁鐵讓電子或帶電粒子，在一個固定的環內持續的做圓週運動，使能量累積，累積到一定程度後，可控制電子或質子加速的速度，在切線的方向，動能就會以光的方式釋放出來，所以加速可以控制放出光的強度和頻率。同步輻射具有以下特性

- ✧ 強度極高
- ✧ 波長連續
- ✧ 準直性佳
- ✧ 光束截面積小
- ✧ 具有時間脈波性與偏振性

若以X光為例，同步輻射在這個波段的亮度比傳統X光機還要強百萬倍以上！過去需要幾個月才能完成的實驗，現在只需幾分鐘便能得到結果。以往因實驗光源亮度不夠而無法探測的結構，現在藉由同步輻射，都可分析得一清二楚，也因此於近年內許多新的研究領域得以開發。目前同步輻射Powder and fiber X-ray diffraction beam lines 提供波長 1.333 Å與 1.03 Å ~ 0.37 Å光源做繞射研究。 Small and wide angle X-ray scattering for nano-materials and soft matter， wavelength 2.48 Å ~ 0.54 Å。X-ray absorption spectroscopy beam lines ， energy range 2~33keV。

How a Synchrotron Light Source Works

- Whenever electrons moving close to the speed of light are deflected by a magnetic field, they radiate a thin beam of radiation tangentially from their path. This beam is called "synchrotron radiation". Taking the NSRRC's synchrotron light source as an example, the electrons are first accelerated in the linear accelerator (LINAC) and the booster ring. They are then sent through the transport line and into the storage ring, where they circulate in vacuum pipes for several hours, emitting synchrotron radiation. The emitted light is channeled through beamlines to the experimental stations where experiments are conducted.
- Experiments using synchrotron radiation attempt to analyze electrons, photons, and other particles that are emitted when synchrotron radiation strikes matter. The resulting data are then used to deduce the matter's chemistry, geometry, electronic structure, or magnetic properties.

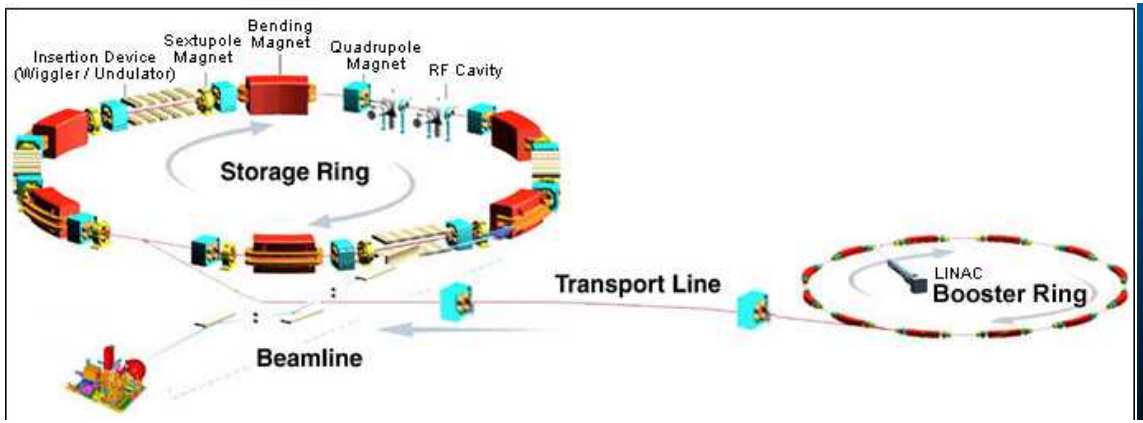

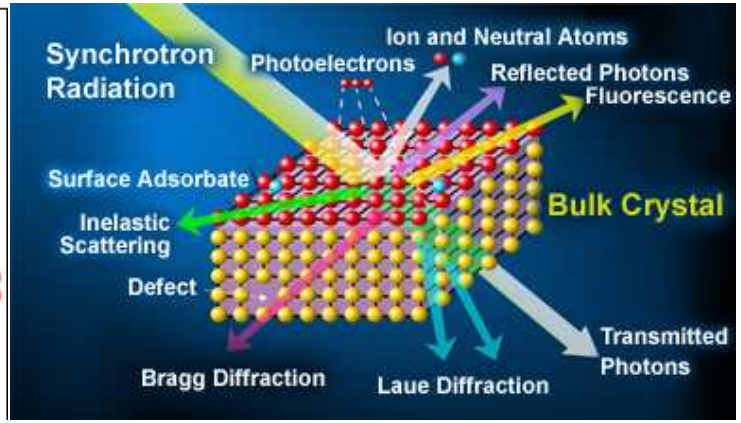

- **Photoelectron spectroscopy**
- **X-ray Absorption Spectroscopy**
- **X-ray Diffraction Spectroscopy**

Photoelectron spectroscopy detects the kinetic energy of the electron escaped from the surface.

- **X-ray Photoelectron Spectroscopy (XPS)**

- using soft x-ray (200-2000 eV) radiation to examine core-levels and valence levels.

- **Ultraviolet Photoelectron Spectroscopy (UPS)**

- using vacuum UV (10-45 eV) radiation to examine valence levels.

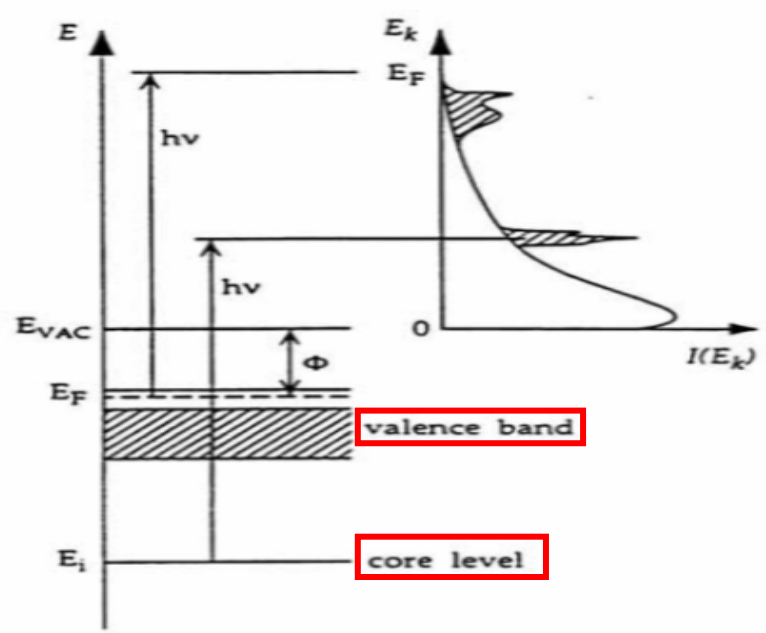

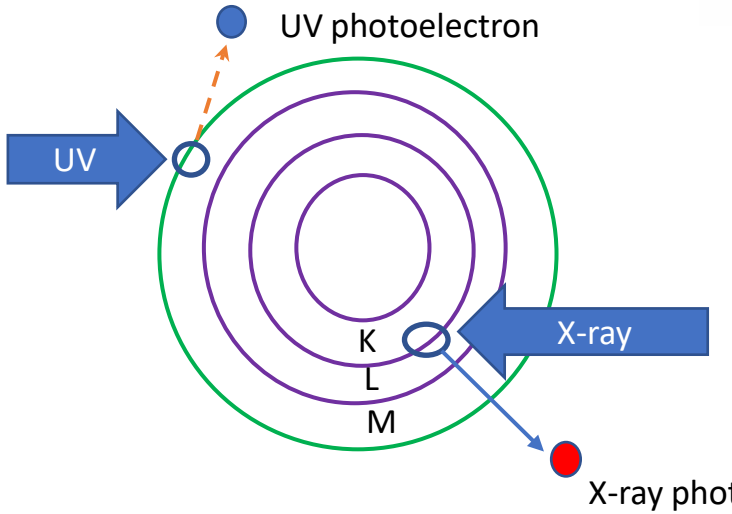

XPS : Core electrons ejected
UPS : Valence electrons ejected

The Photoelectric Effect

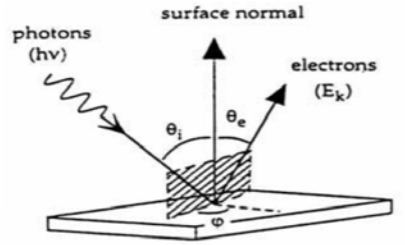

Albert Einstein considered electromagnetic energy to be bundled into little packets called photons.

- **E(Energy of photon) = hv**

h = Planck constant (6.62 x 10-34 J s)

v = frequency (Hz) of the radiation

- **hv = B.E. + K.E + Φ**

- Photons of light hit surface electrons and transfer their energy
- The energized electrons overcome their attraction and escape from the surface

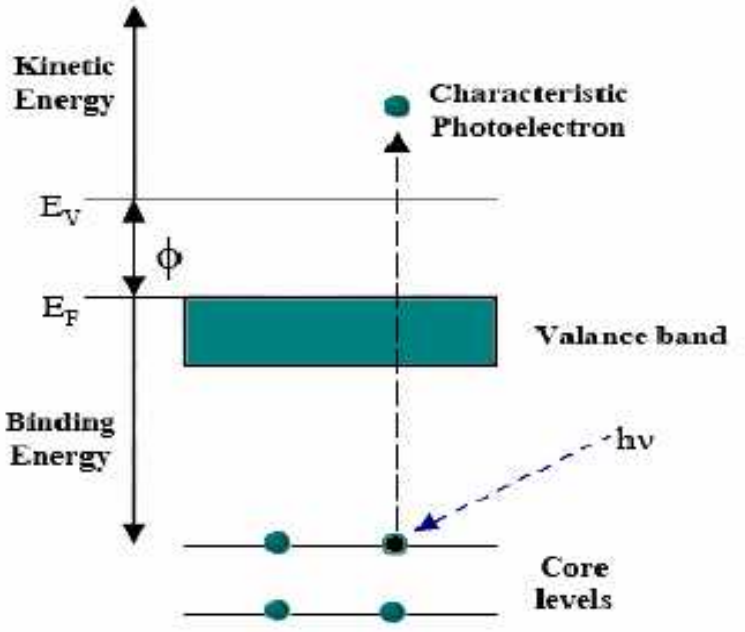

Ultraviolet Photoelectron Spectroscopy (UPS)

- The UPS instrument measures the kinetic energy and angular distribution of the photoelectrons, information on the electronic structure (band structure) of the material under investigation can be extracted with surface sensitivity.

UPS	XPS
▪ Low Escape Depth High Surface Sensitivity	▪ Core Levels & Valence Band
▪ High Resolution	▪ Sharp Lines Qualitative & Quantitative Analysis
▪ Access to: Valence Band Features, Bonding Process	▪ Chemical Shifts

Binding Energy Shifts
(Chemical Shifts- Electronegativity Effects)

Carbon-Oxygen Bond

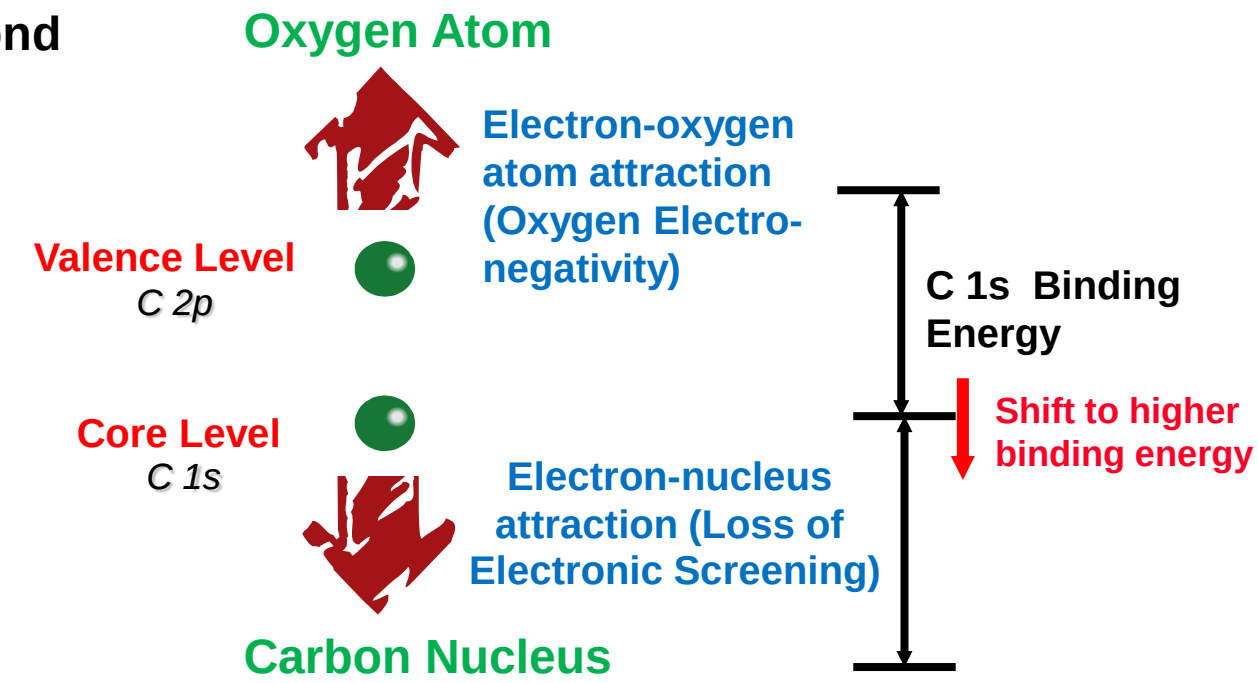

Binding Energy Shifts
(Chemical Shifts- Electronegativity Effects)

Functional Group		Binding Energy (eV)
hydrocarbon	C-H, C-C	285.0
amine	C-N	286.0
alcohol, ether	C-O-H, C-O-C	286.5
Cl bound to C	C-Cl	286.5
F bound to C	C-F	287.8
carbonyl	C=O	288.0

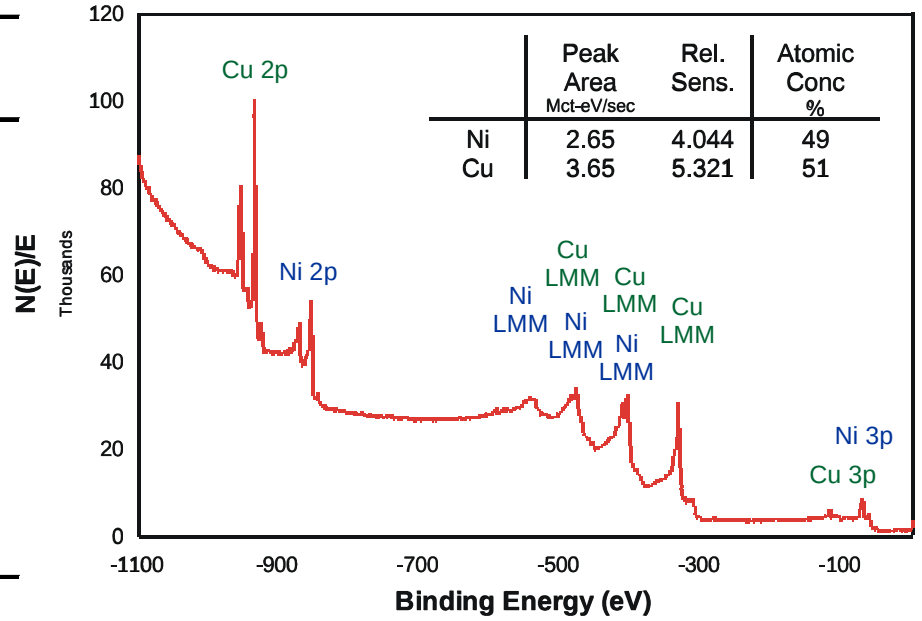

XPS of Copper-Nickel alloy

Surface Survey

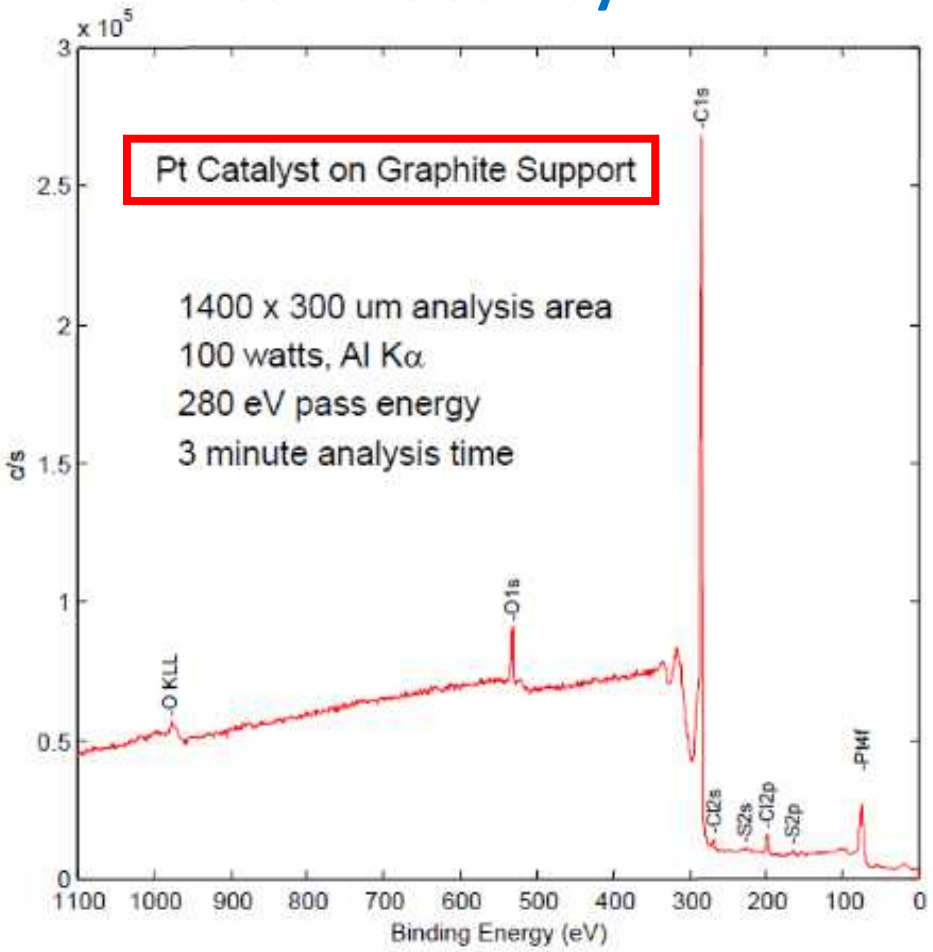

Surface composition (atom %)	
C	95.1
O	3.3
Cl	0.9
Pt	0.6
S	0.2

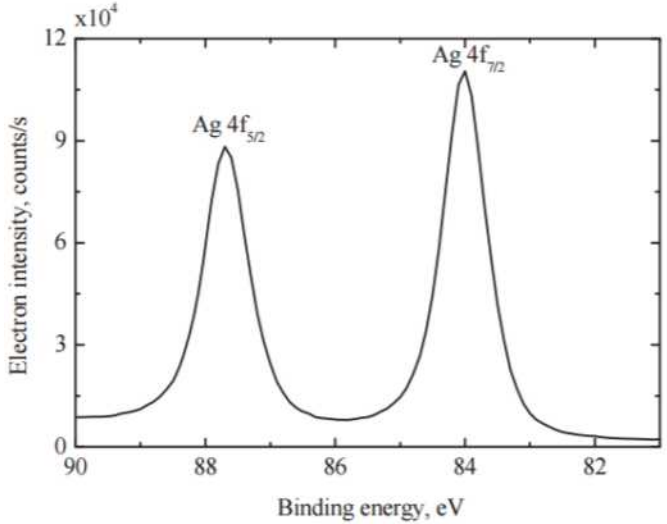

Narrow Scan

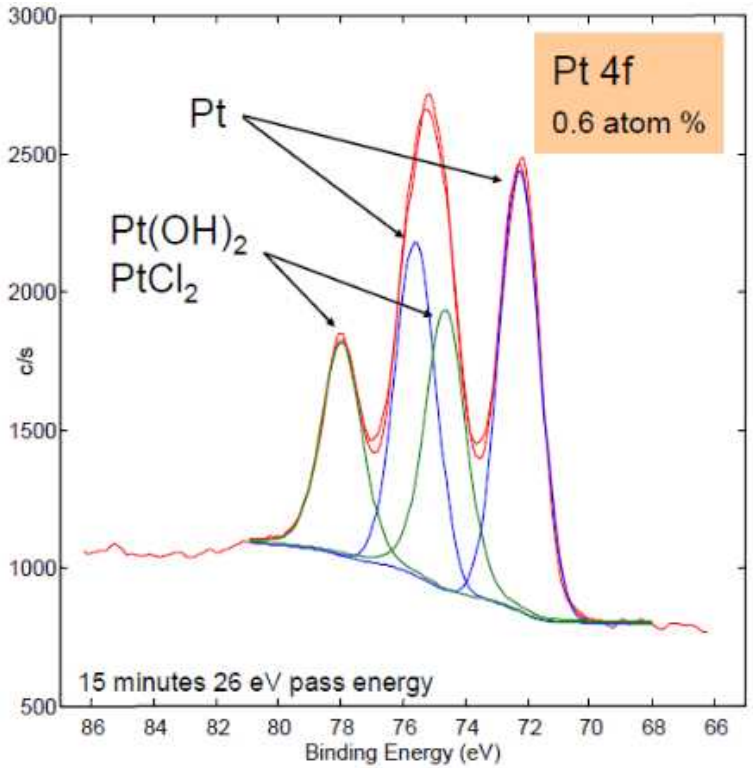

Depth Profile

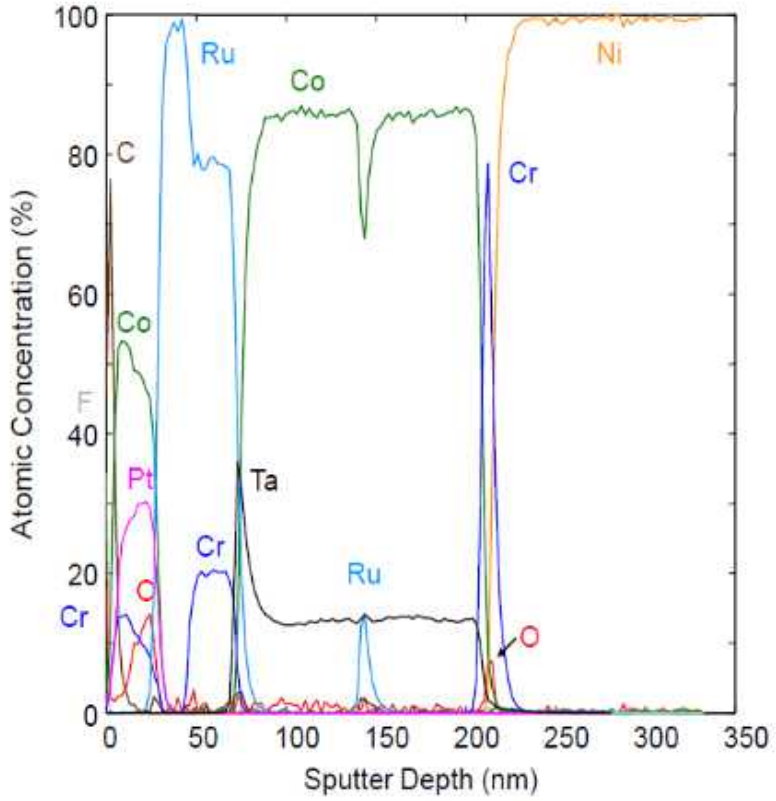

- **Photoelectron spectroscopy**
- **X-ray Absorption Spectroscopy**
- **X-ray Diffraction Spectroscopy**

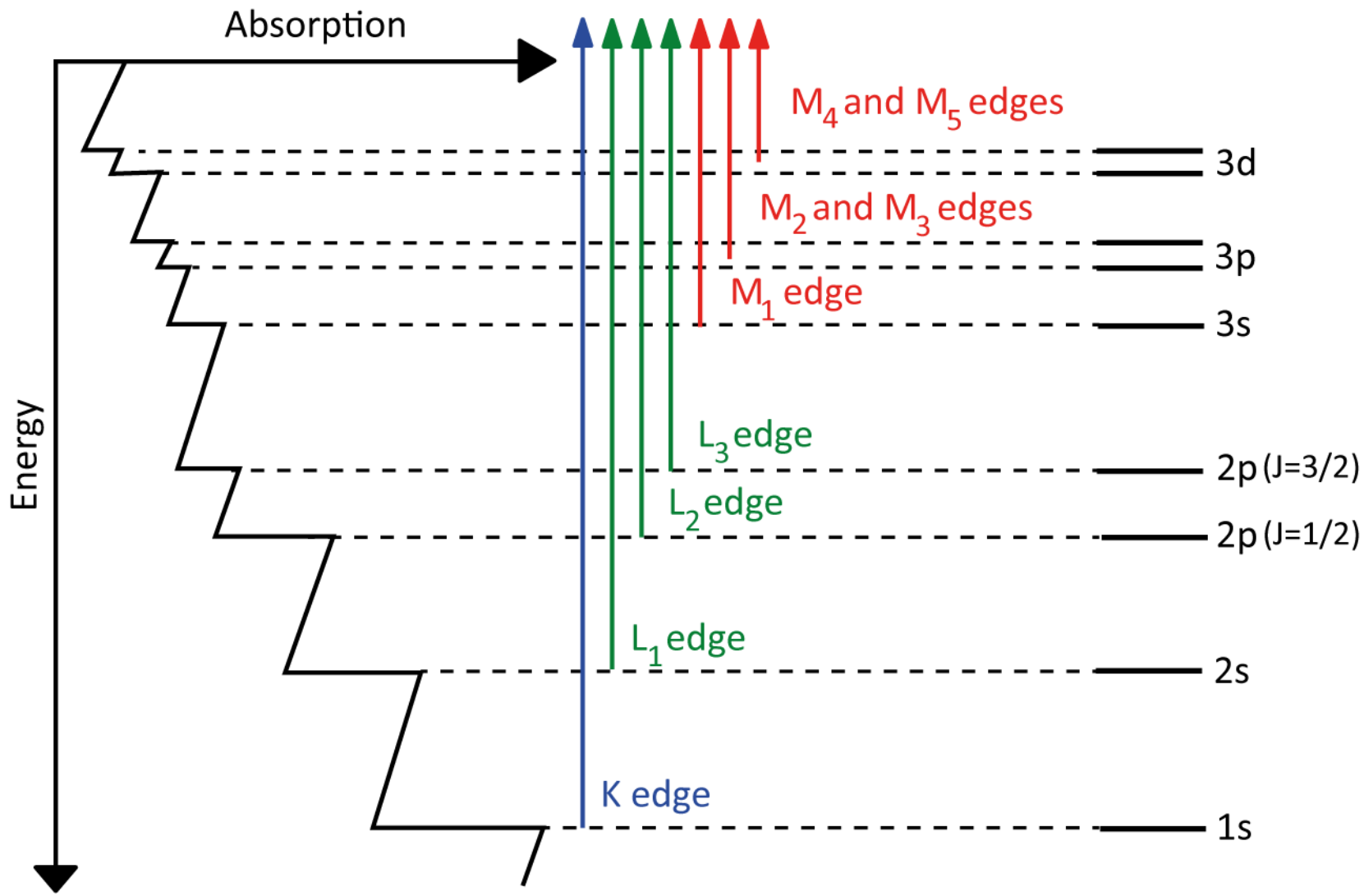
Absorption
Energy
M4 and M5 edges
M2 and M3 edges
M1 edge
L3 edge
L2 edge
L1 edge
K edge
3d
3p
3s
2p (J=3/2)
2p (J=1/2)
2s
1s

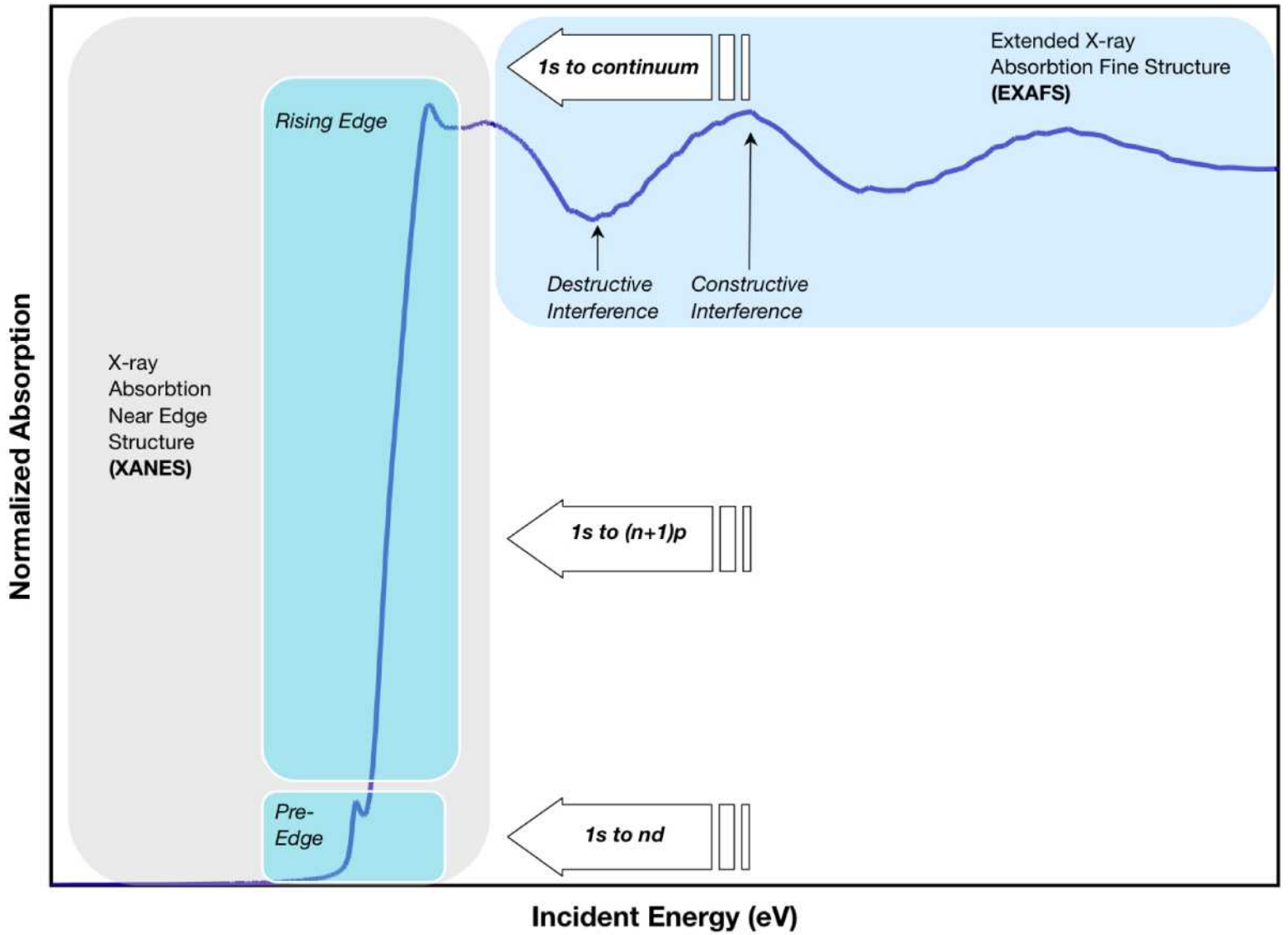
Normalized Absorption
X-ray
Absorbtion
Near Edge
Structure
(XANES)
Rising Edge
Pre-
Edge
1s to continuum
1s to (n+1)p
1s to nd
Extended X-ray
Absorbtion Fine Structure
(EXAFS)
Destructive
Interference
Constructive
Interference
Incident Energy (eV)

XANES

- Average oxidation state
- Local coordination environment
- Electronic structure (empty density of state)

Oxidation state

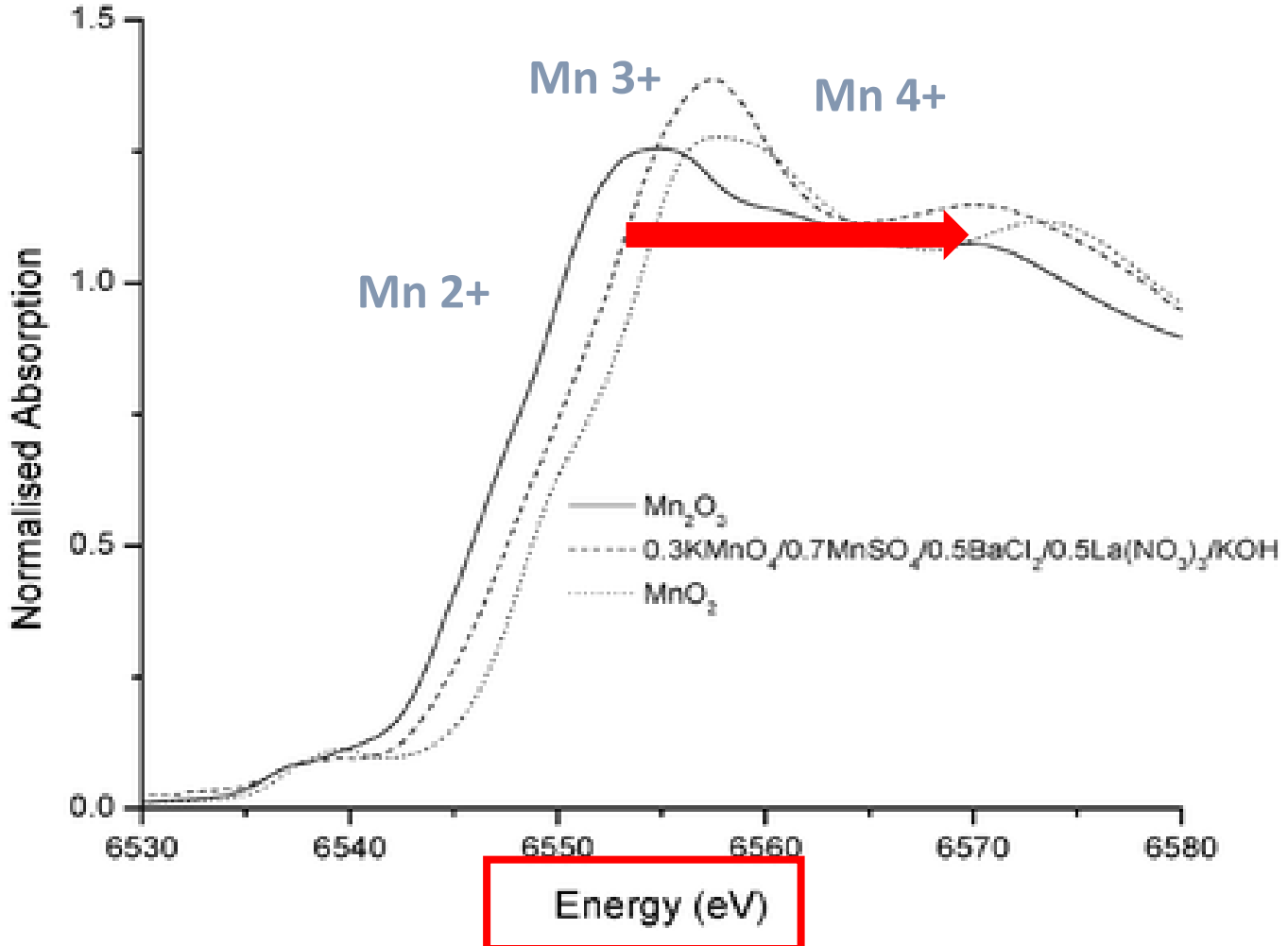

Local coordination environment

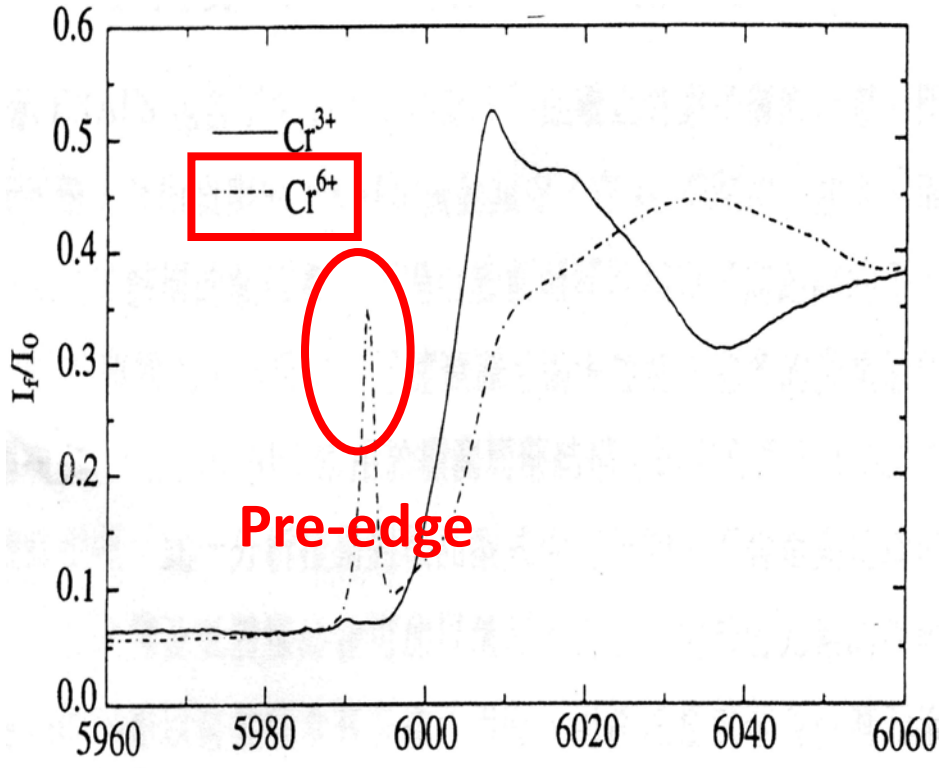

Pure octahedral case

Centro-symmetric: no p-d mixing allowed; only quadrupolar transitions – very low intensity

Distortion from octahedral

p-d mixing allowed: dipole transition in pre-edge – increasingly larger intensity.

Pure tetrahedral

Largest pre-edge intensity.

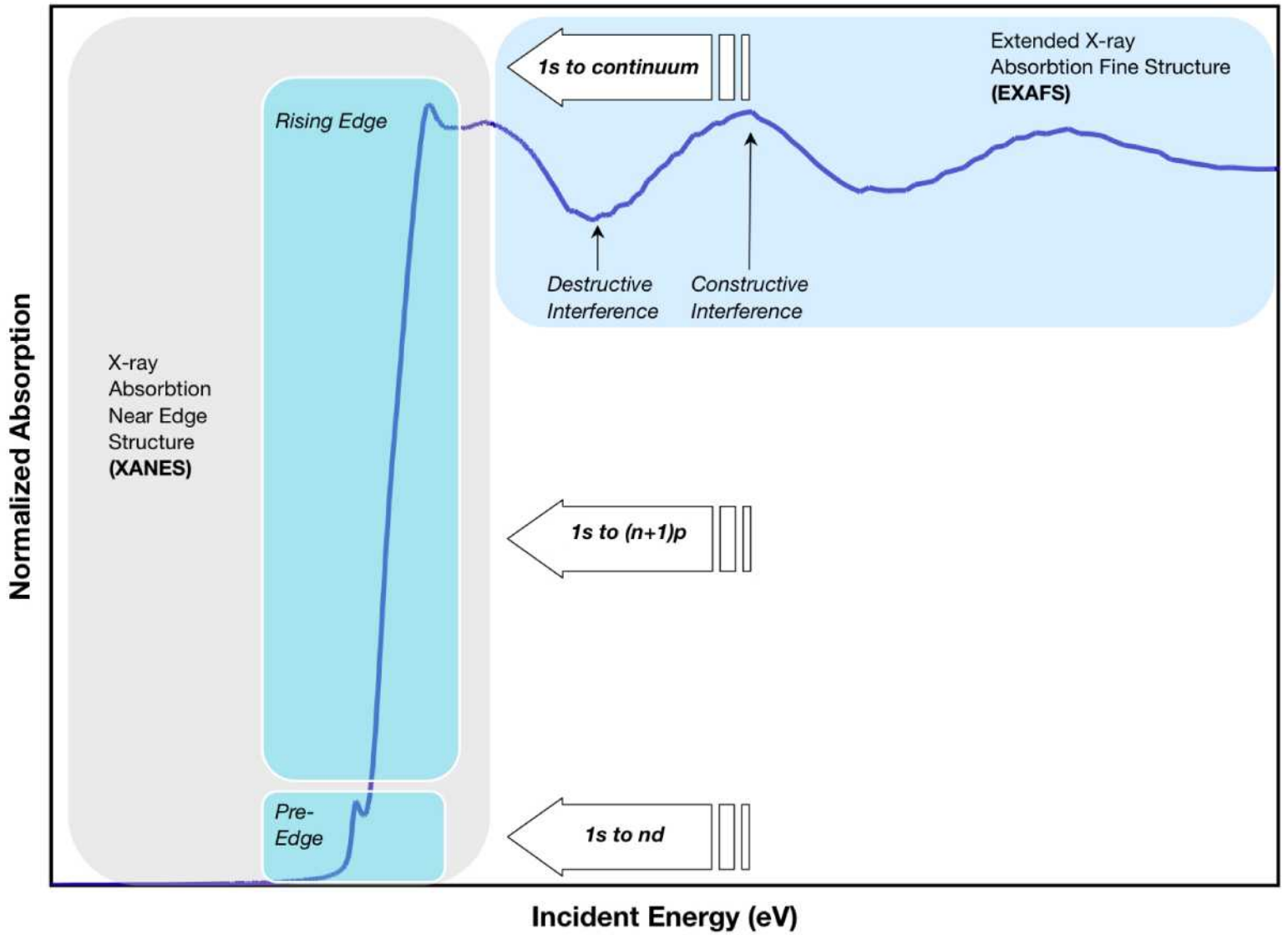
Normalized Absorption
X-ray
Absorbtion
Near Edge
Structure
(XANES)
Rising Edge
Pre-
Edge
1s to continuum
1s to (n+1)p
1s to nd
Extended X-ray
Absorbtion Fine Structure
(EXAFS)
Destructive
Interference
Constructive
Interference
Incident Energy (eV)

EXAFS

- Distance to neighboring atoms (average bond length)
- Coordination number and type of the neighboring atoms
- Order or disorder for atom arrangement

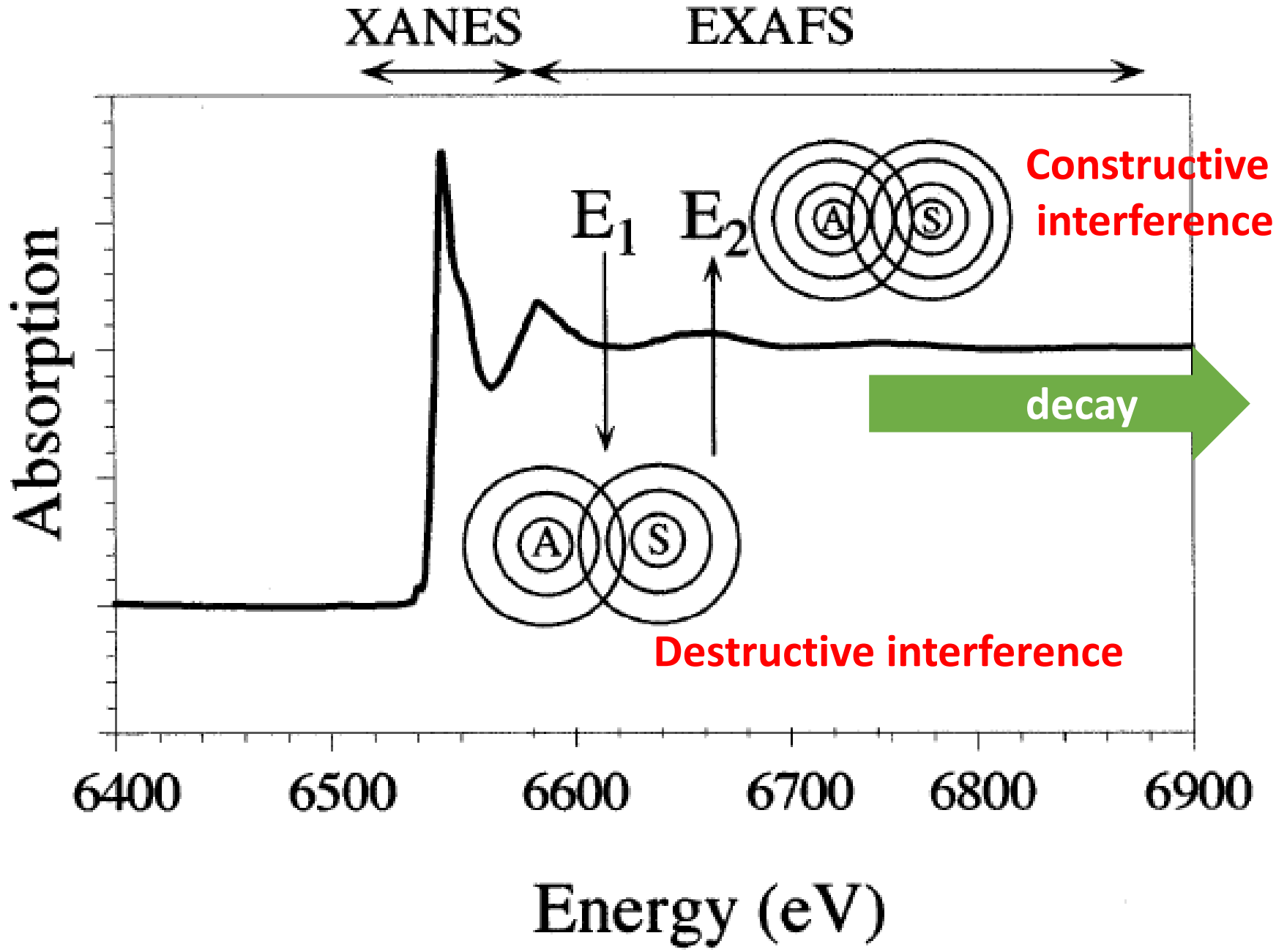
XANES
EXAFS
Absorption
E1
E2
A
S
Constructive interference
decay
A
S
Destructive interference
6400
6500
6600
6700
6800
6900
Energy (eV)

K (wave number)

$$k = \left[\frac{2m}{\hbar^2}\left(E - E_0\right)\right]^{1/2}$$

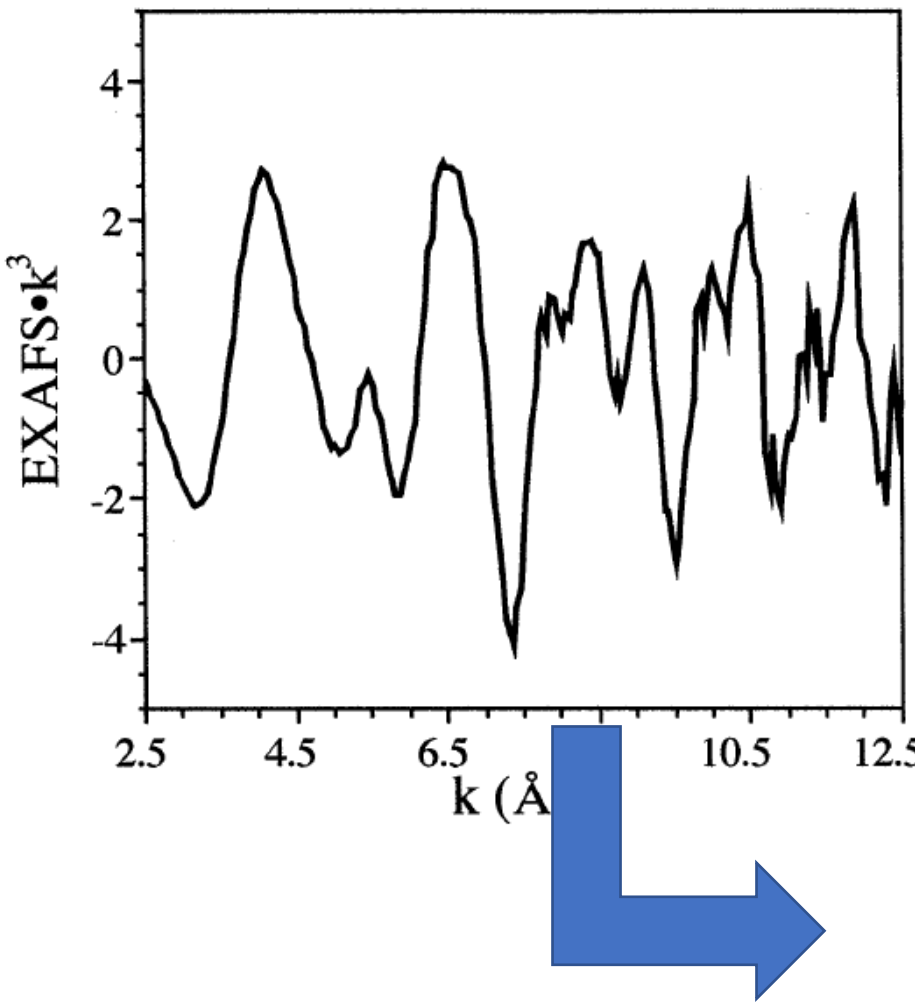

Fourier transformation

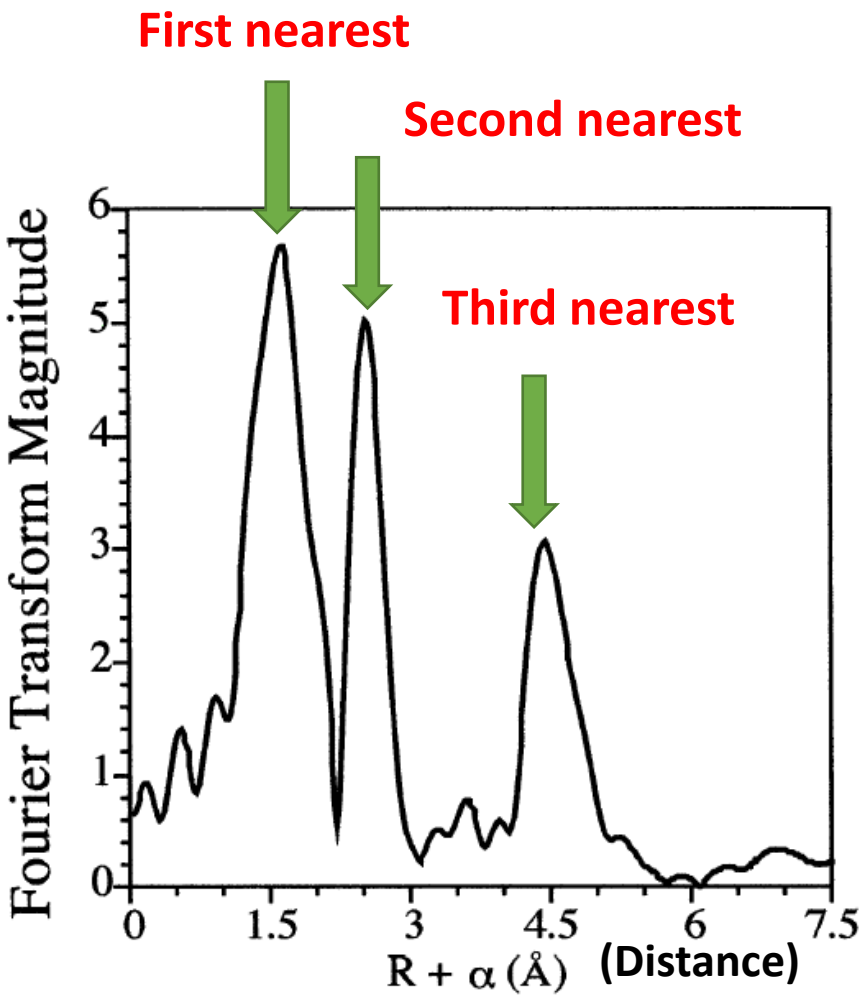

$$\chi(k) = \sum_j \frac{N_j S_0^2 f_j(k) e^{-2R_j/\lambda(k)} e^{-2k^2\sigma_j^2}}{kR_j^2} \sin[2kR_j + \delta_j(k)]$$

where $f(k)$ and $\delta(k)$ are *photo-electron scattering properties* of the neighboring atom.

If we know these properties, we can determine:

R	distance to neighboring atom.
N	coordination number of neighboring atom.
σ^2	mean-square disorder of neighbor distance.

The scattering amplitude $f(k)$ and phase-shift $\delta(k)$ depend on atomic number *Z* of the scattering atom, so we can also determine the species of the neighboring atom.

Nickel Oxide

Crystal structure : face centered cubic (fcc)
Lattice constant a : 4.178 Å
Ni occupies corner site: (000)
O occupies body center site: (½½½)

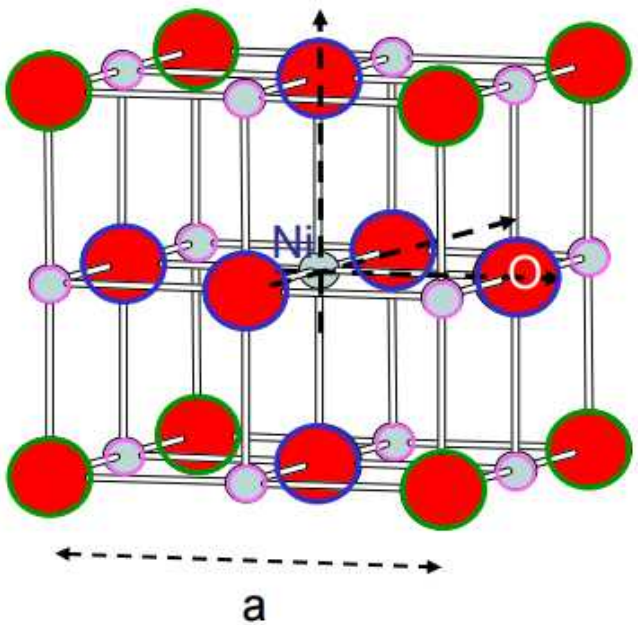

absorbing atom: Ni

Shell	element	distance (Å)	coordination no.
1st	O	2.09	6
2nd	Ni	2.95	12
3rd	O	3.62	8

3. Crystal field splitting & 3d orbital symmetry

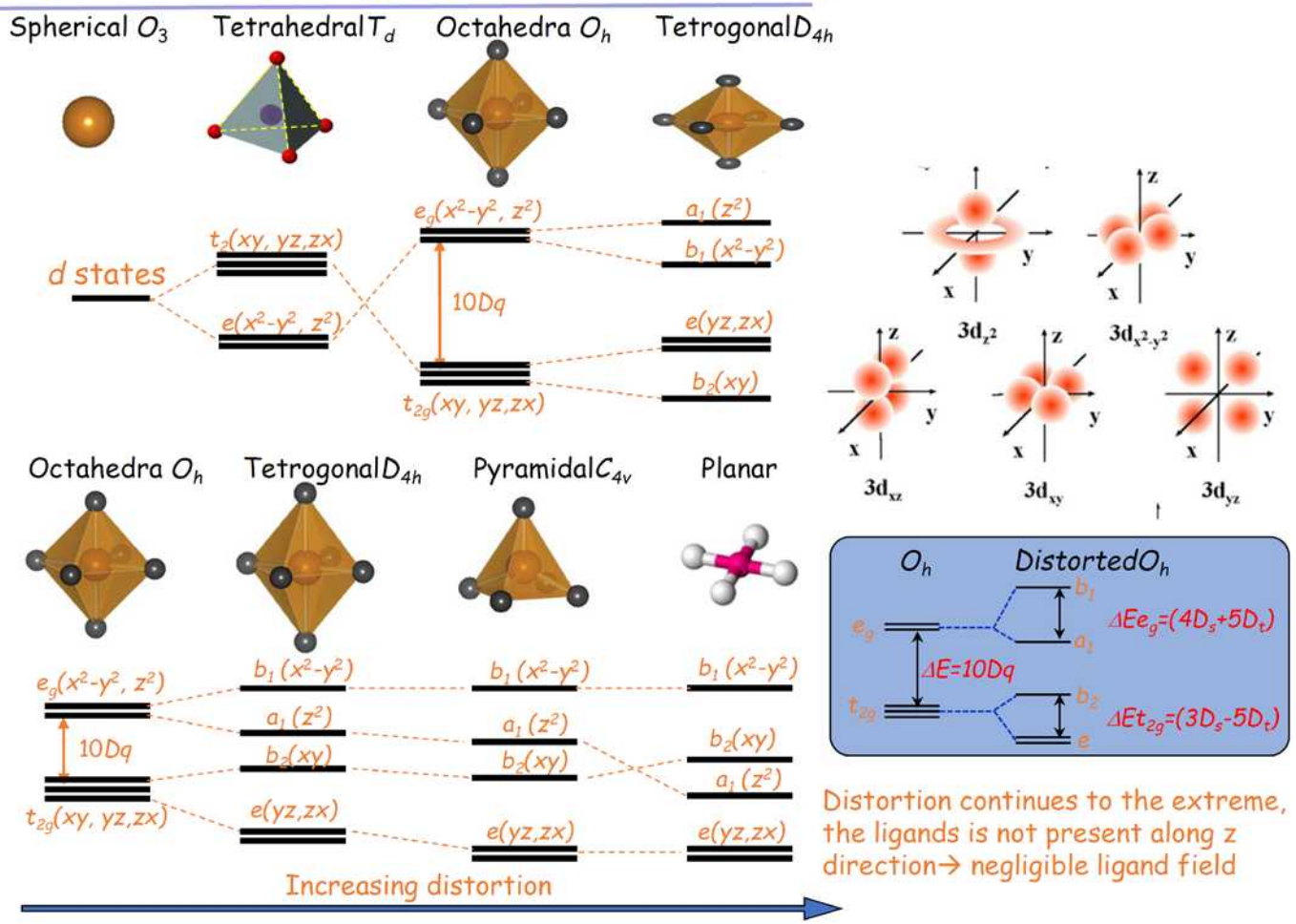

Distortion continues to the extreme, the ligands is not present along z direction→ negligible ligand field

3d orbital symmetry

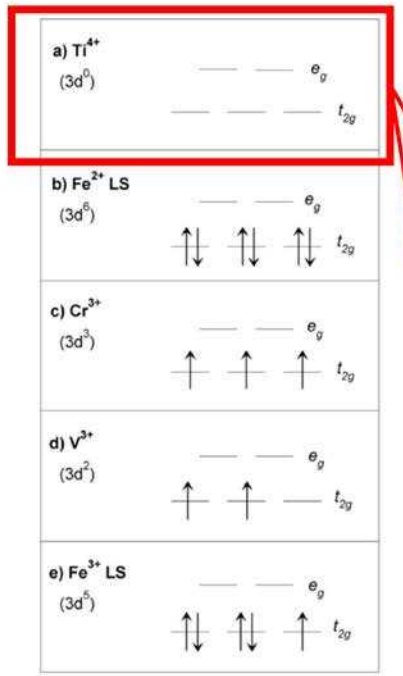

Representation of the 3d levels electronic occupation (in O_h symmetry) of the transition metal ions investigated.

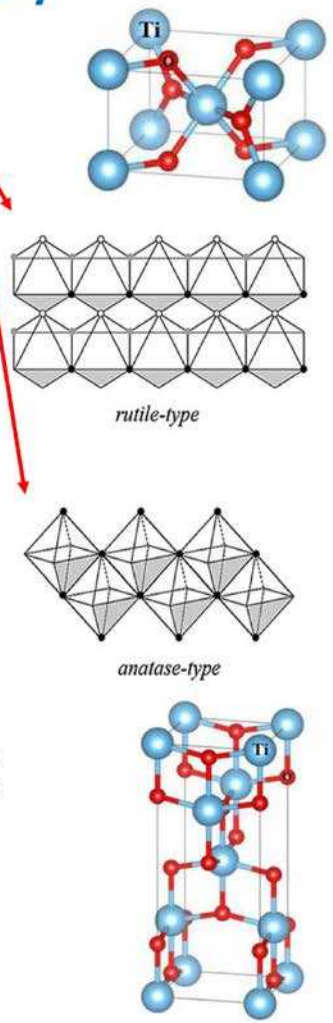

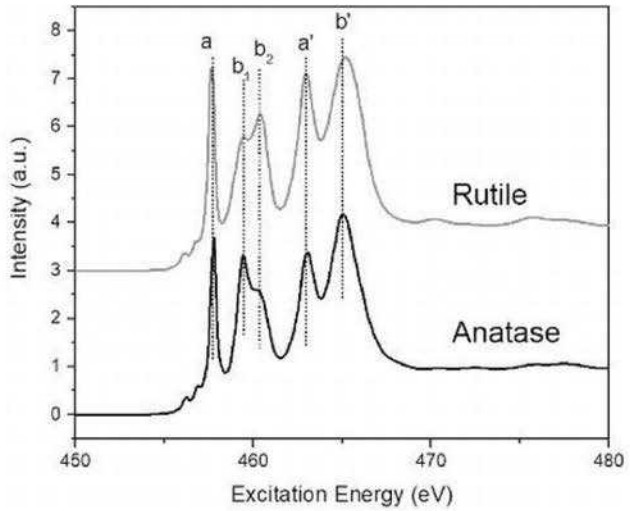

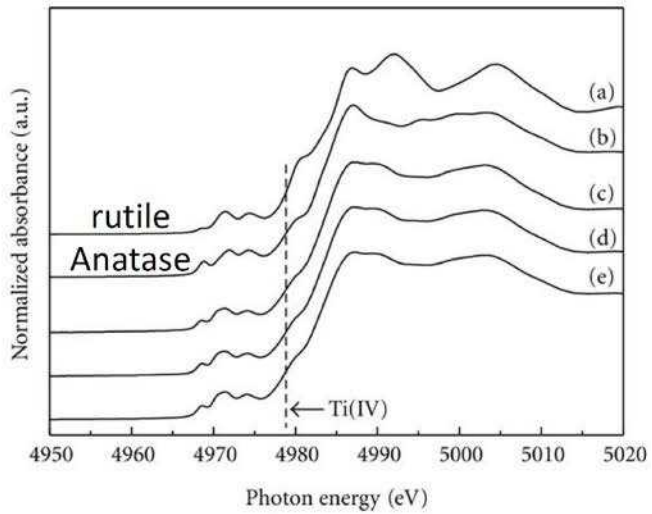

Result

- XAS

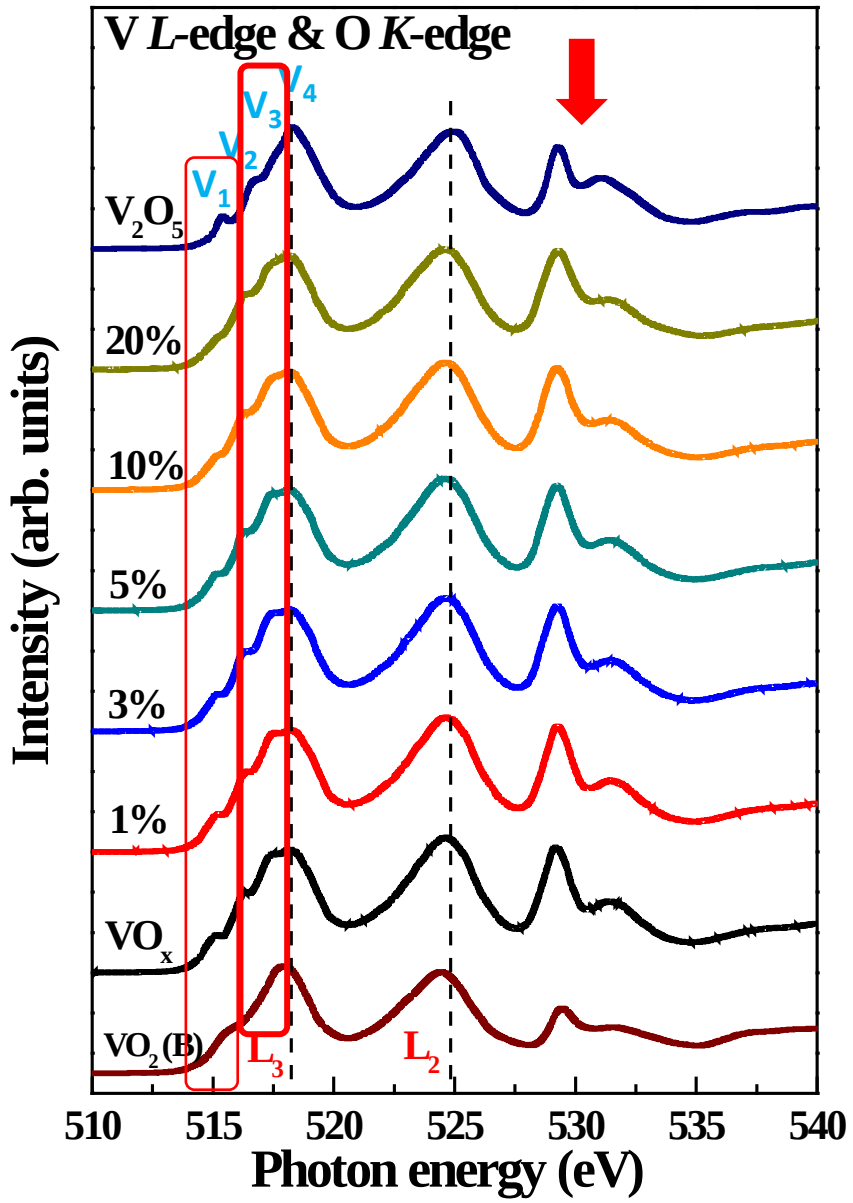

O K-edge

O 1s ➡ O 2p

t_{2g} : O 2p – V 3d (t_{2g})

e_g : O 2p – V 3d (e_g)

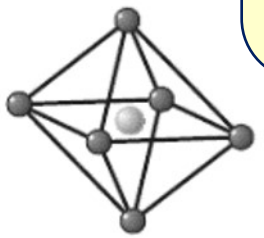

octahedral

pyramid

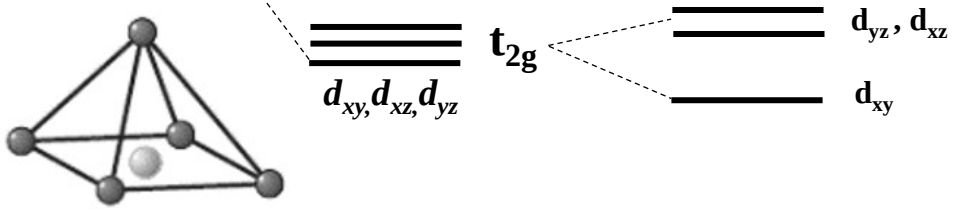

V L_3-edge

V_1 : $3d_{xy}$

V_3 : $3d_{x^2-y^2}$

V_2 : $3d_{xz}+3d_{yz}$

V_4 : $3d_{z^2}$

Adv. Mater. ***3****, 244 (1997)*

Physical Review B ***77****, 075118(2008)*

Result

- XAS

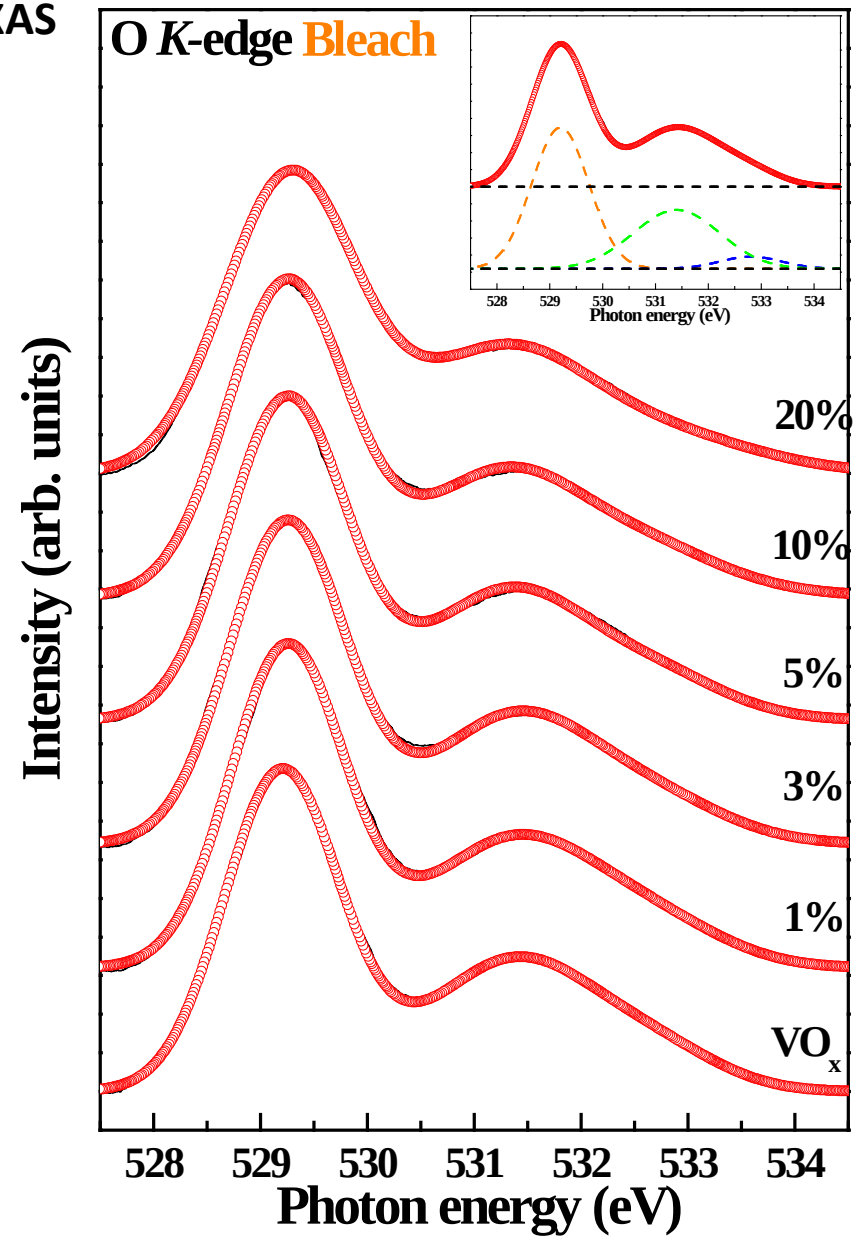

$b_1\ (x^2-y^2)$
$a_1\ (z^2)$
$b_2\ (xy)$
$e\ (yz, zx)$

Physical Review B ***77****, 075118*(2008)

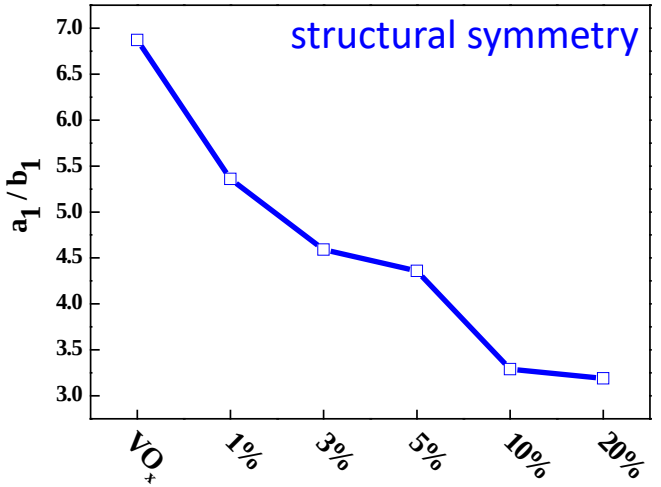

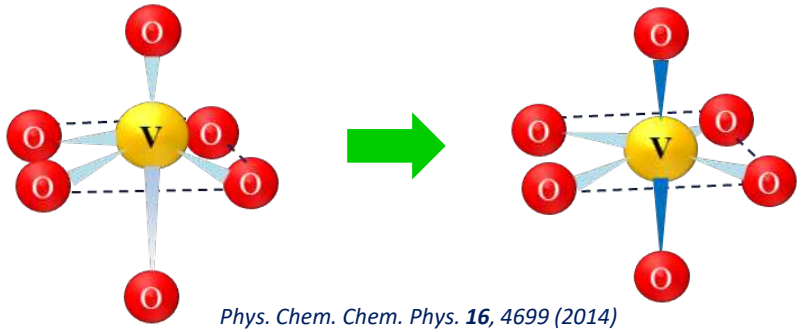

Phys. Chem. Chem. Phys. ***16****, 4699 (2014)*

Central V atom is closer to the plane

- **Photoelectron spectroscopy**
- **X-ray Absorption Spectroscopy**
- **X-ray Diffraction Spectroscopy**

XRD

- NSRRC: continuum spectrum
- In house XRD: characteristics spectrum

- X-ray diffraction is a rapid analytical technique primarily used for phase identification of a crystalline material and can provide information on unit cell dimensions.

The theory of XRD

- The wavelength of x-ray is 10^{-12}~10^{-8}m.
- The wavelength of X-rays are similar to the distance between atoms.
- Diffraction occurs when light is scattered by a periodic array with long-range order, producing constructive interference at specific angles.

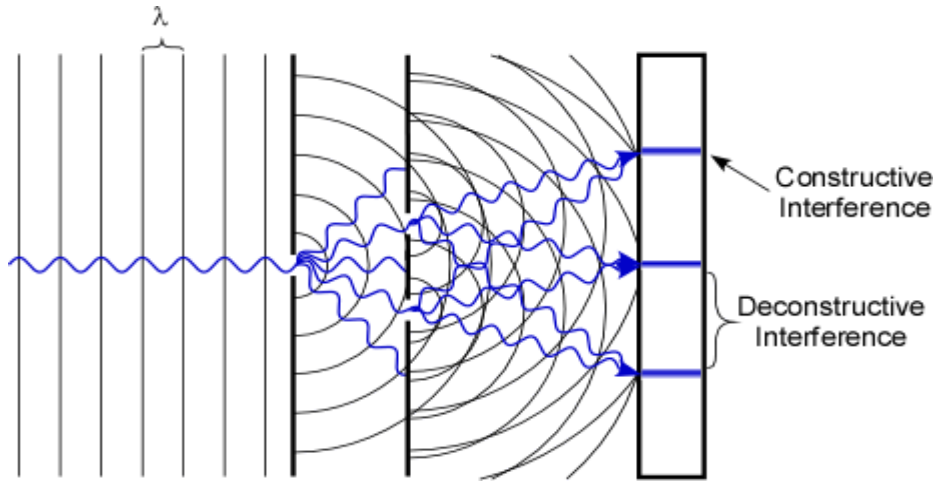

Bragg's law

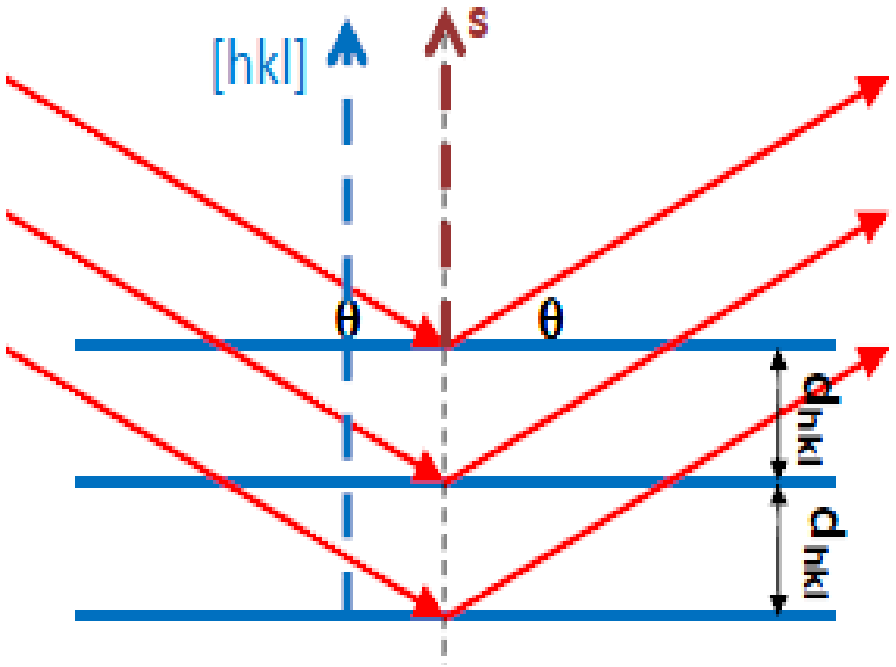

$n\lambda = 2\, d \sin\theta$

- For parallel planes of atoms, with a space dhkl between the planes, constructive interference only occurs when Bragg's law is satisfied.
- Additionally, the plane normal [hkl] must be parallel to the diffraction vectors

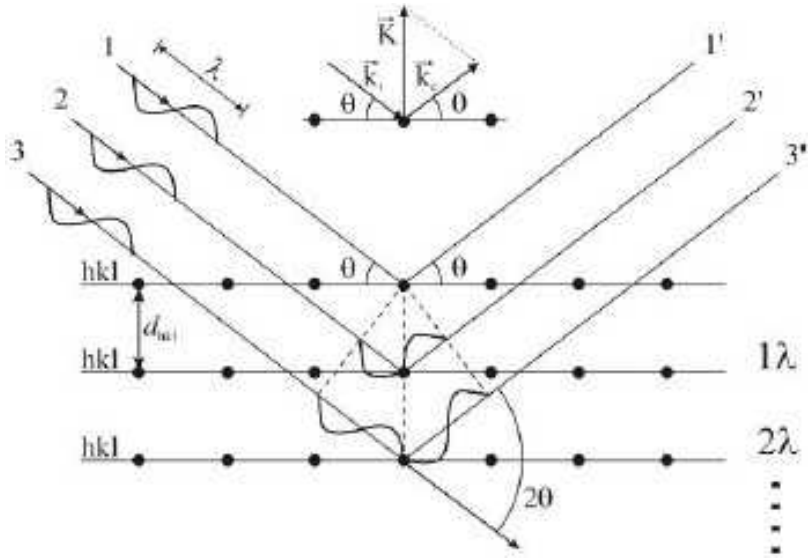

The theory of XRD

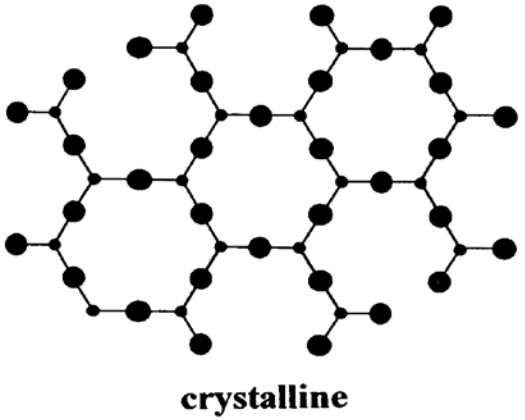

crystalline

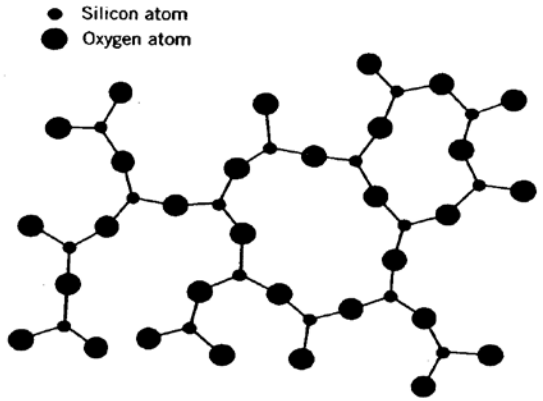

non-crystalline

- The scattering of X-rays from atoms produces a diffraction pattern, which contains information about the atomic arrangement within the crystal.
- Amorphous materials like glass do not have a periodic array with long-range order, so they do not produce a diffraction pattern.

Miller index (hkl)

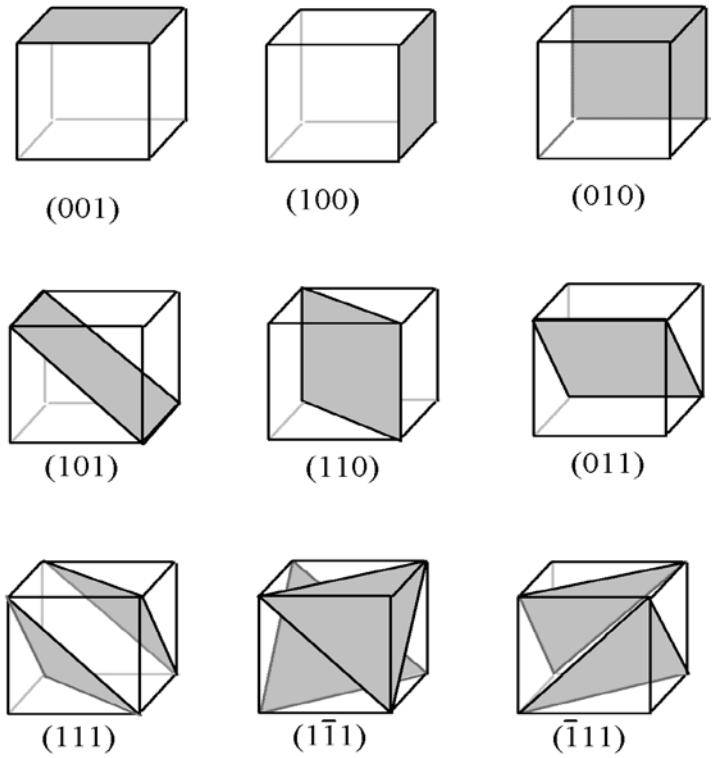

The (200) planes of atoms in NaCl

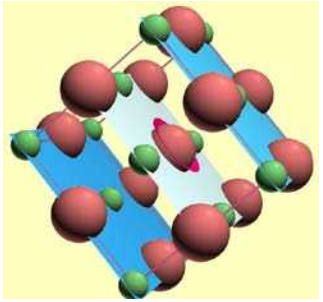

The (220) planes of atoms in NaCl

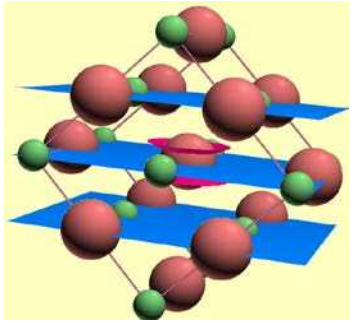

- Miller indices (hkl) are used to identify different planes of atoms.

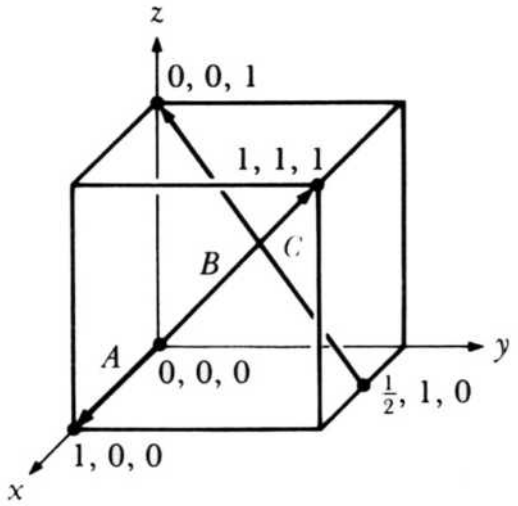

Crystal structure

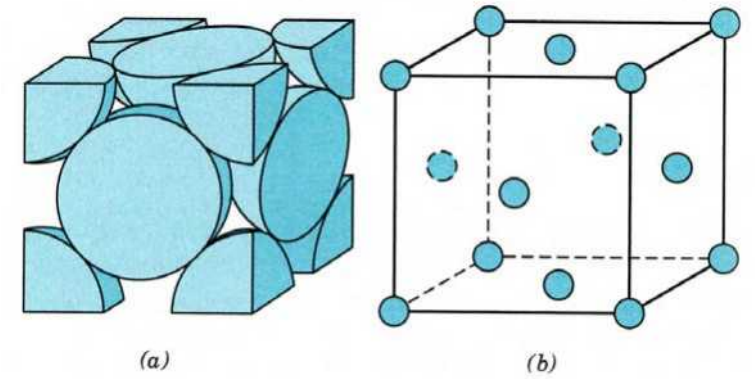

The Face-centered Cubic Crystal Structure

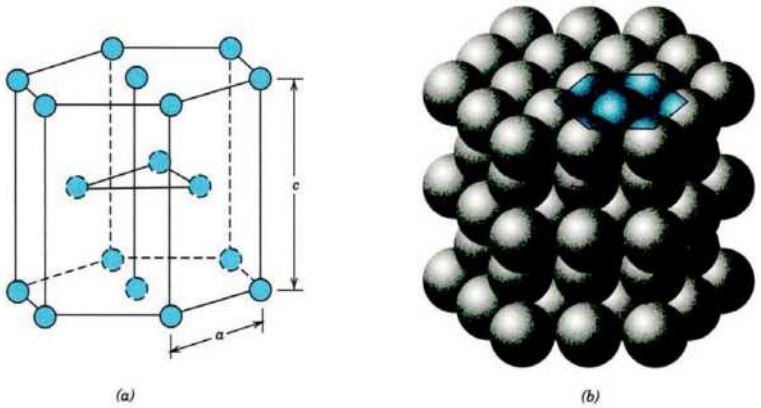

The Hexagonal Close-packed Crystal Structure

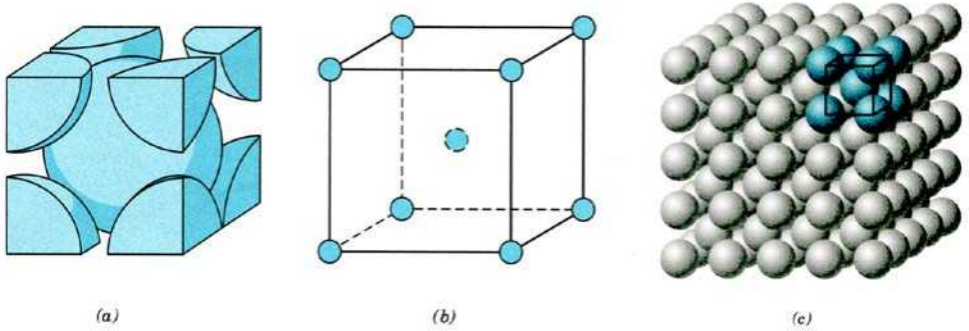

The Body-centered Cubic Crystal Structure

The measurement of XRD

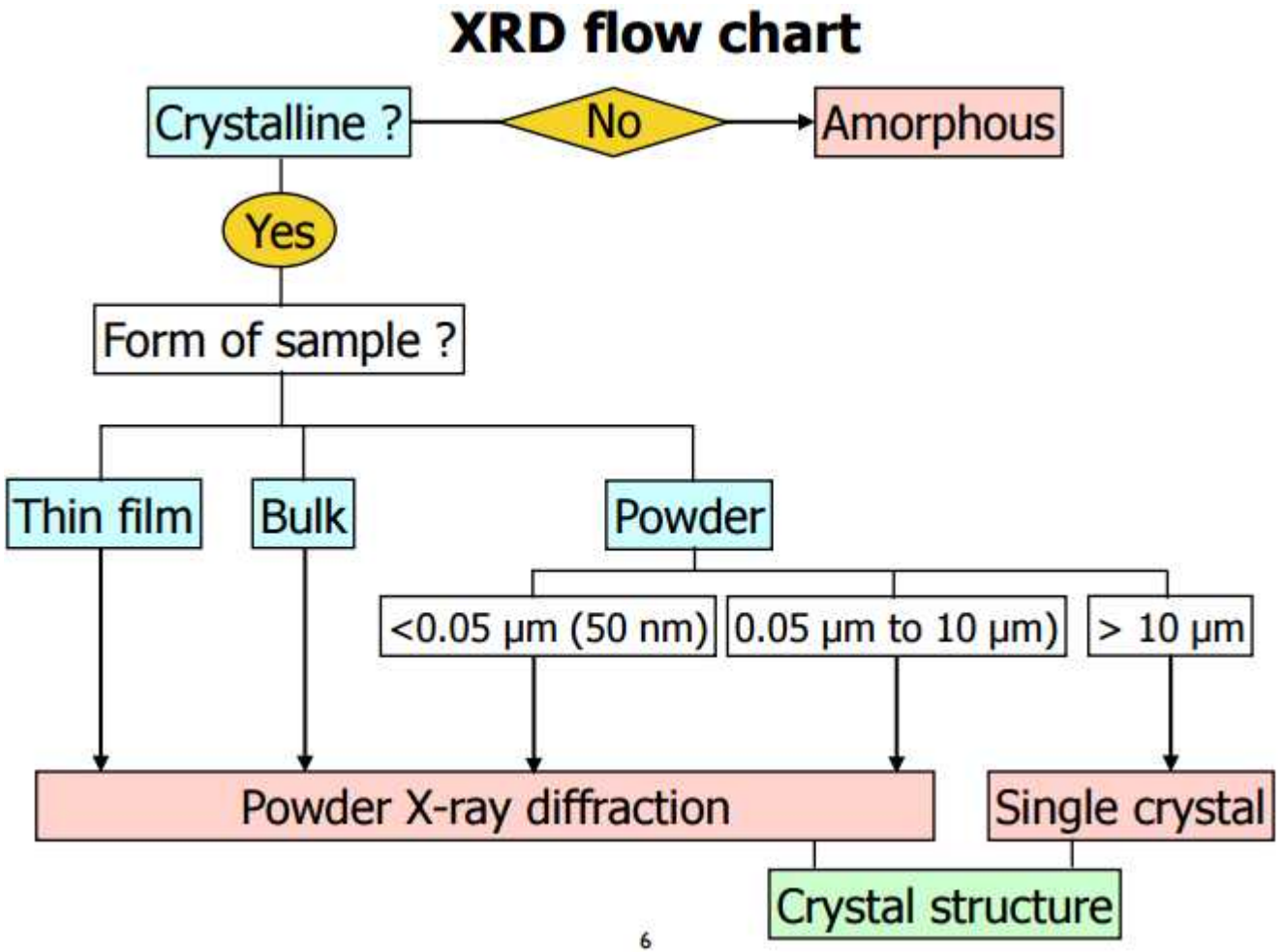

Diffraction peaks are associated with planes of atoms

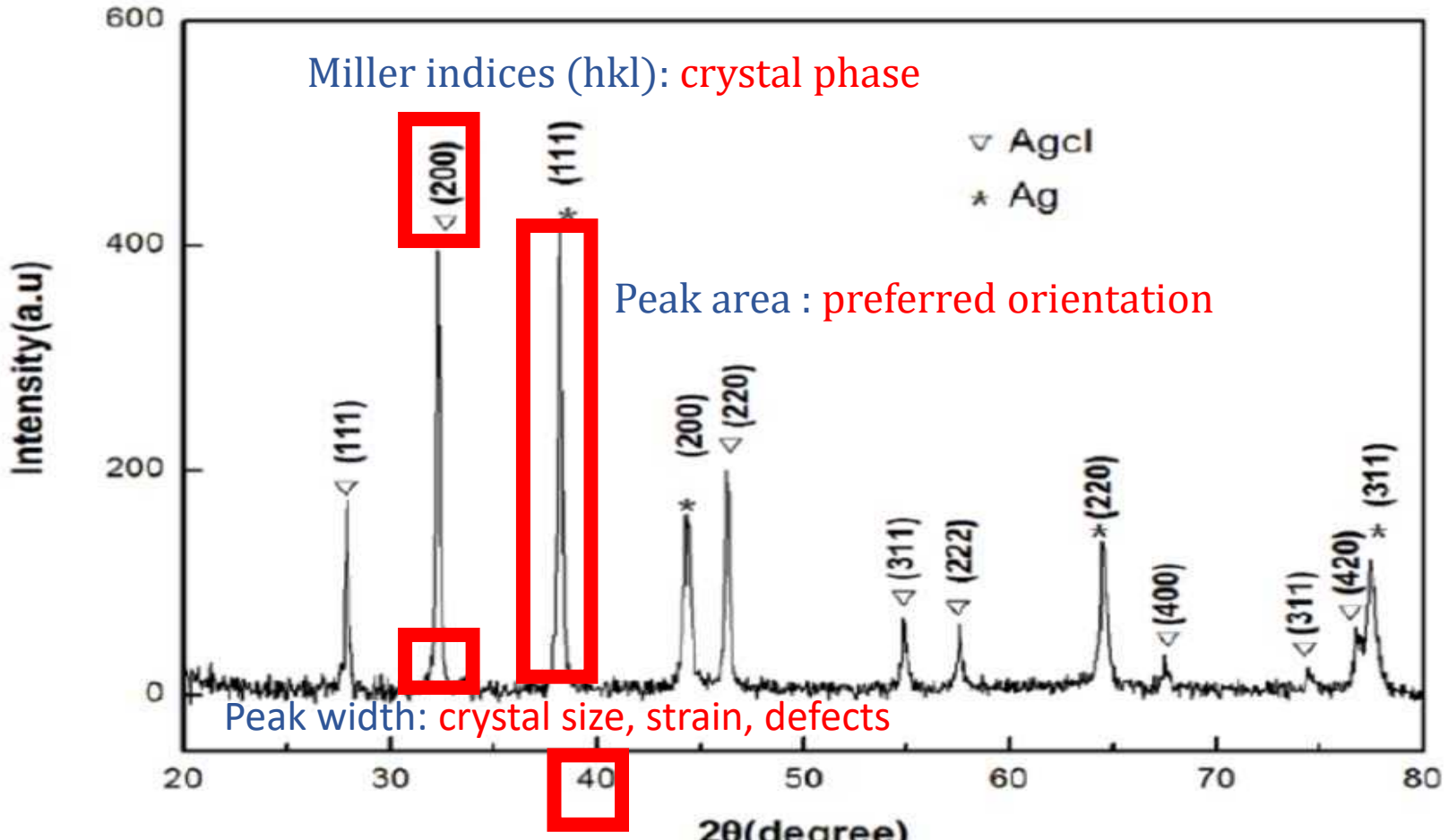

XRD vs XAS

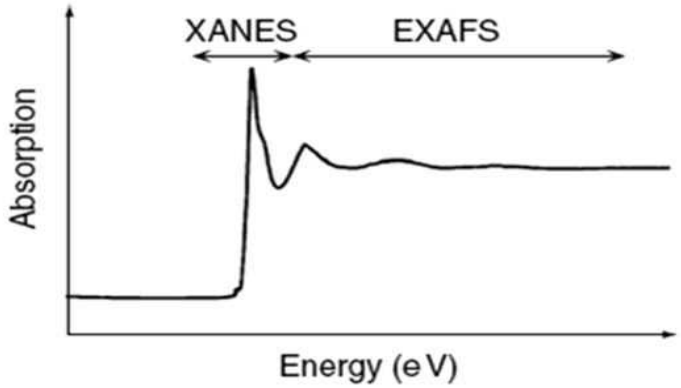

XAS

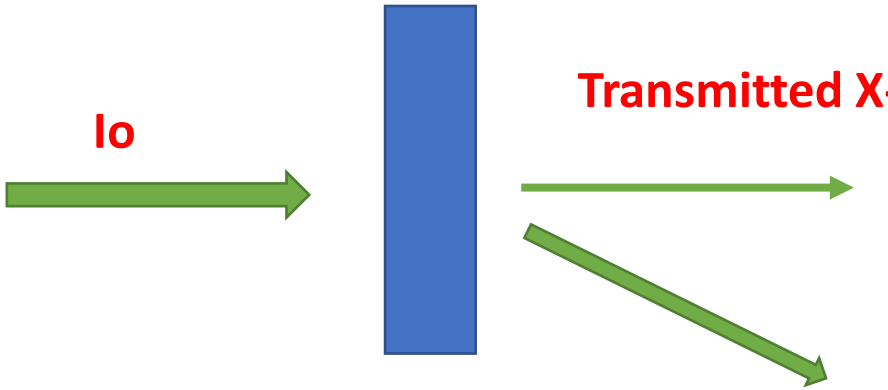

Short range order < 5Å

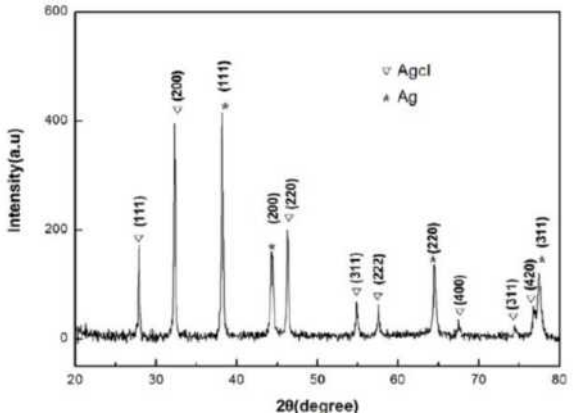

XRD

Long range order > 5 Å

Energy Generation-Solar energy

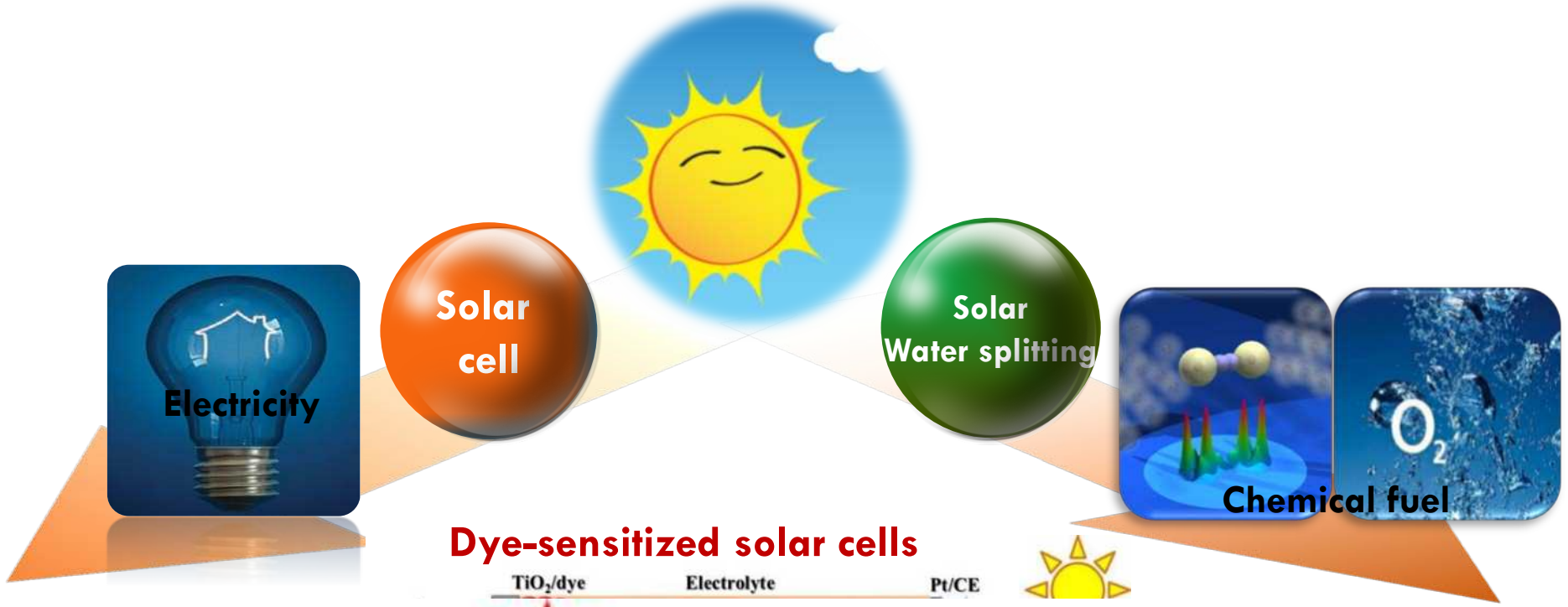

Dye-sensitized solar cells

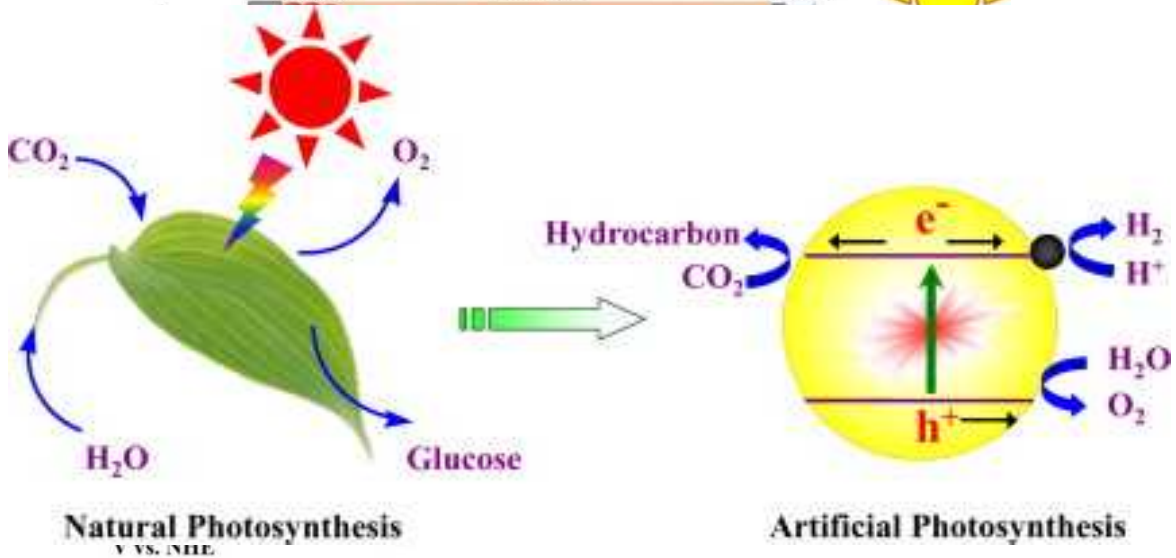

Natural Photosynthesis

Artificial Photosynthesis

Chinese Journal of Catalysis, 2013, 34, 524


H2

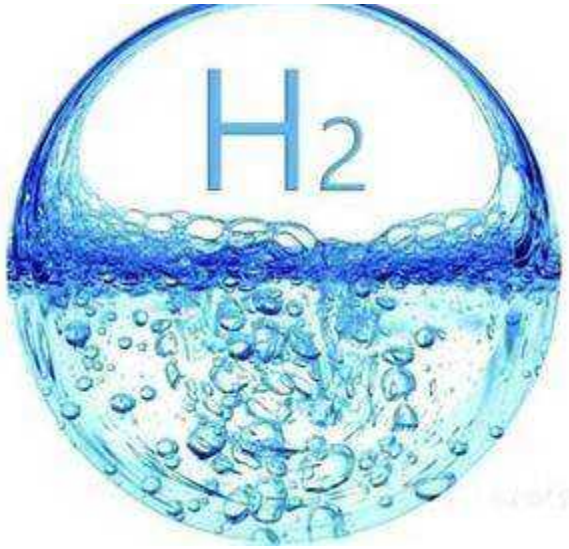
H2


STORAGE
ENERGY
Production
SUN
ENERGY
Fuel
H2O

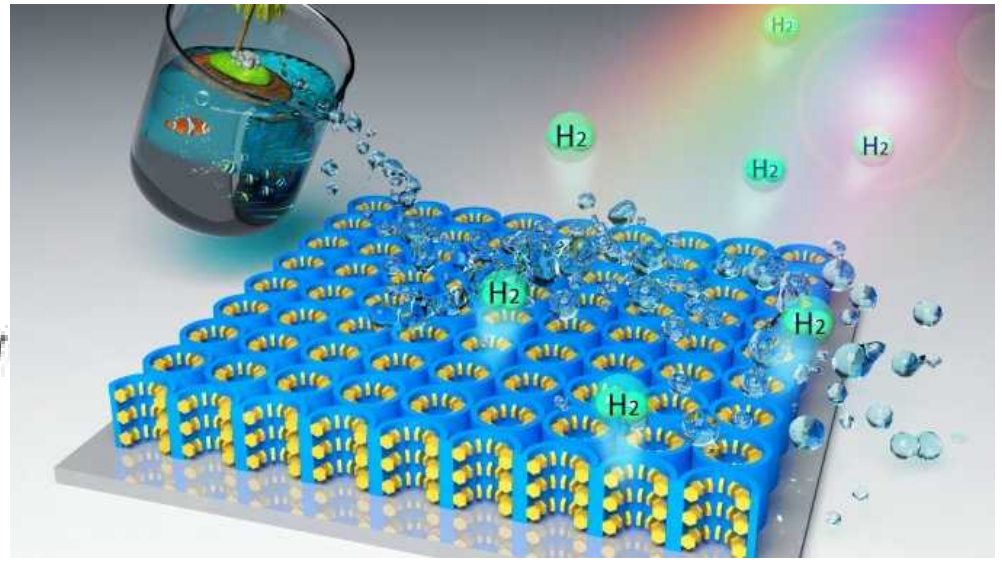
H2
H2
H2
H2
H2
H2

Application of the Chemical Fuel – H_2

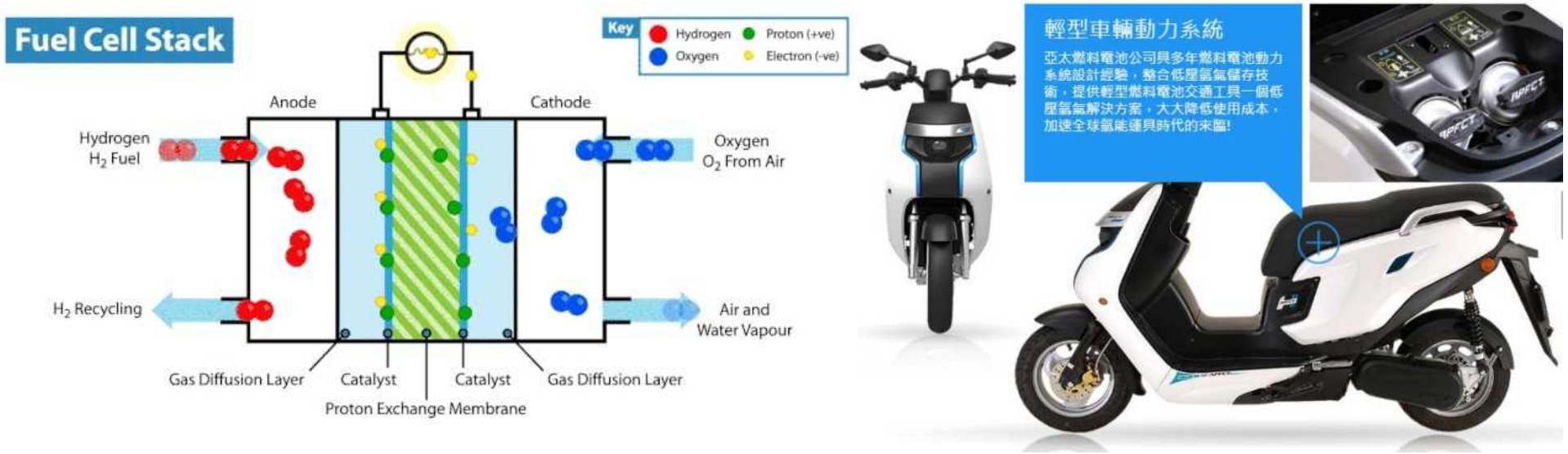

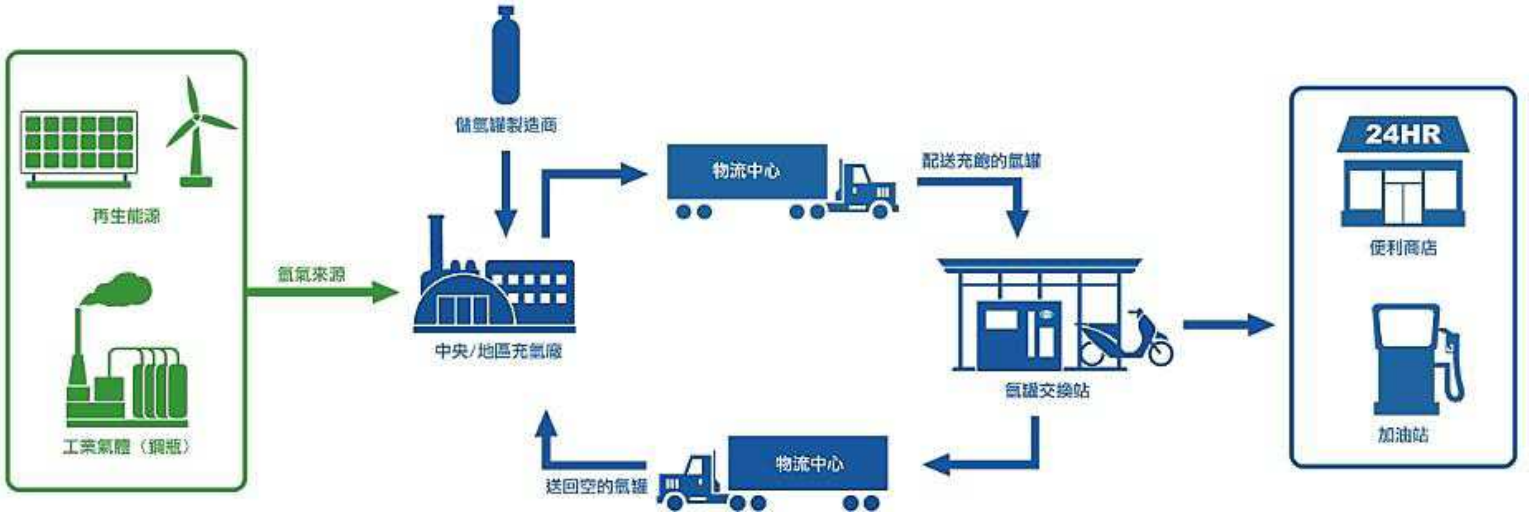

http://www.apfct.com/tw/#

Application

大型發電廠的應用

全球第一輛量產的燃料電池車
(2015)

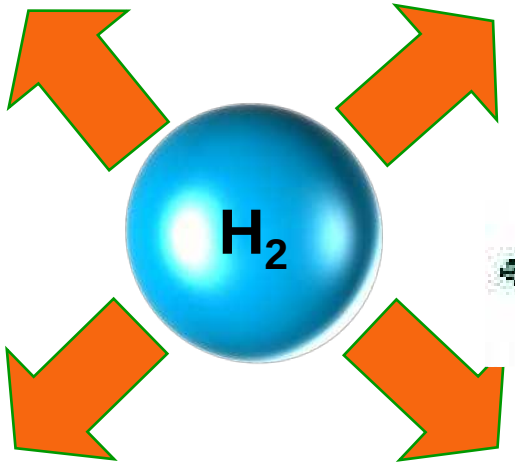

定置型電熱共生系統
(同時產生電力與熱能，供應家庭使用)

3C產品行動電源

Future

日本推動乾淨能源 2021奧運打造「**氫氣城**（hydrogen town）」選手村用

東京都政府為因應氫能源政策，已決定將選手村打造成未來感十足的「氫氣城」。
（擷取自《The Japan News》）

火車正駛向「零碳排」的歷史新頁：首輛「氫能驅動」鐵路列車將在德國上路

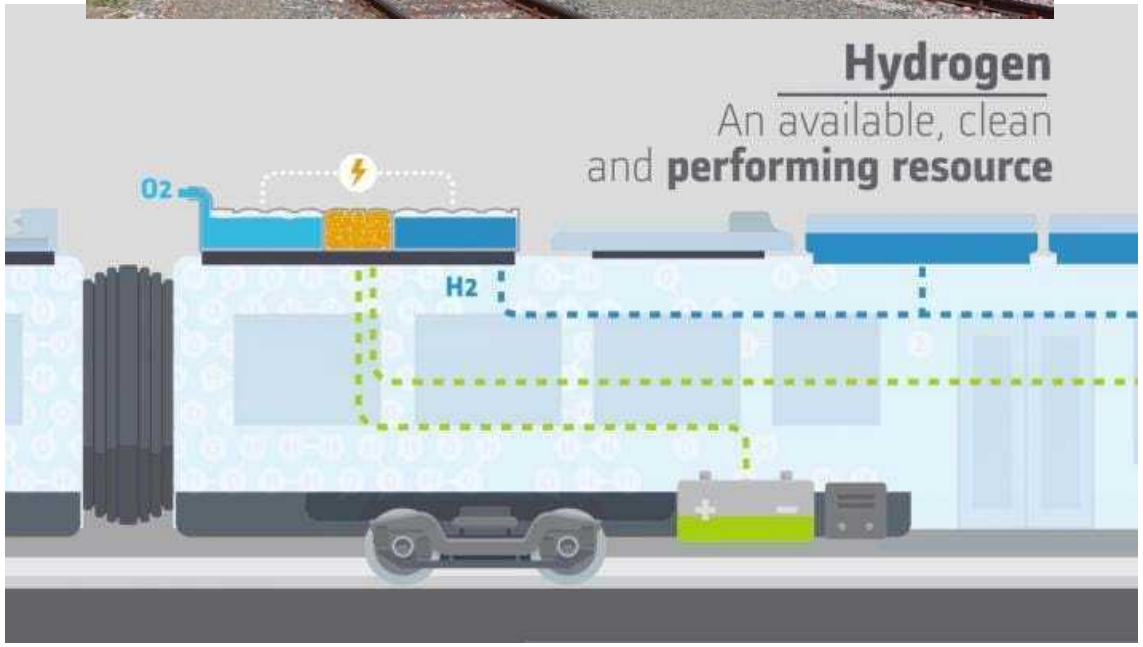

淨零科技方案重點

目　標	推動永續及前瞻能源、低碳、負碳、循環、人文社會科學等五大領域，協助國家達成2050淨零碳排目標
經　費	112年投入119億元
2030年前效益	打造出全球首座百ＭＷ級浮動式離岸風機商轉、1ＭＷ級甲烷裂解去碳燃氫機組，在跨部會協作下，建構數位淨零體系
2030年後效益	發展出深層地熱電廠總裝置量達GW級，並擴大低碳製程與氫能燃燒等技術，協助產業減碳達2,000萬噸

資料來源：國科會　　製表：彭婉琳

Solar to Hydrogen Device

Photosynthesis vs. Artificial Photosynthesis

Photosynthesis

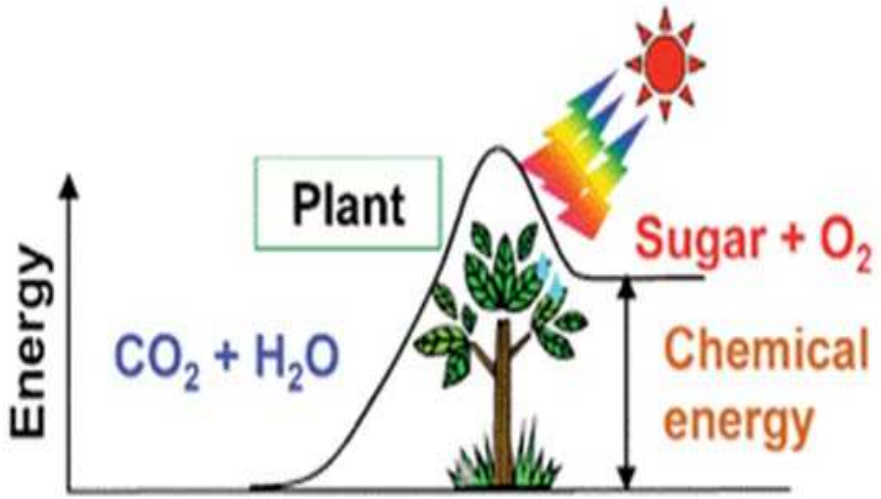

$$6CO_2 + 6H_2O \xrightarrow{\text{Photosynthesis}} C_6H_{12}O_6 + 6O_2$$

carbon dioxide — water — glucose — oxygen

Artificial Photosynthesis (uphill reaction)

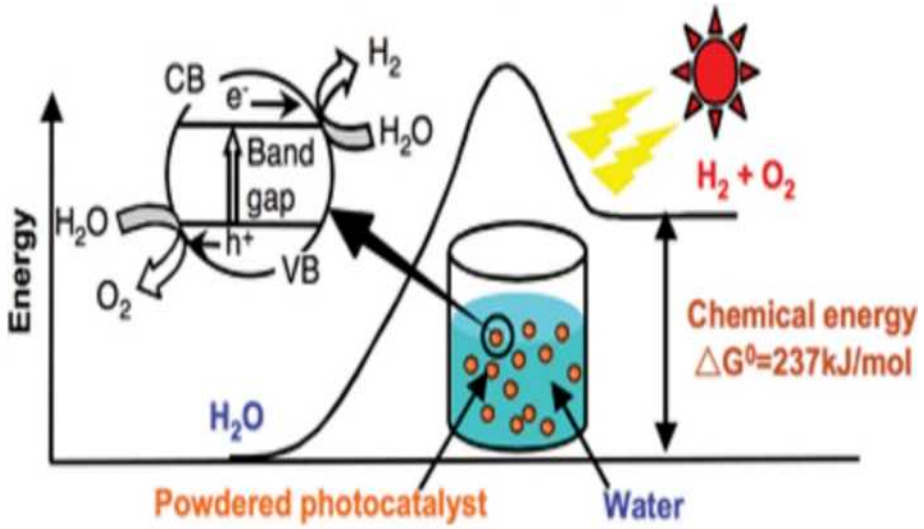

H_2O Oxidation | Charge carrier generation | CO_2 reduction

$$2\,H_2O \rightarrow 2H_2 + O_2$$

$2H^+ + 2e^- \rightarrow H_2$ photocathode

$2H_2O + 4h^+ \rightarrow O_2 + 4H^+$ photoanode

Chem. Soc. Rev., 2009, **38**, 253-278

Approach: Modification of band structure by doping

Accomplishments: Mo-doped ZnO nanorods

Experimental process

Cyclic voltammetric method

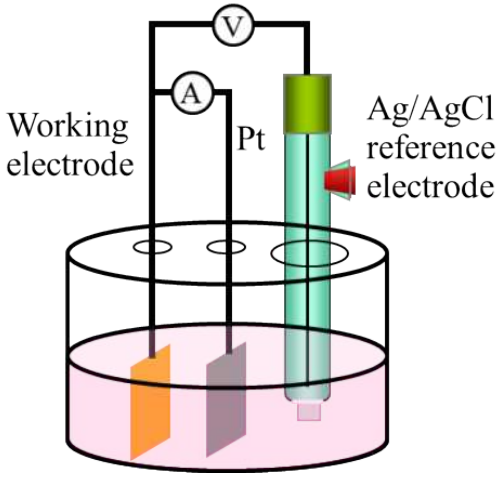

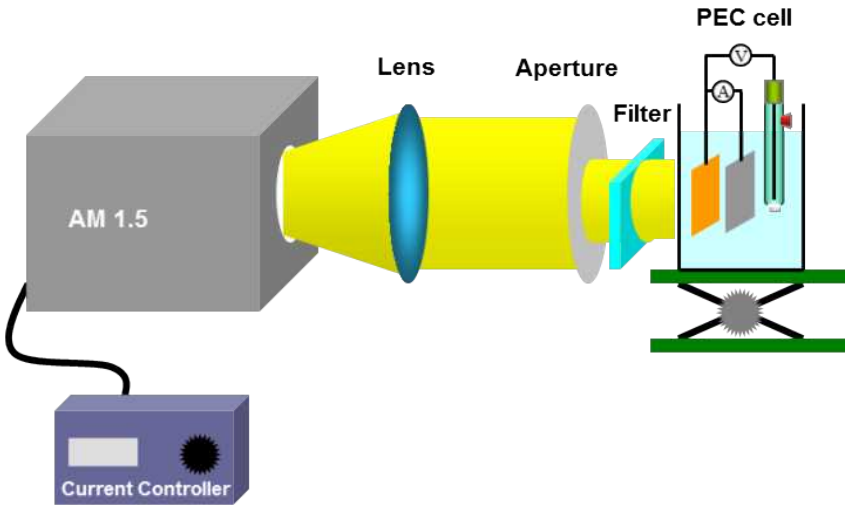

Solutions:

Zinc chloride $ZnCl_2$

Sodium molybdate Na_2MoO_4

Applied Potential: -0.8V (*Ag/AgCl*)

Reaction Temp: 80 ℃

Deposit time: 30 min

- ✓ PEC measurement
- ✓ IPCE measurement
- ✓ Mott-Schottky analysis

Mott-Schottky Analysis

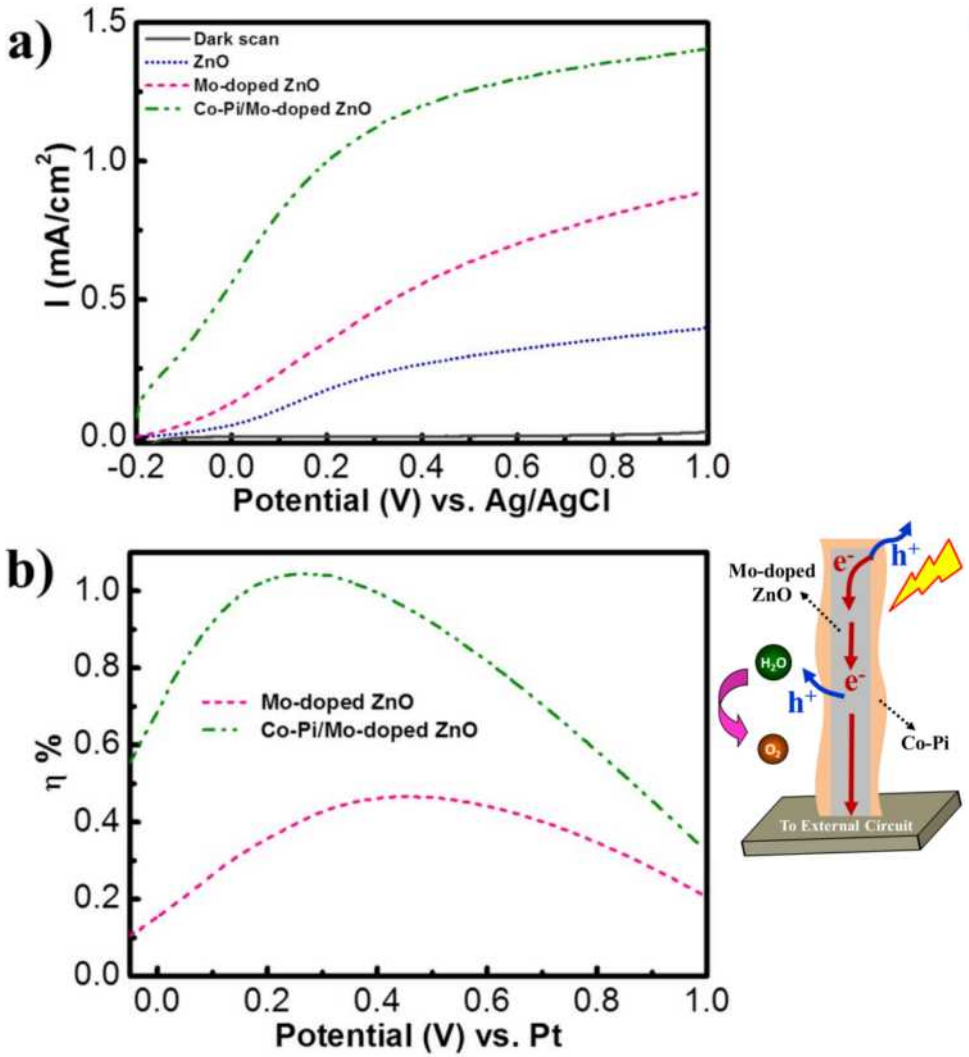

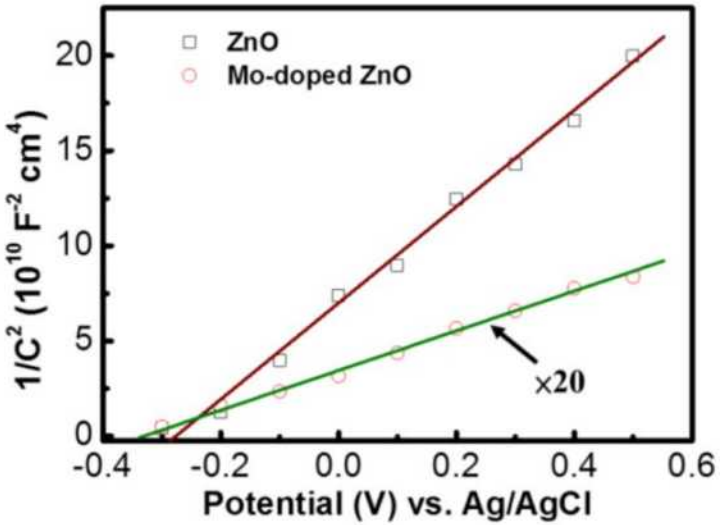

- **Mo incorporation improve overall PEC activity**

Fitting results:

ZnO

$N_D = 6\times10^{18}$ cm^{-3}

$V_{FB} = -0.28$ V vs Ag/AgCl

Mo-ZnO

$N_D = 3\times10^{20}$ cm^{-3}

$V_{FB} = -0.34$ V vs Ag/AgCl

ChemSusChem, **7**, 2748 (2014)

Approach: Modification of band structure by doping

Accomplishments: Mo-doped ZnO nanorods

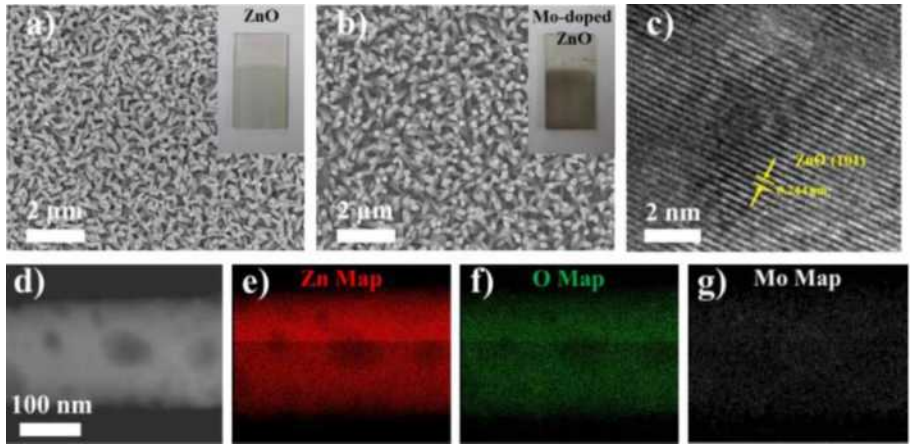

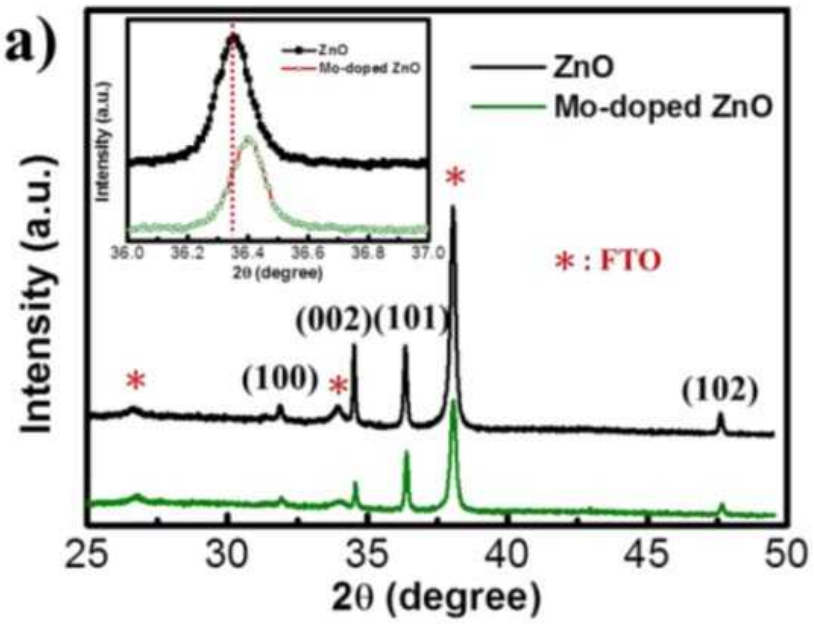

ZnO vs Mo-doped ZnO

- Morphology unchange
- Contraction of ZnO lattice
  Smaller Mo atom has substituted for the larger Zn atom
- Red-shift of the band gap

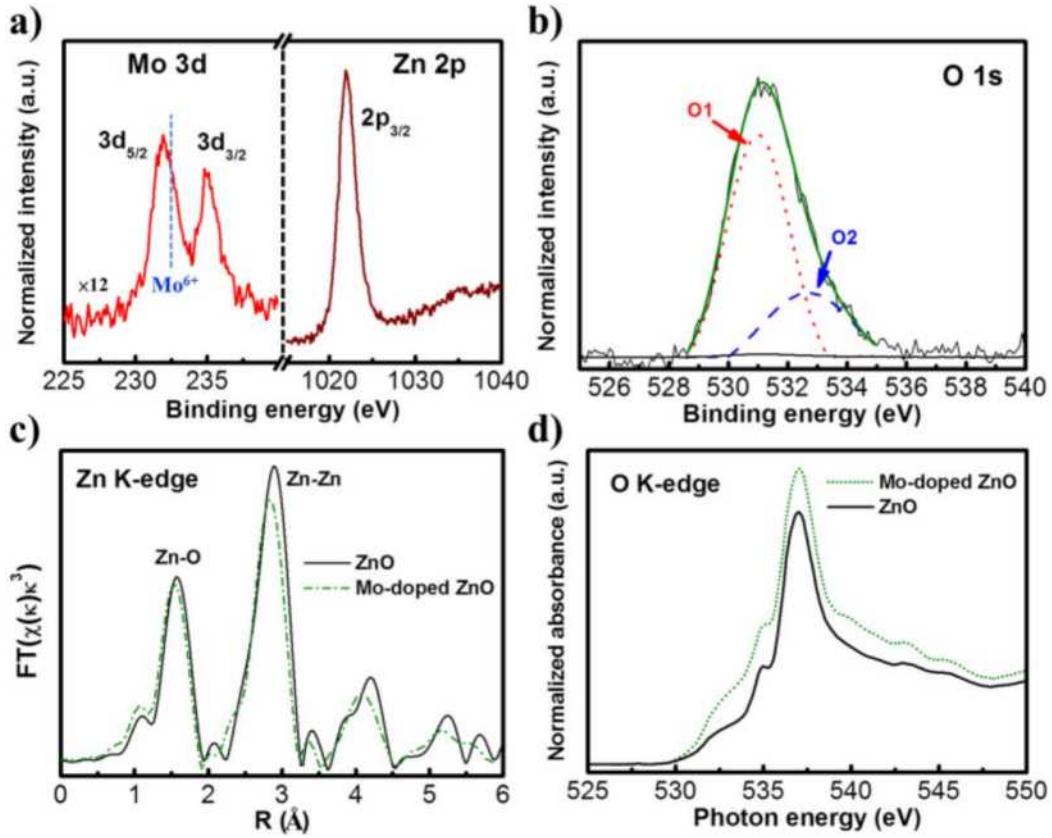

sample	shell	N	R_j (Å)	σ^2 (Å^2)	$\triangle E_0$ (eV)	R-factor
ZnO	Zn-O	3.3	1.96	0.003	4.8	0.003
	Zn-Zn	13.2	3.23	0.015	3.9	0.003
Mo-doped ZnO	Zn-O	3.2	1.94	0.004	2.7	0.004
	Zn-Zn	11.8	3.18	0.02	3.5	0.003

◆ **Insertion of Mo into ZnO**
→ partial reduction of Mo^{6+}
→ charge transfer from O to Mo
→ 1.7 at. % Mo in ZnO

530-538 eV
O 2p–Zn 4s hybrid states
539-550 eV
O 2p–Zn 4p hybrid states

→ increase in number of unoccupied hybrid states
→ e^- transfer from O 2p to Mo

ChemSusChem, **7**, 2748 (2014)

In recent work: Why MnO_2?

■ Typical metal oxides with low recombination loss

➡ TiO_2 and ZnO Ti: [Ar].$3d^2 4s^2$ Zn: [Ar].$3d^{10} 4s^2$

photo electron and hole separate via metal 3*d* or 4*s*(CB) and oxygen 2*p*(VB)

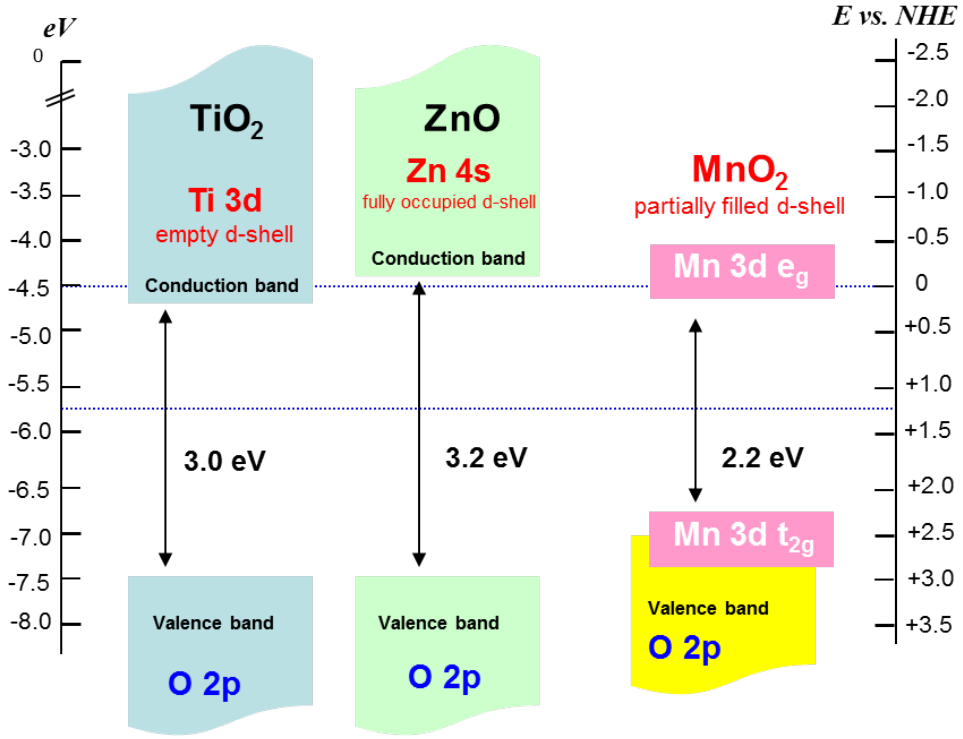

Sakai, N. et al. *J. Phys. Chem.* B **109** (2005) 9651.
Xu, Y. et al. *Am. Mineral.* **85** (2002) 543.

Advantages :

✓ Low cost

✓ Visible-light response

Drawbacks :

■ **In the case of Mn(IV)O_2,**

VB → O(2p) & occupied Mn(3d) t_{2g} orbital

CB → unoccupied Mn(3d) e_g orbital

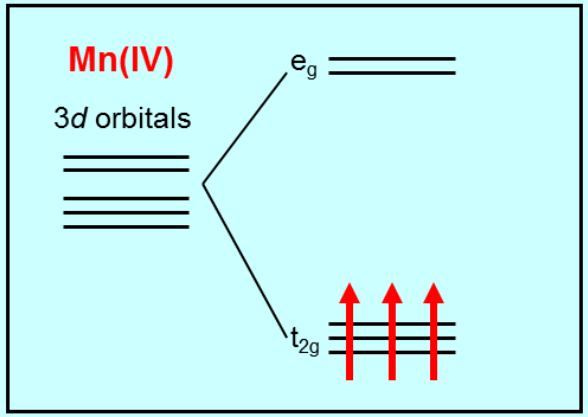

photo electron and hole via **d-d transitions**

➢ **Difficult migration**

➢ **Rapid recombination**

Sherman, D.M. et al. *Am. Mineral.* **69** (1984) 788.

Approach: Modification of band structure by doping

Accomplishments: Ca-doped MnO_2 nanorod bundles

Experimental process

Cyclic voltammetric method

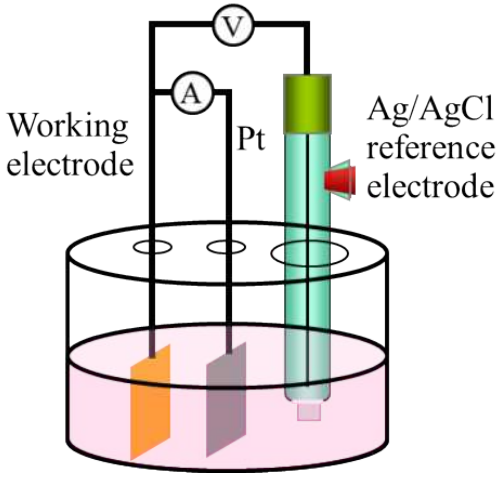

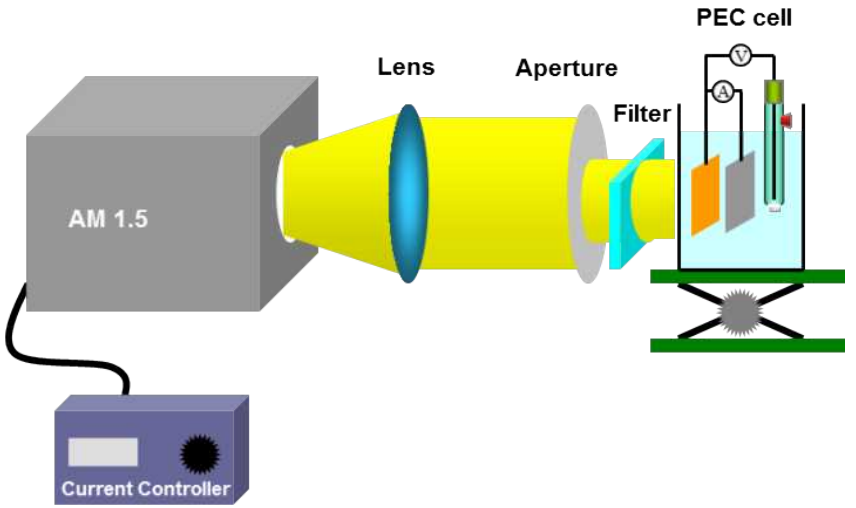

Solutions: (at 25 °C)

Manganese acetate $Mn(CH_3COO)_2$

Calcium nitrate $Ca(NO_3)_2$

Potential window: 0V~0.7V

Scan rate: 500mV/s

Deposit time: 15 mins

- ✓ PEC measurement
- ✓ IPCE measurement
- ✓ Mott-Schottky analysis

PEC results

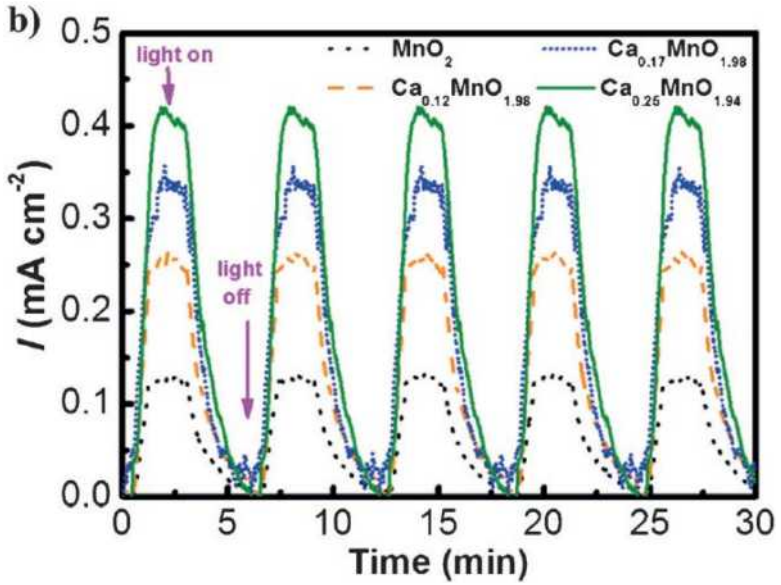

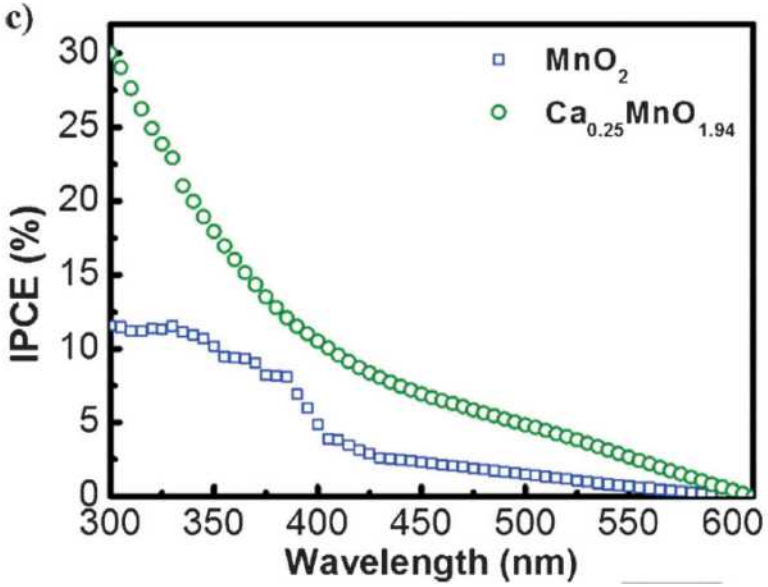

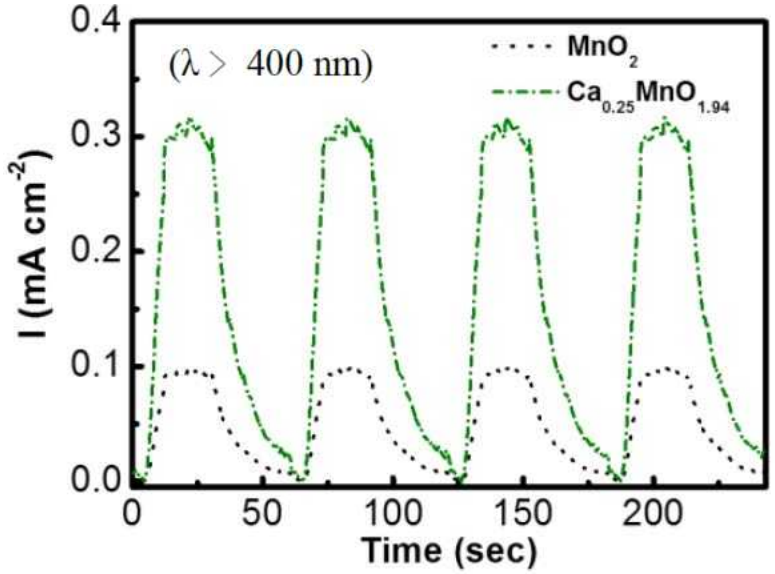

$$\text{IPCE}\,[\%] = \frac{1240 \times \text{photocurrent density}\ [\text{mA cm}^{-2}]}{\text{wavelength}\ [\text{nm}] \times \text{photon flux}\ [\text{mW cm}^{-2}]} \times 100$$

- **Ca incorporation improve overall visible-light absorption and PEC activity.**

Chemcatchem, **6**, 1684 (2014)

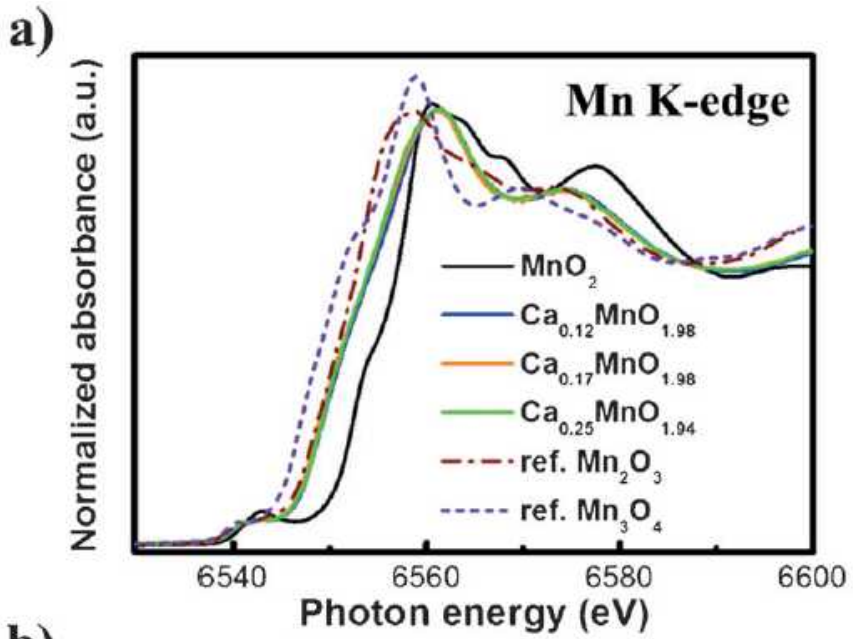

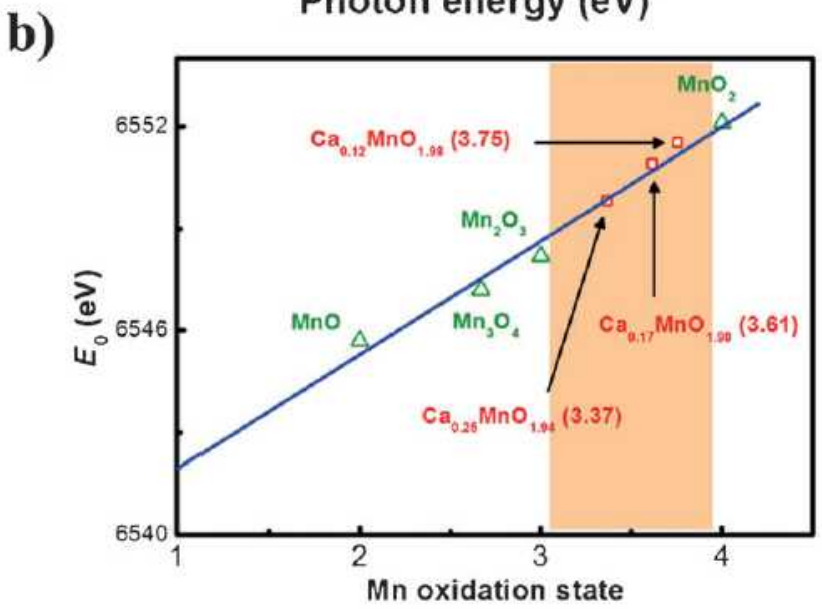

Table 1. Characteristics of pristine and Ca-containing MnO_2 samples.

Sample composition	$[Ca^{2+}]$ initial content (M)	Ca:Mn atomic ratio[a]	Mean Mn oxidation state[b]	Element ratio (Mn^{3+}/Mn^{4+})[b]
MnO_2	-	0 : 1	4	0
$Ca_{0.12}MnO_{1.98}$	0.5	0.12 : 1	3.75	0.33
$Ca_{0.17}MnO_{1.98}$	1	0.17 : 1	3.61	0.64
$Ca_{0.25}MnO_{1.94}$	1.5	0.25 : 1	3.37	1.7

[a] Atomic ratios were determined by ICP. [b] Valence states and element ratios were calculated by XAS.

- **Insertion of Ca into MnO_2**

→ **decreases Mn oxidation state**

→ **charge transfer from Ca to Mn**

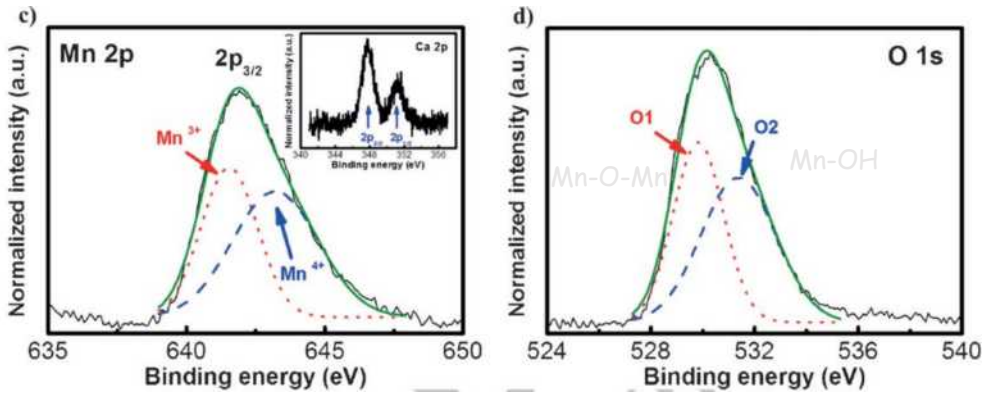

7.8 at. % Ca in MnO_2

Chemcatchem, **6**, 1684 (2014)

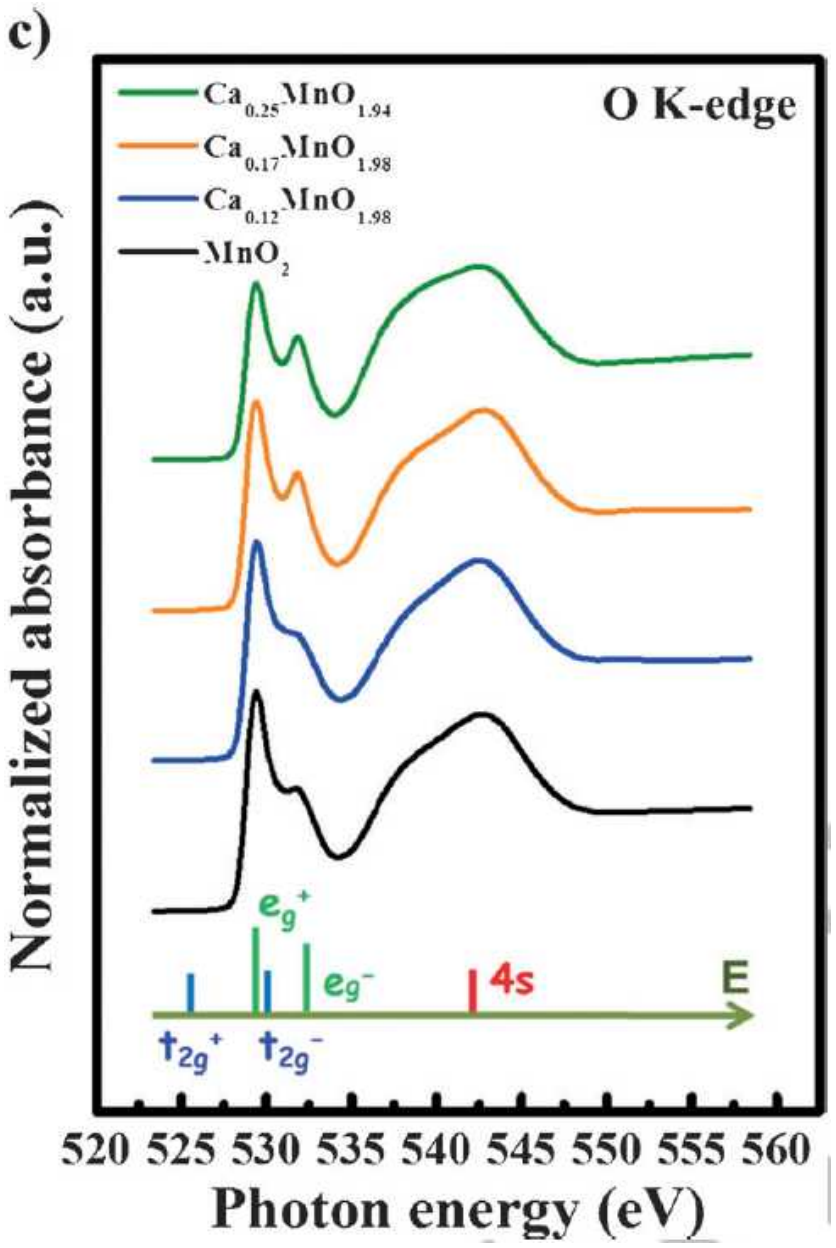

545 eV
O 1s to Mn 4sp transition
531 eV
O1s to mixing O 2p and Mn 3d transition

- **Insertion of Ca into MnO_2**

→ decreases t_{2g} ↓ and/or e_g ↑
→ increases e_g ↓
→ Mn^{III} Jahn–Teller ion arises accompanying insertion of Ca
→ Mn^{IV} ion is distorted from octahedral symmetry

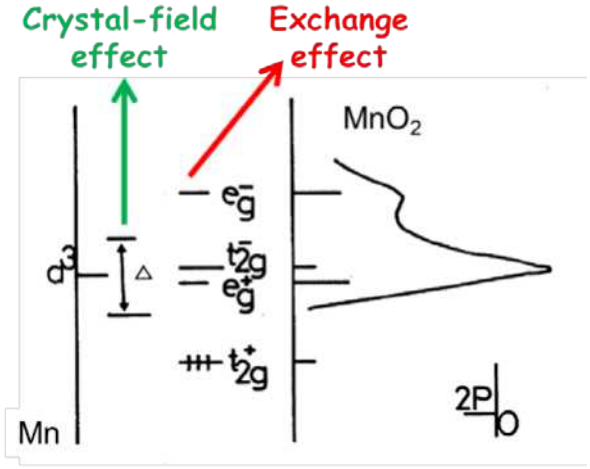

β-$SnWO_4$ Photocatalyst with Controlled Morphological Transition of Cubes to Spikecubes

Experimental process

Polyol method

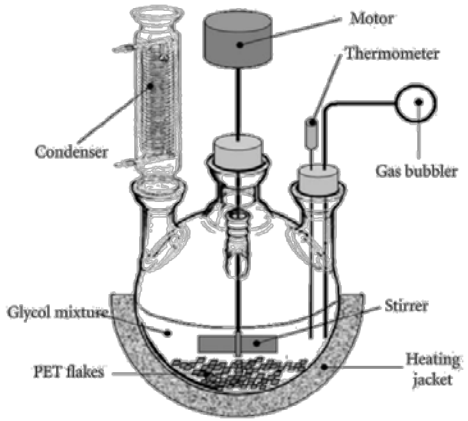

Solutions:
24mM $Na_2WO_4 \cdot 2H_2O$ in diethylene glycol
0.6 M $SnCl_2 \cdot 2H_2O$ in DI H_2O

Reaction temp. :
120°C, 160°C, 190°C

Reaction time :
60 (min)

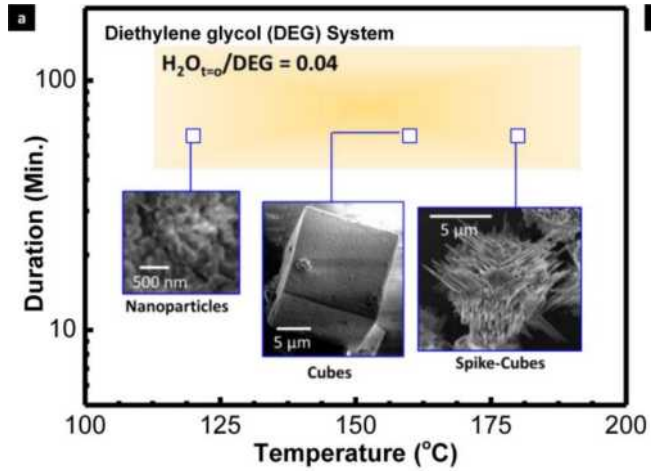

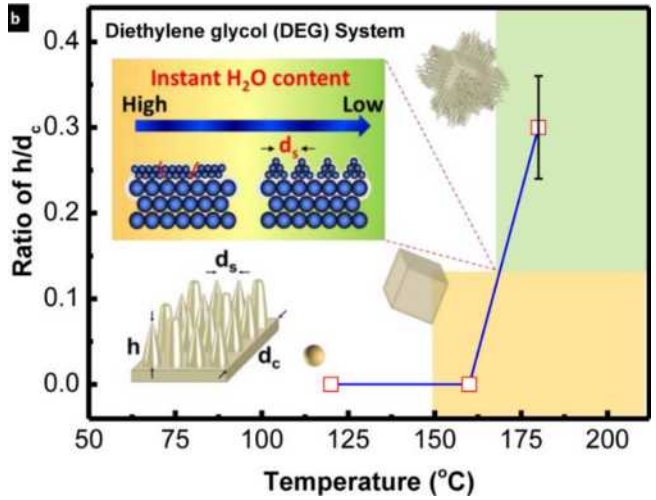

Cube vs Spikecube

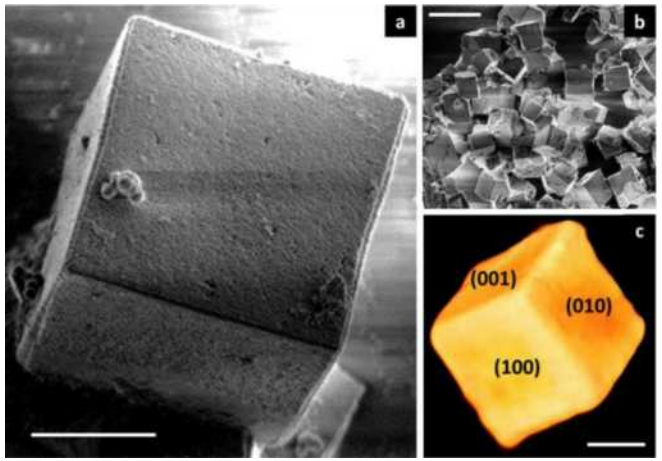

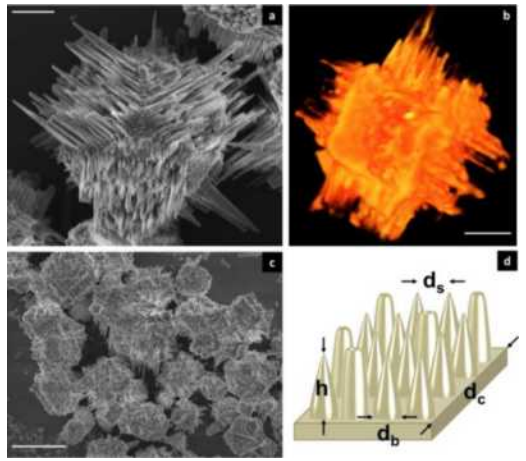

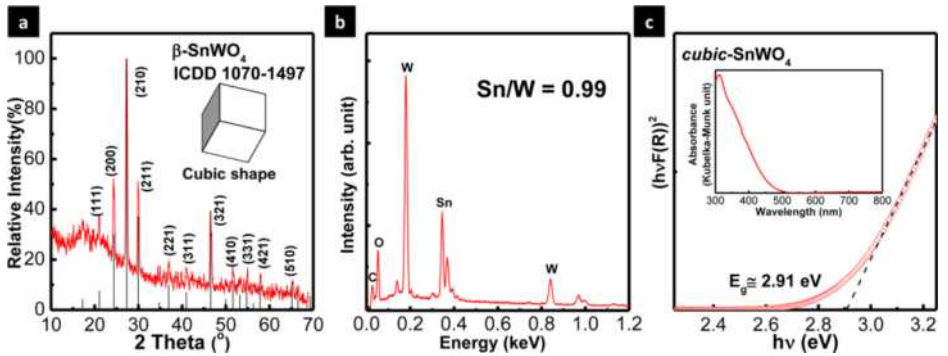

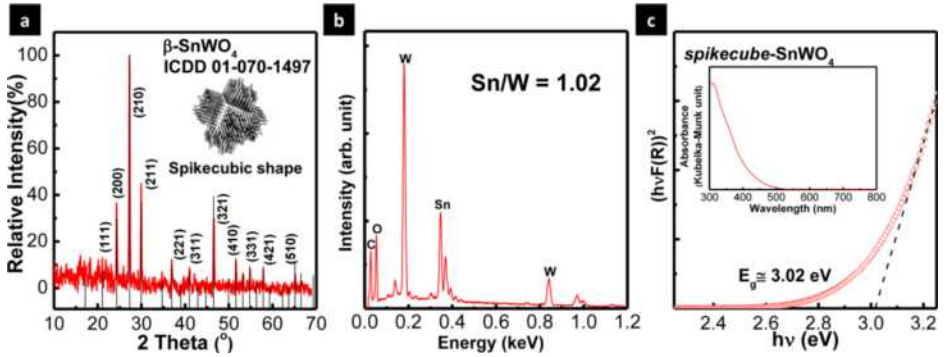

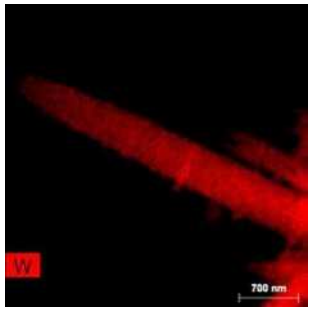

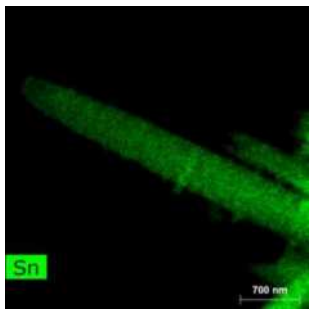

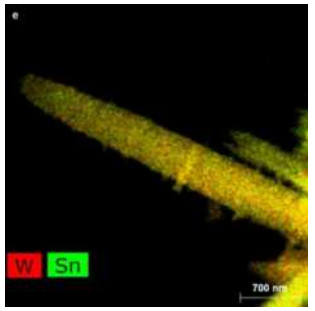

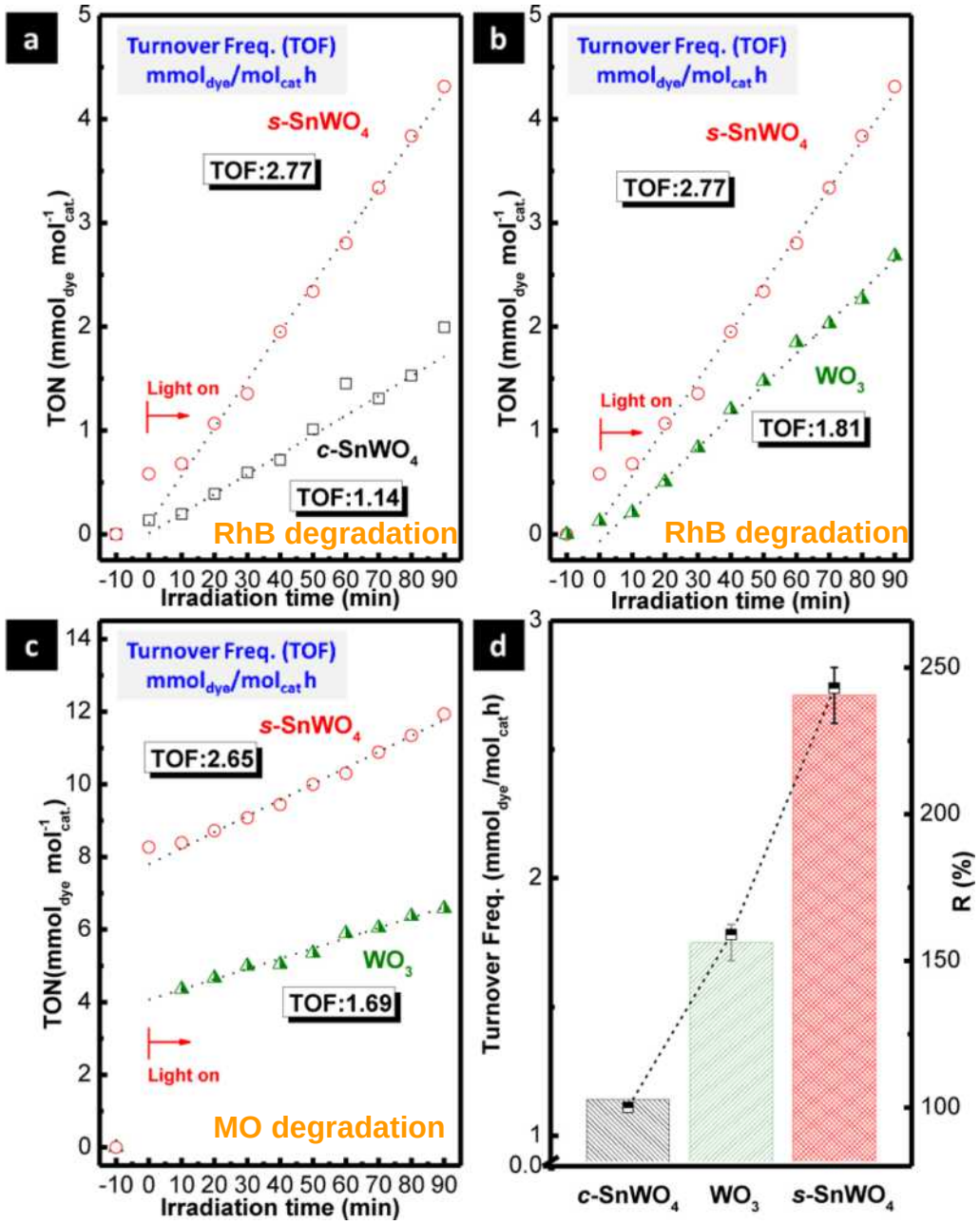

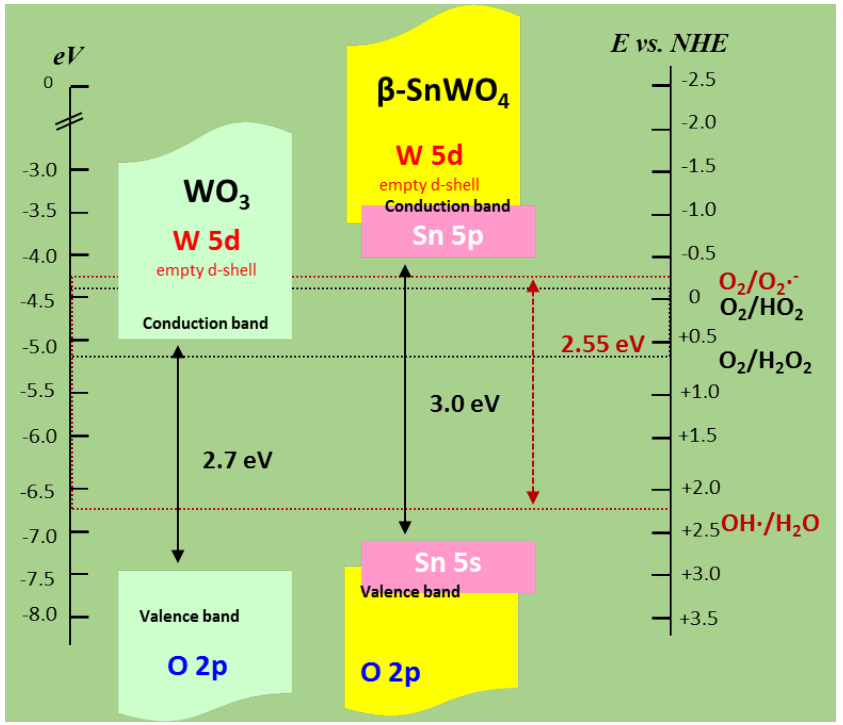

$$\text{TON} = \frac{\text{Number of reacted molecules}}{\text{Number of atoms in a photocatalyst}}$$

$$\text{TOF} = \frac{\text{TON}}{\text{reaction duration}}$$

ACS Catal., **6**, 2357 (2016)

XAS - W L_3-edge

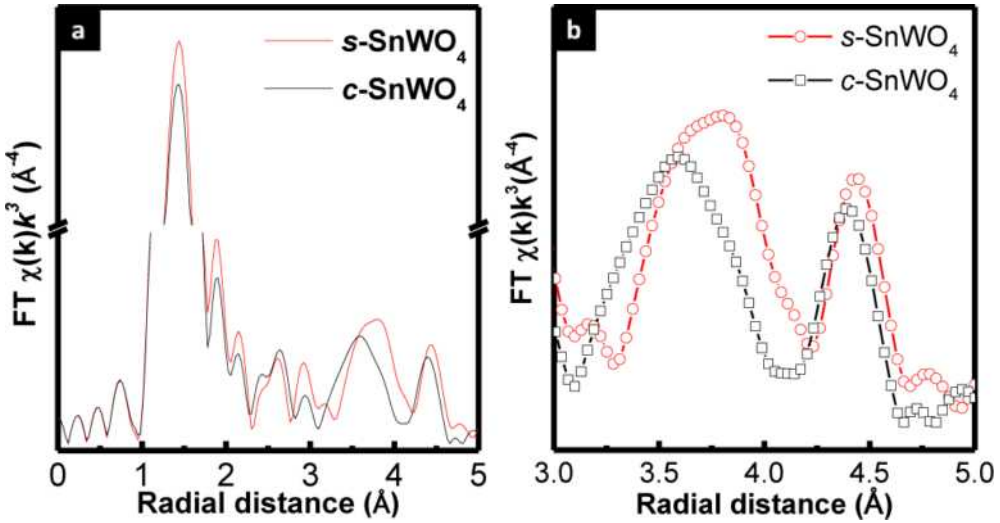

absorber-backscatter pair	$N^{a,b}$	$R^{a,b}$ (Å)	$\sigma^{2a,b}$ (Å^2)
Spikecubic Shape			
W–O	4	1.780(1)	0.0010(2)
W–Sn(1)	2.1(9)	4.050(74)	0.0067(8)
W–Sn(2)	1.6(7)	4.240(66)	0.0043(59)
W–W	0.6(3)	4.540(24)	0.0010(59)
absorber-backscatter pair	$N^{a,b}$	$R^{a,b}$ (Å)	$\sigma^{2a,b}$ (Å^2)
Cubic Shape			
W–O	4	1.780(12)	0.0010(2)
W–Sn(1)	4.0(1.7)	4.080(35)	0.0147(40)
W–Sn(2)	0.9(4)	4.250(25)	0.0029(20)
W–W	0.5(4)	4.540(31)	0.0010(59)

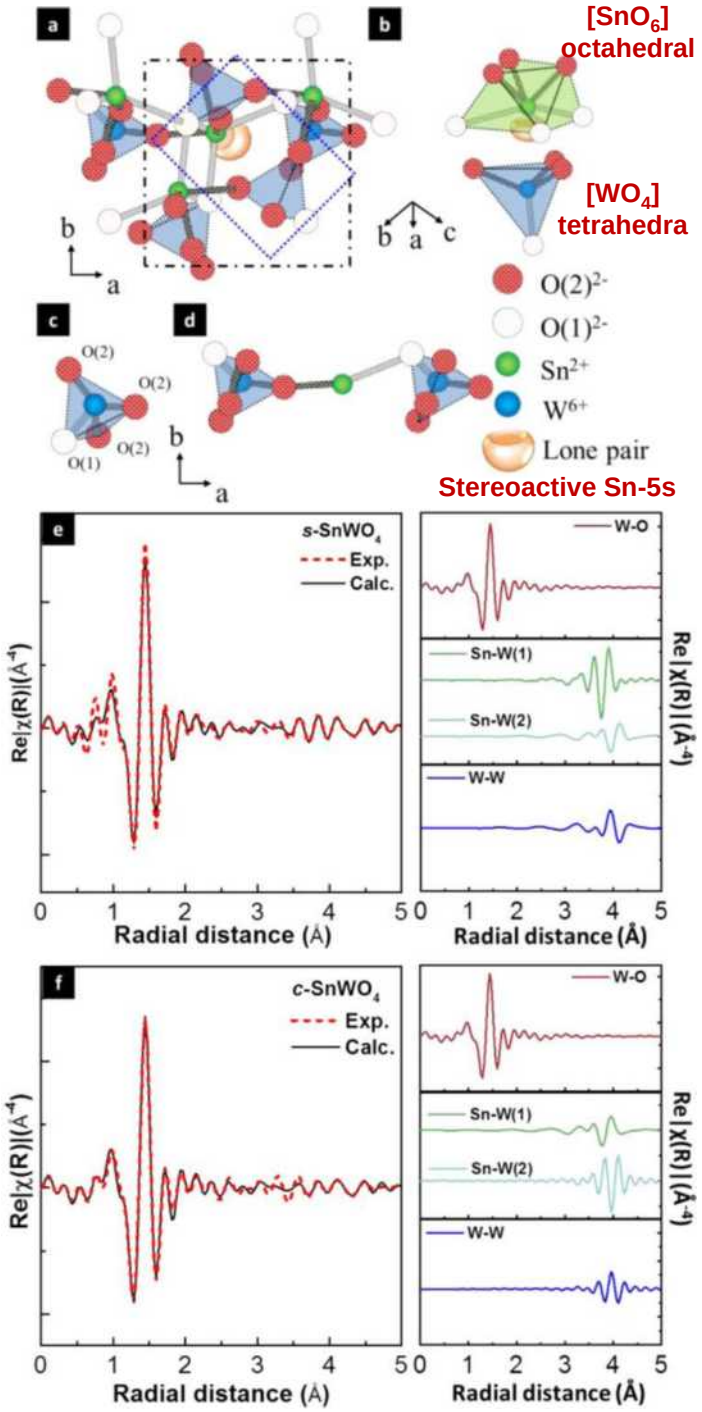

XAS - O K-edge

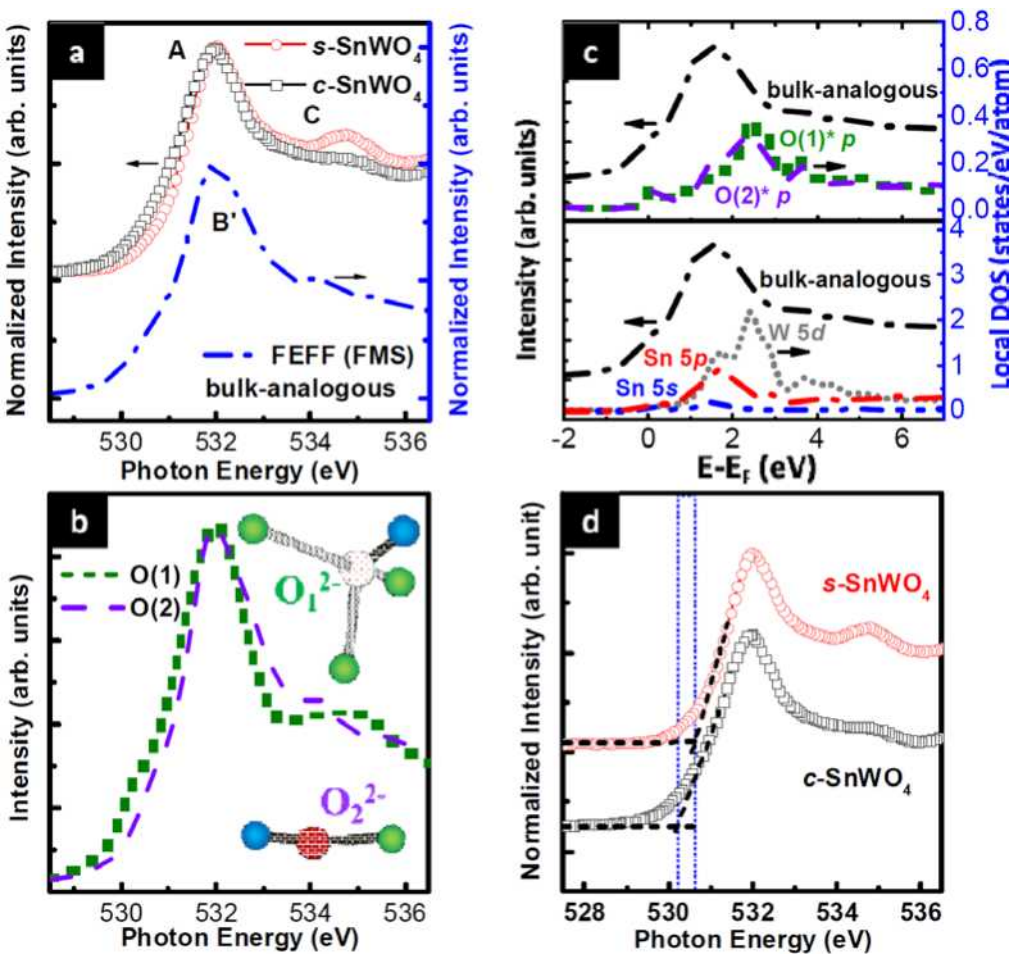

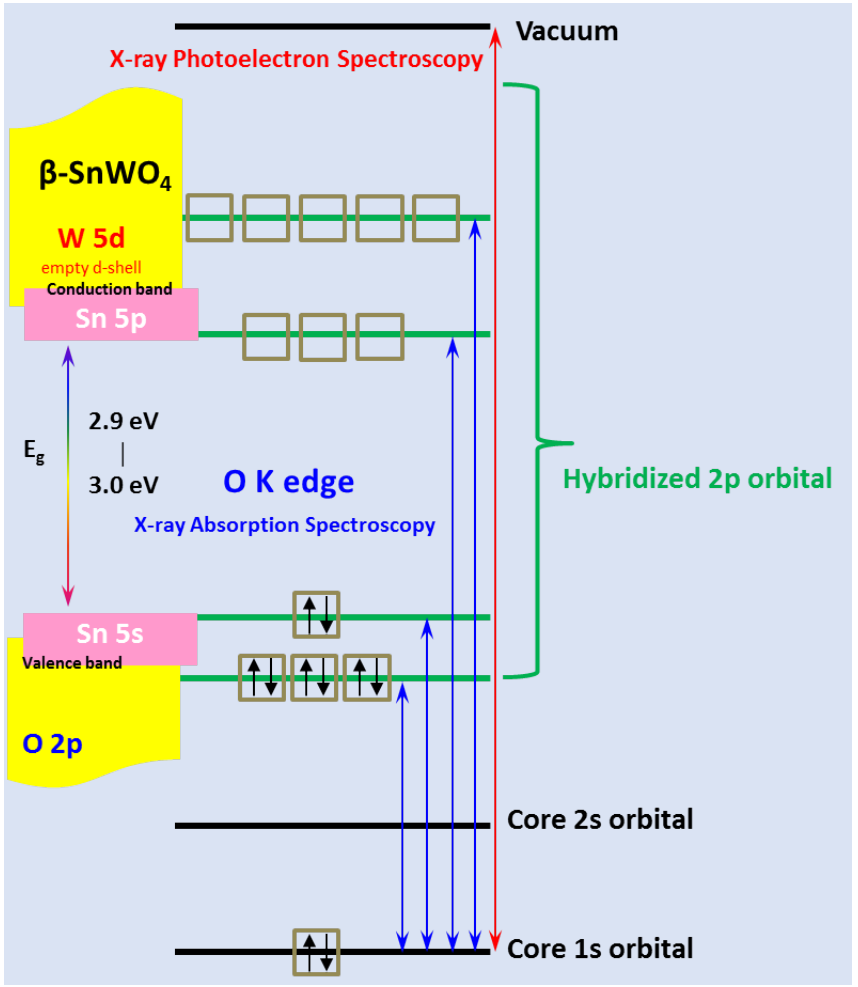

***ab initio* FMS computation**
Full multiple scattering (FMS)

Enhanced SOFT and covalence effects account for band gap opening via the energy shift of CBM !

ACS Catal., **6**, 2357 (2016)

Electronic Structure of β-$SnWO_4$

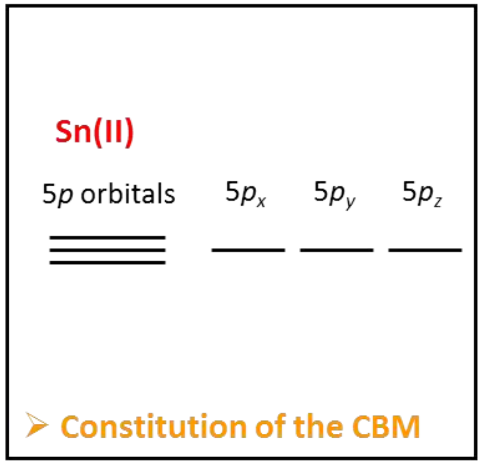

➢ Constitution of the CBM

- The **localized Sn 5s lone pair** strongly favors a **second-order Jahn-Teller (SOJT) distortion** and results in a lower symmetry structure (**distorted [SnO_6]**).
- **SOJT enables the Sn 5s and Sn $5p_z$ (CBM) states to mix in order to stabilize the antibonding state (VBM).**
- **Elevation of CBM**
- **Increased band gap**

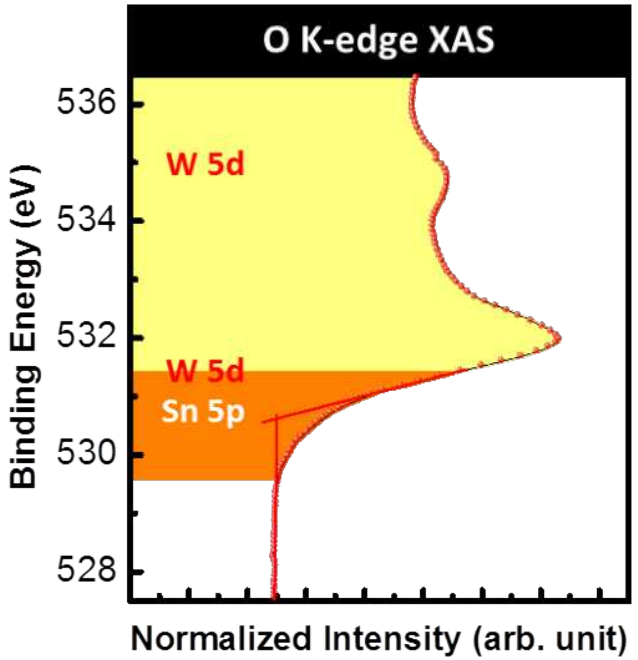

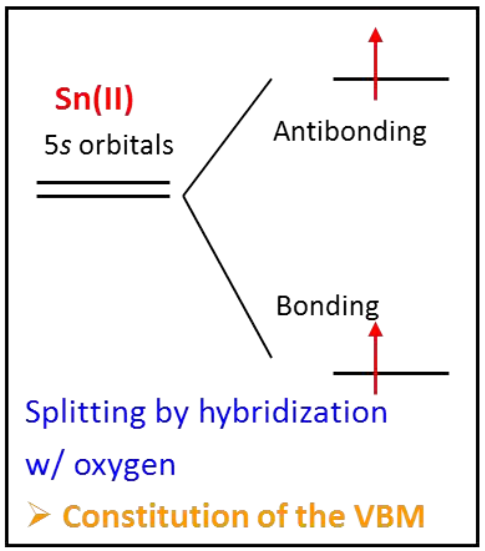

Splitting by hybridization w/ oxygen

➢ Constitution of the VBM

- One of the basic concepts of **molecular orbital theory** is that interactions where **both the bonding and antibonding levels are equally filled** have a **destabilizing influence.**

- The dependence of **hybridization** on **coordinated site symmetry**.
- **Symmetry → destabilized VBM**
- **Distortion → stabilized VBM**

Regular [SnO_6] **Irregular [SnO_6]**

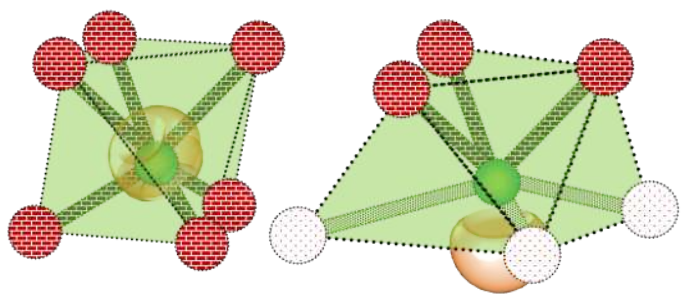

Modeling and Synthesis of CQD/H-ZnO_{1-x}/ZnO Photoanodes

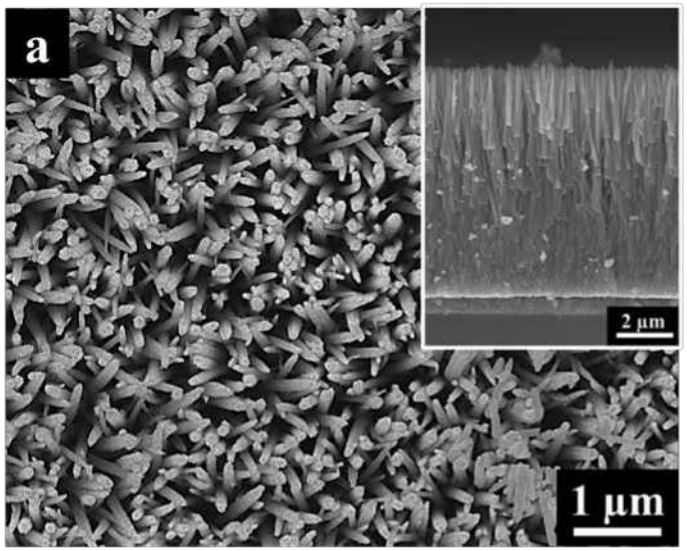

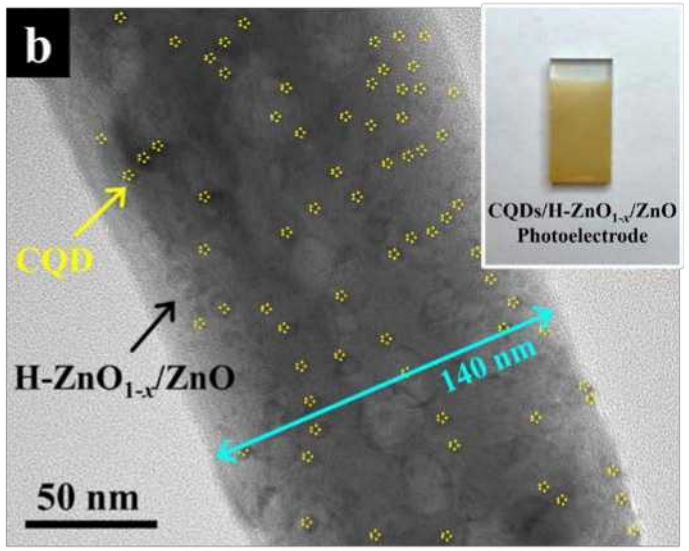

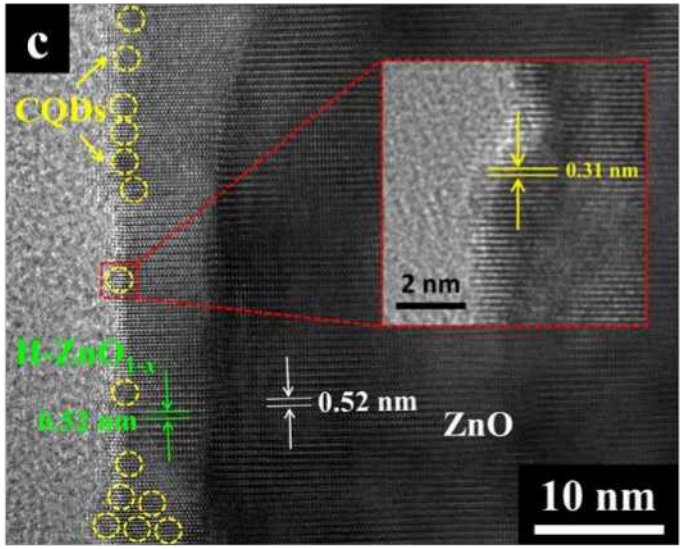

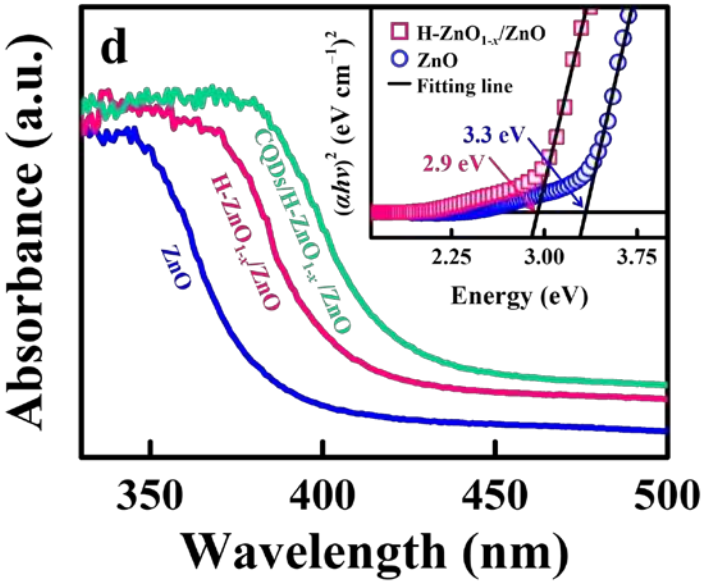

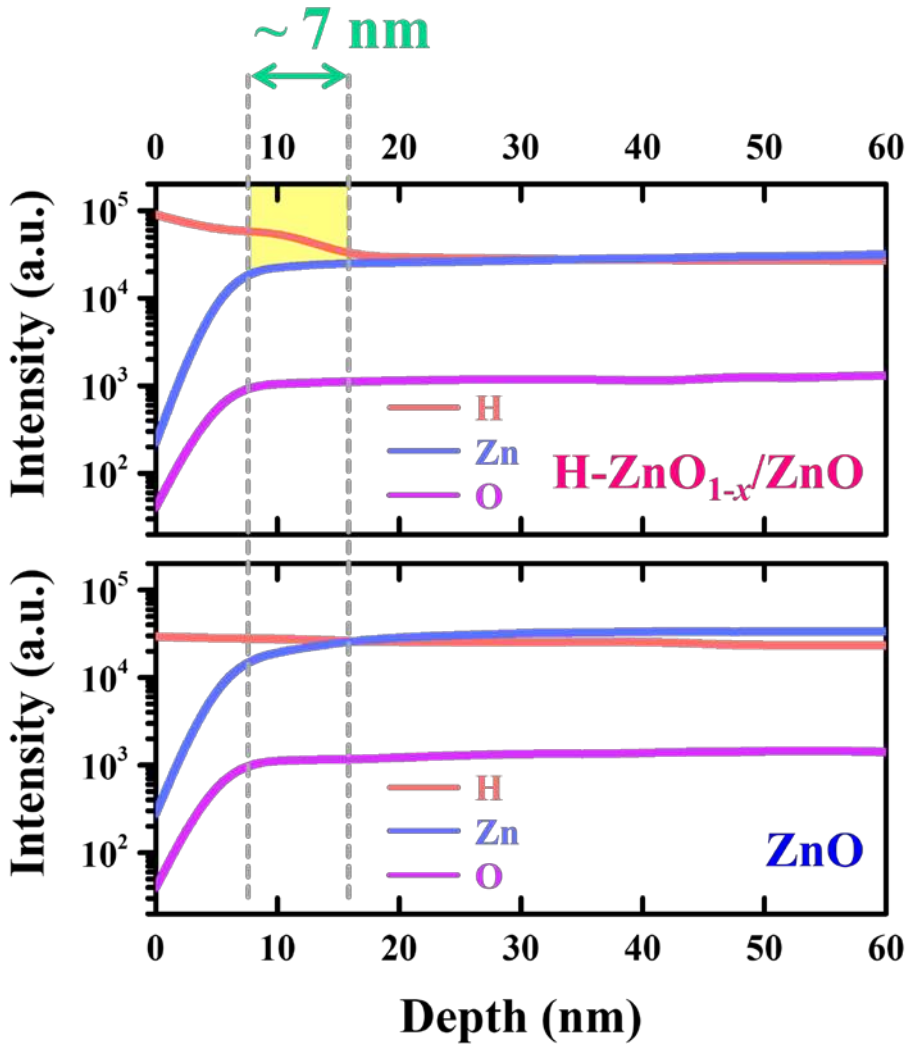
~ 7 nm
Intensity (a.u.)
H
Zn
O
H-ZnO1-x/ZnO
ZnO
Depth (nm)

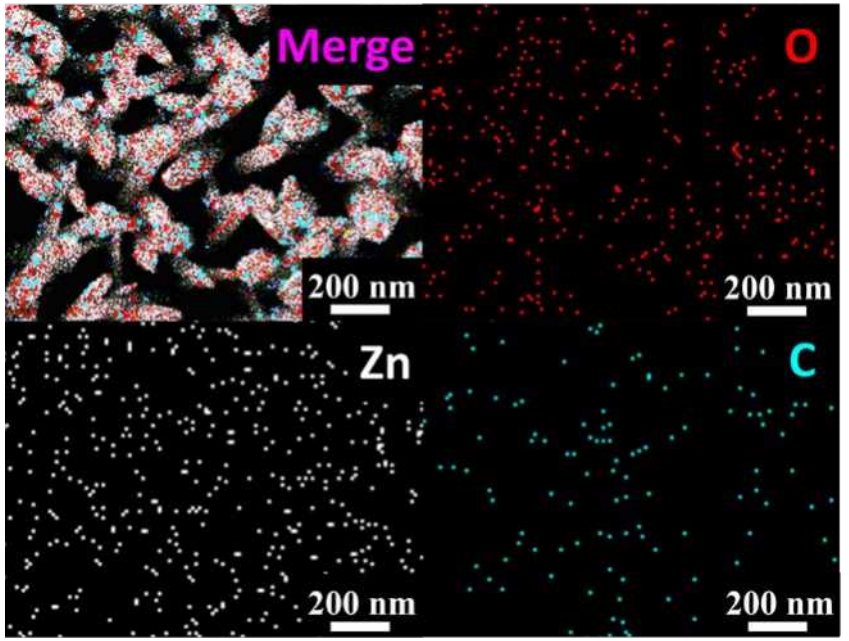
Merge
O
Zn
C
200 nm

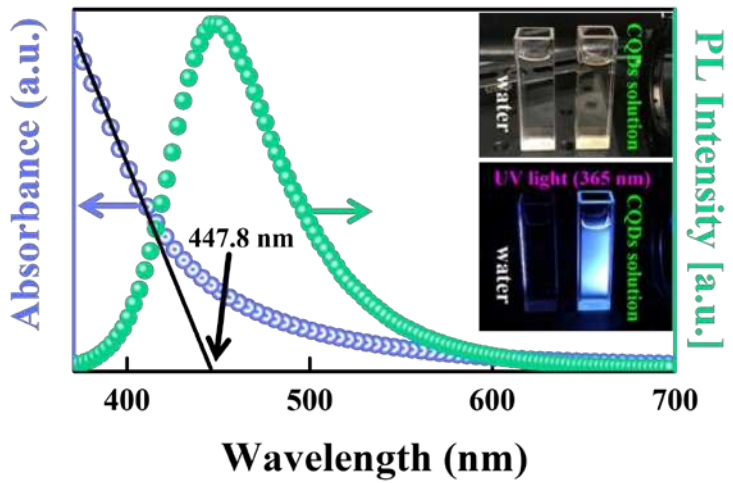
Absorbance (a.u.)
PL Intensity [a.u.]
447.8 nm
water
CQDs solution
UV light (365 nm)
Wavelength (nm)

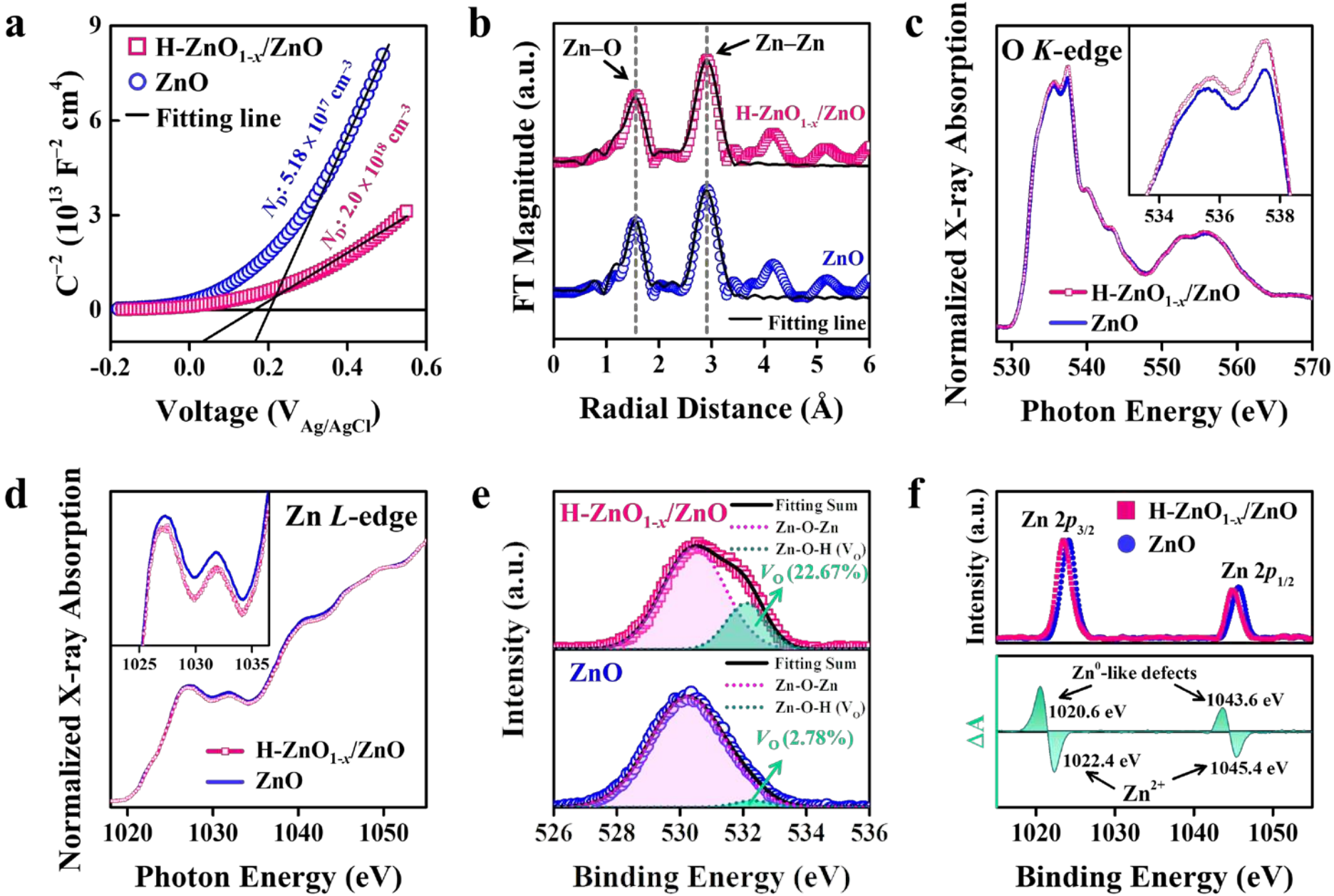
a
H-ZnO1-x/ZnO
ZnO
Fitting line
ND: 5.18 × 10^17 cm^-3
ND: 2.0 × 10^18 cm^-3
C^-2 (10^13 F^-2 cm^4)
Voltage (VAg/AgCl)
b
Zn–O
Zn–Zn
H-ZnO1-x/ZnO
ZnO
Fitting line
FT Magnitude (a.u.)
Radial Distance (Å)
c
O K-edge
H-ZnO1-x/ZnO
ZnO
Normalized X-ray Absorption
Photon Energy (eV)
d
Zn L-edge
H-ZnO1-x/ZnO
ZnO
Normalized X-ray Absorption
Photon Energy (eV)
e
H-ZnO1-x/ZnO
Fitting Sum
Zn-O-Zn
Zn-O-H (VO)
VO (22.67%)
ZnO
VO (2.78%)
Intensity (a.u.)
Binding Energy (eV)
f
Zn 2p3/2
Zn 2p1/2
H-ZnO1-x/ZnO
ZnO
Zn0-like defects
1020.6 eV
1022.4 eV
1043.6 eV
1045.4 eV
Zn2+
ΔA
Intensity (a.u.)
Binding Energy (eV)

Summary of the FT-EXAFS fitting data for H-ZnO_{1-x}/ZnO and ZnO.

Sample	Path	CN^a	R (Å)^b	σ^2 (10^{-3}Å^2)^c	ΔE_0 (eV)^d
ZnO	Zn-O	3.6	1.9647	6.8	1.9221
	Zn-Zn	11.0	3.2285	10	-1.2996
H-ZnO_{1-x}/ZnO	Zn-O	3.2	1.9647	7.0	1.9888
	Zn-Zn	10.9	3.2285	11	-1.3873

*The effective parameters for EXAFS fitting includes coordination number (CN)^a, interatomic distance (R)^b, Debye-Waller factor (σ^2)^c, and potential correction ΔE_0^{d}. Typically, ZnO with wurtzite structure was used as the model of EXAFS fitting, where Zn is coordinated with 4 O atoms (Zn-O path, first shell) and second near-neighbor 12 Zn atoms (Zn-Zn, second shell). The k^3-weight EXAFS data was fit in k-space in the region of 2.0-12.5 Å^{-1} with Hanning-shaped window. The R-space with the range of 1.0-3.6 Å to fit all the EXAFS data. All samples were fit simultaneously, yielding a normalized sum of squared residuals [R-factor = $\sum$(data-fit)^2 /$\sum$data^2) of 0.02 (2%)]. The amplitude reduction factor S_0^2 is defined at 1 to fit all samples for Zn K-edge.

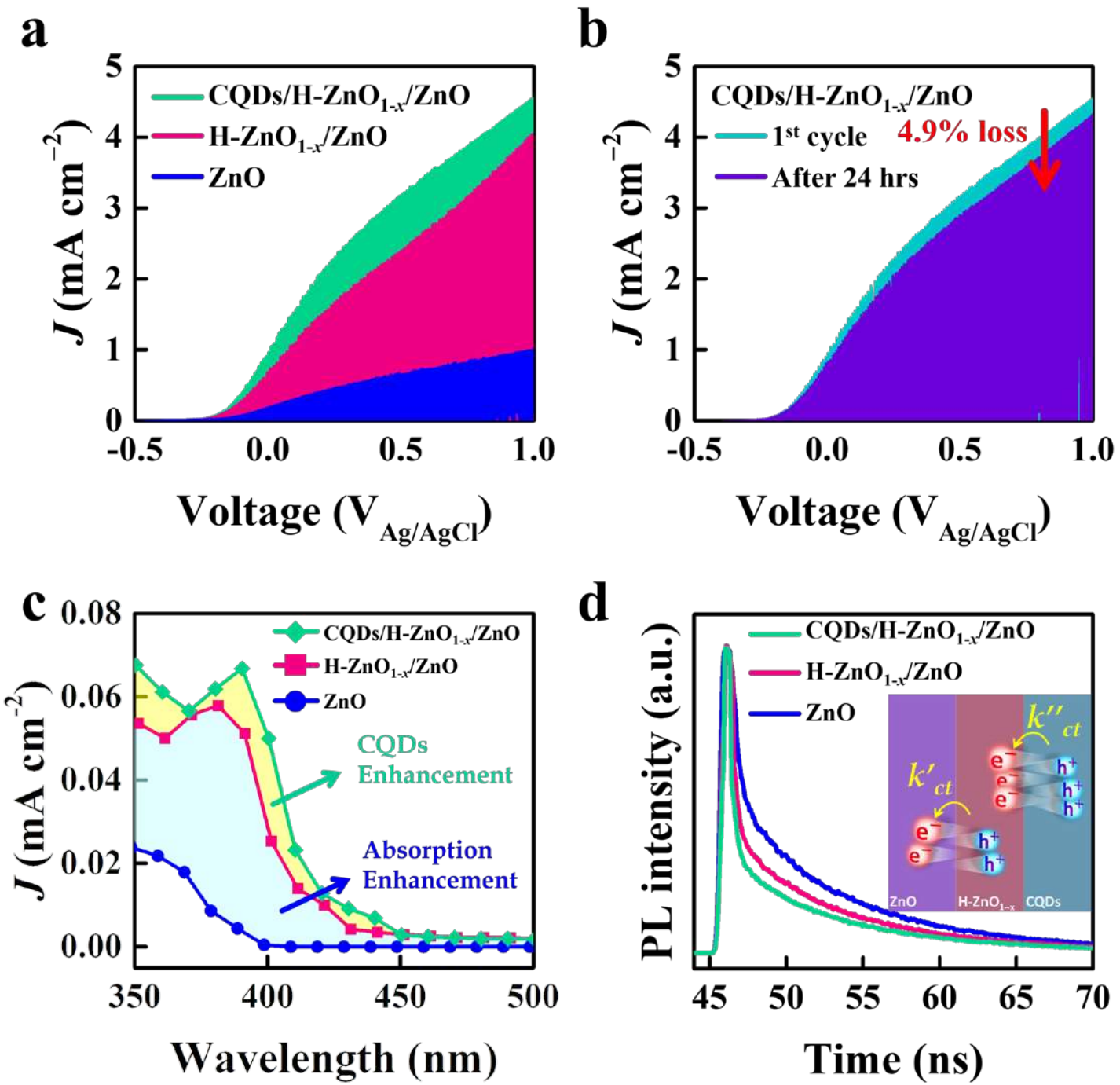
a
CQDs/H-ZnO1-x/ZnO
H-ZnO1-x/ZnO
ZnO
J (mA cm-2)
Voltage (VAg/AgCl)
b
CQDs/H-ZnO1-x/ZnO
1st cycle
4.9% loss
After 24 hrs
J (mA cm-2)
Voltage (VAg/AgCl)
c
CQDs/H-ZnO1-x/ZnO
H-ZnO1-x/ZnO
ZnO
CQDs Enhancement
Absorption Enhancement
J (mA cm-2)
Wavelength (nm)
d
CQDs/H-ZnO1-x/ZnO
H-ZnO1-x/ZnO
ZnO
k'ct
k''ct
ZnO
H-ZnO1-x
CQDs
PL intensity (a.u.)
Time (ns)

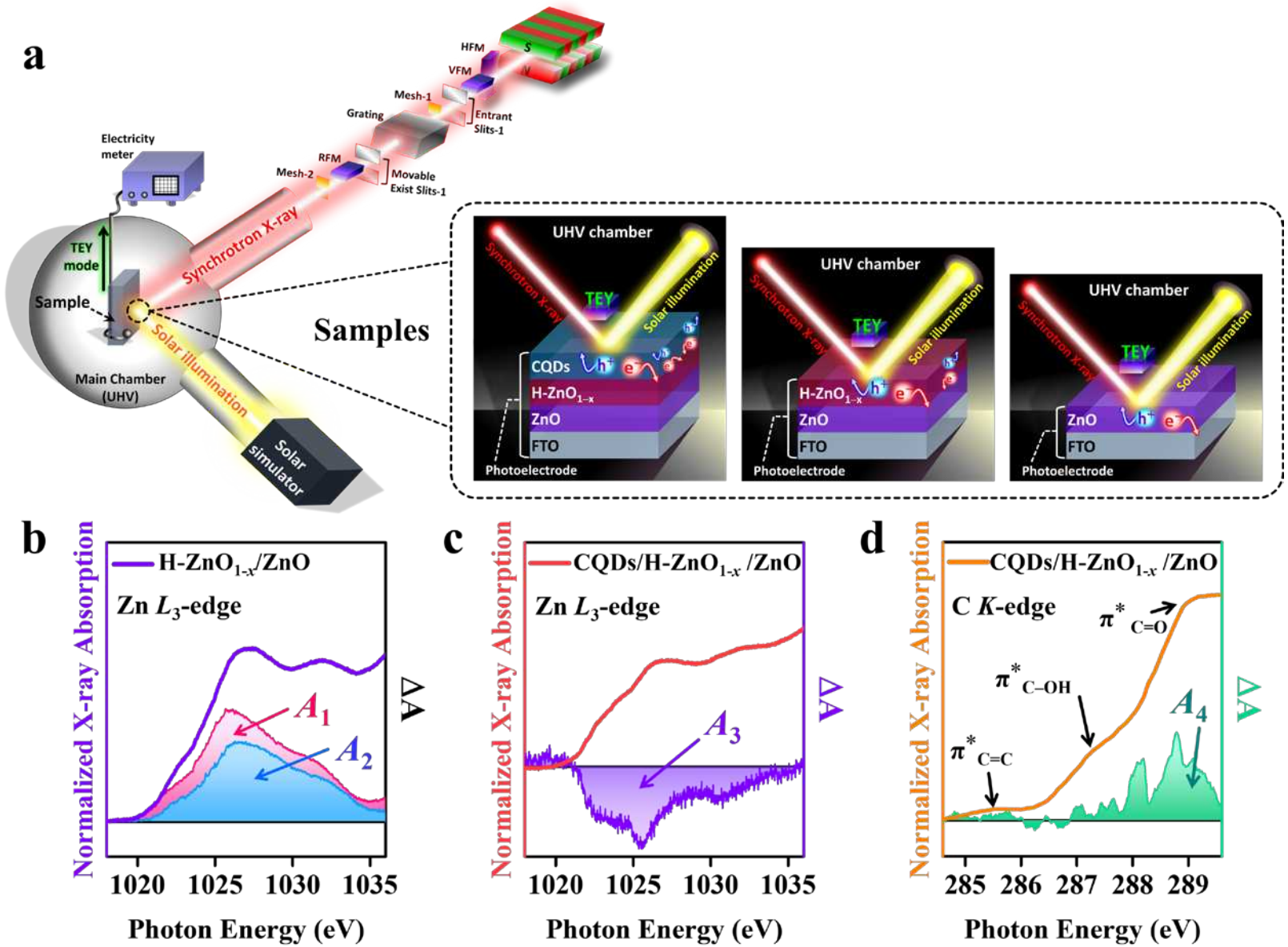
a
HFM
VFM
Mesh-1
Grating
Entrant Slits-1
RFM
Mesh-2
Movable Exist Slits-1
Electricity meter
TEY mode
Sample
Synchrotron X-ray
Solar illumination
Main Chamber (UHV)
Solar simulator
Samples
UHV chamber
TEY
CQDs
H-ZnO1-x
ZnO
FTO
Photoelectrode
b
H-ZnO1-x/ZnO
Zn L3-edge
A1
A2
ΔA
Normalized X-ray Absorption
Photon Energy (eV)
c
CQDs/H-ZnO1-x /ZnO
Zn L3-edge
A3
d
C K-edge
π* C=O
π* C–OH
π* C=C
A4

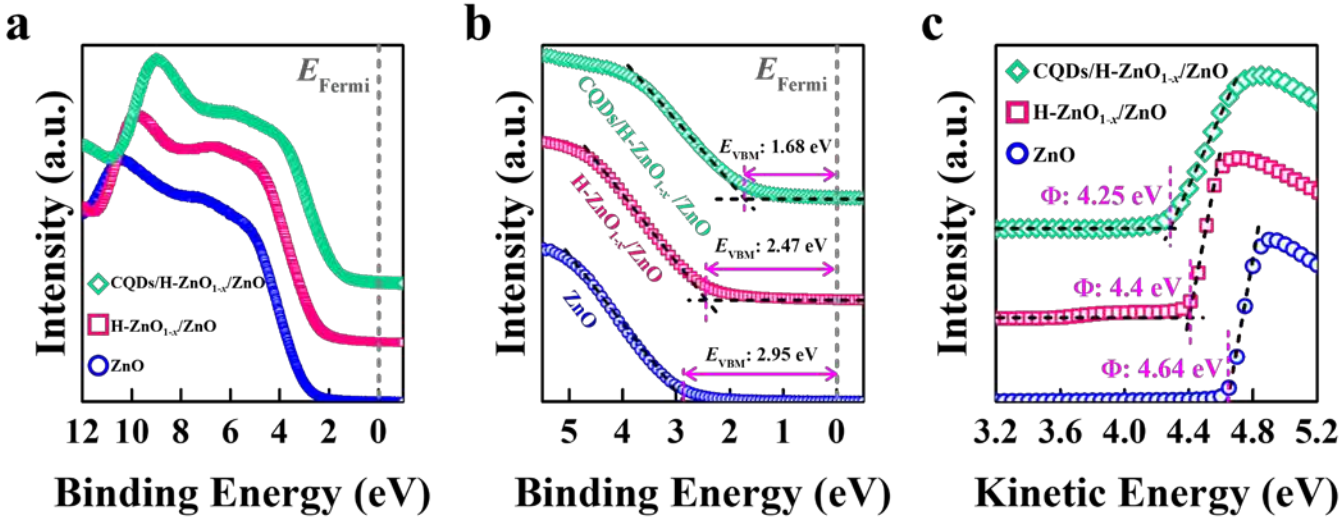

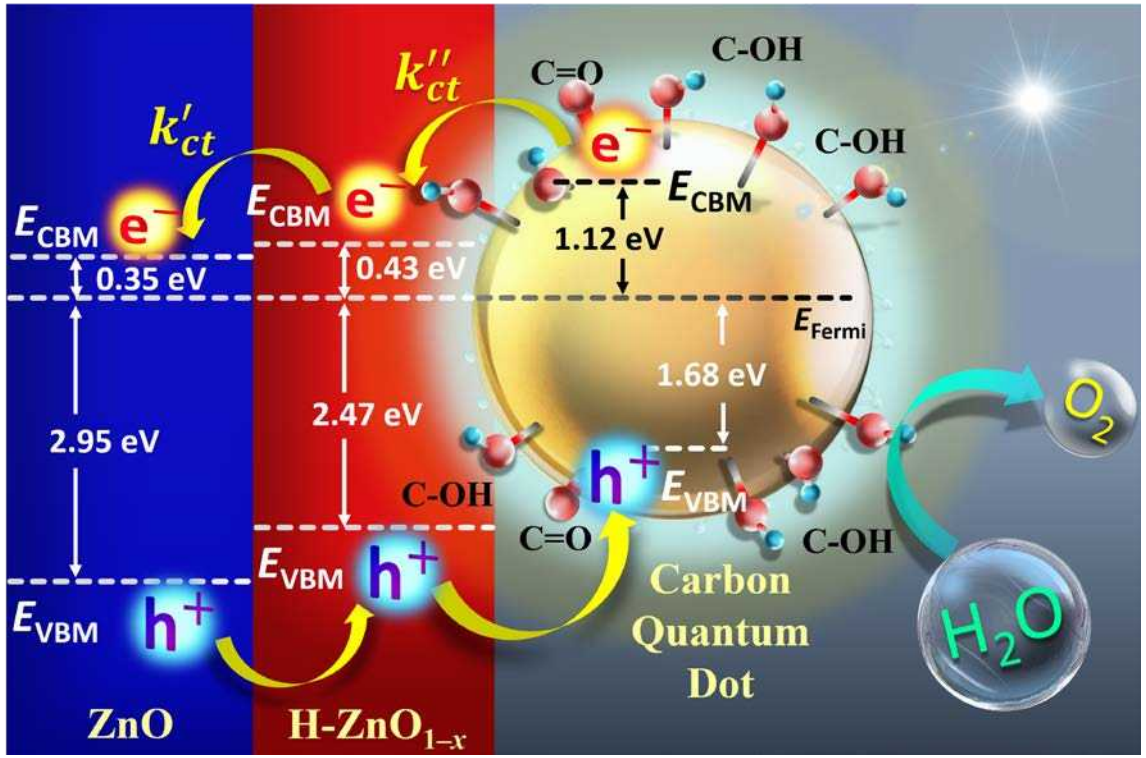

Appl. Catal. B: Environ., **285**, 119846 (2021)

Boron-Triggered Electronic-Structure Reorientation of Os for hydrogen evolution reaction (HER)

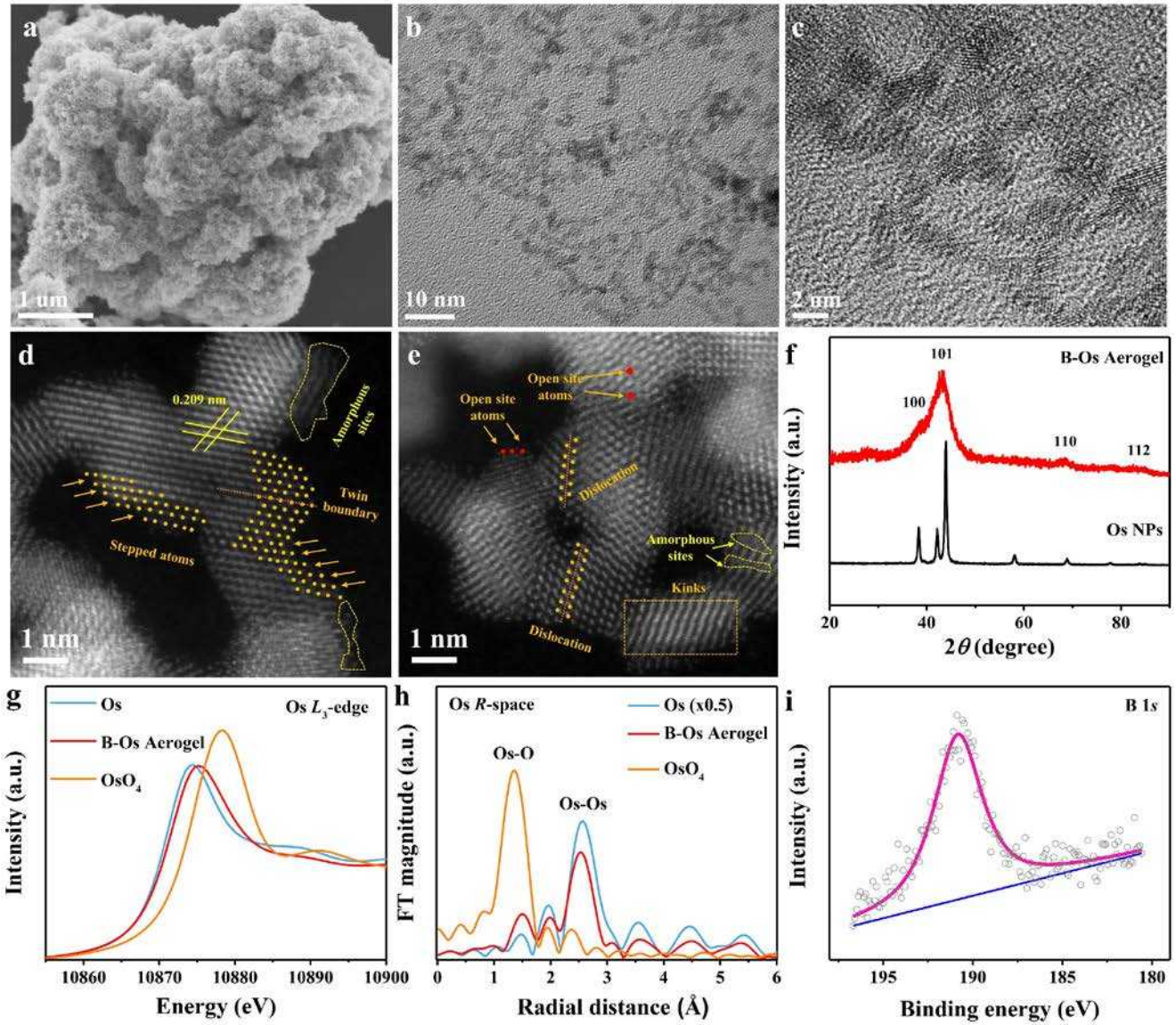

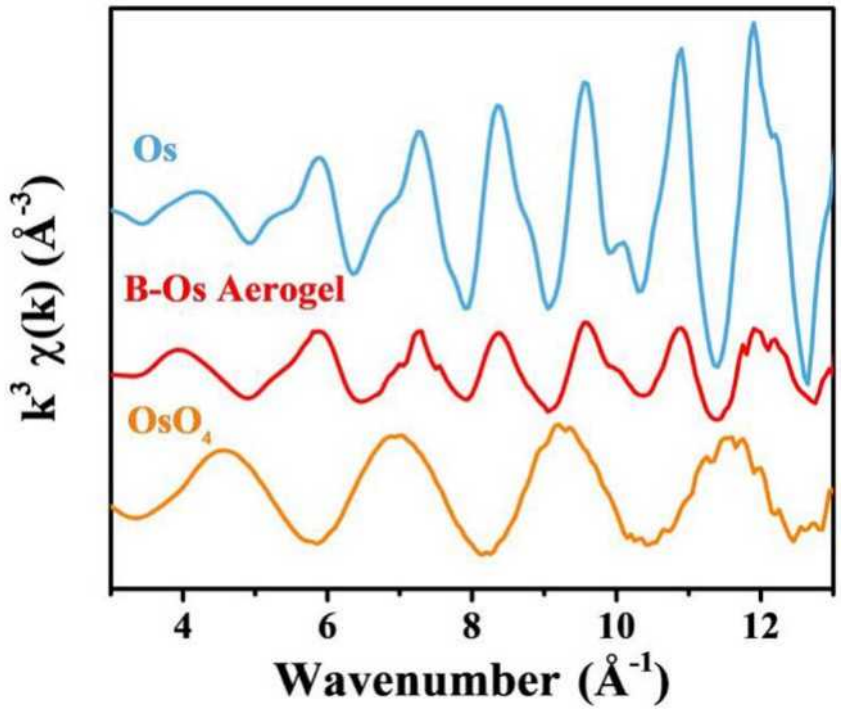

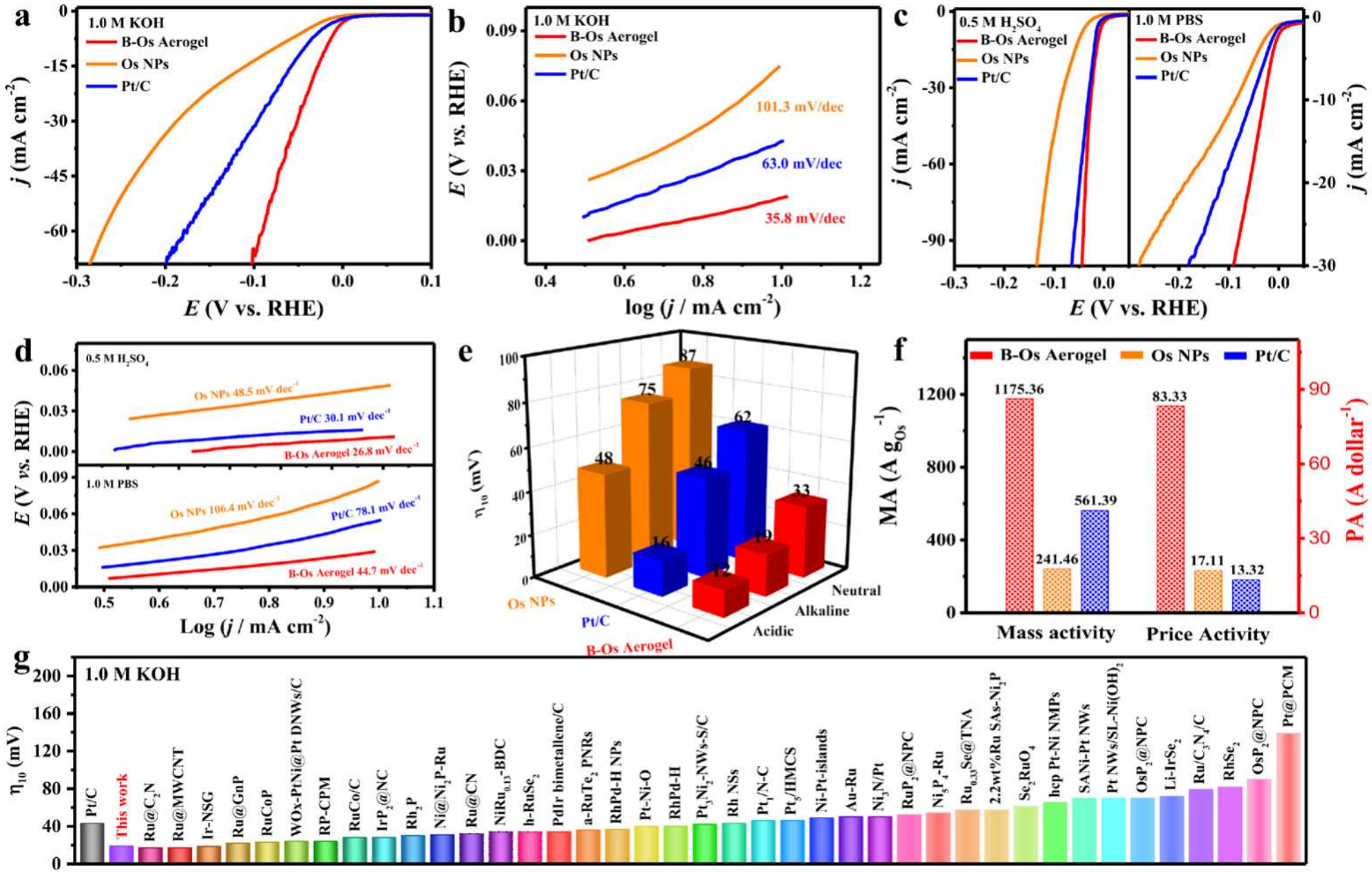
a
1.0 M KOH
B-Os Aerogel
Os NPs
Pt/C
j (mA cm-2)
E (V vs. RHE)
b
1.0 M KOH
B-Os Aerogel
Os NPs
Pt/C
101.3 mV/dec
63.0 mV/dec
35.8 mV/dec
E (V vs. RHE)
log (j / mA cm-2)
c
0.5 M H2SO4
1.0 M PBS
B-Os Aerogel
Os NPs
Pt/C
j (mA cm-2)
E (V vs. RHE)
d
0.5 M H2SO4
Os NPs 48.5 mV dec-1
Pt/C 30.1 mV dec-1
B-Os Aerogel 26.8 mV dec-1
1.0 M PBS
Os NPs 106.4 mV dec-1
Pt/C 78.1 mV dec-1
B-Os Aerogel 44.7 mV dec-1
E (V vs. RHE)
Log (j / mA cm-2)
e
η10 (mV)
Os NPs
Pt/C
B-Os Aerogel
Neutral
Alkaline
Acidic
f
B-Os Aerogel
Os NPs
Pt/C
MA (A gOs-1)
PA (A dollar-1)
1175.36
241.46
561.39
83.33
17.11
13.32
Mass activity
Price Activity
g
1.0 M KOH
η10 (mV)
Pt/C
This work
Ru@C2N
Ru@MWCNT
Ir-NSG
Ru@GnP
RuCoP
WOx-PtNi@Pt DNWs/C
RP-CPM
RuCo/C
IrP2@NC
Rh2P
Ni@Ni2P-Ru
Ru@CN
NiRu0.13-BDC
h-RuSe2
PdIr bimetallene/C
a-RuTe2 PNRs
RhPd-H NPs
Pt-Ni-O
RhPd-H
Pt3Ni2-NWs-S/C
Rh NSs
Pt1/N-C
Pt5/HMCS
Ni-Pt-islands
Au-Ru
Ni3N/Pt
RuP2@NPC
Ni5P4-Ru
Ru0.33Se@TNA
2.2wt%Ru SAs-Ni2P
Se2RuO4
hcp Pt-Ni NMPs
SANi-Pt NWs
Pt NWs/SL-Ni(OH)2
OsP2@NPC
Li-IrSe2
Ru/C3N4/C
RhSe2
OsP2@NPC
Pt@PCM

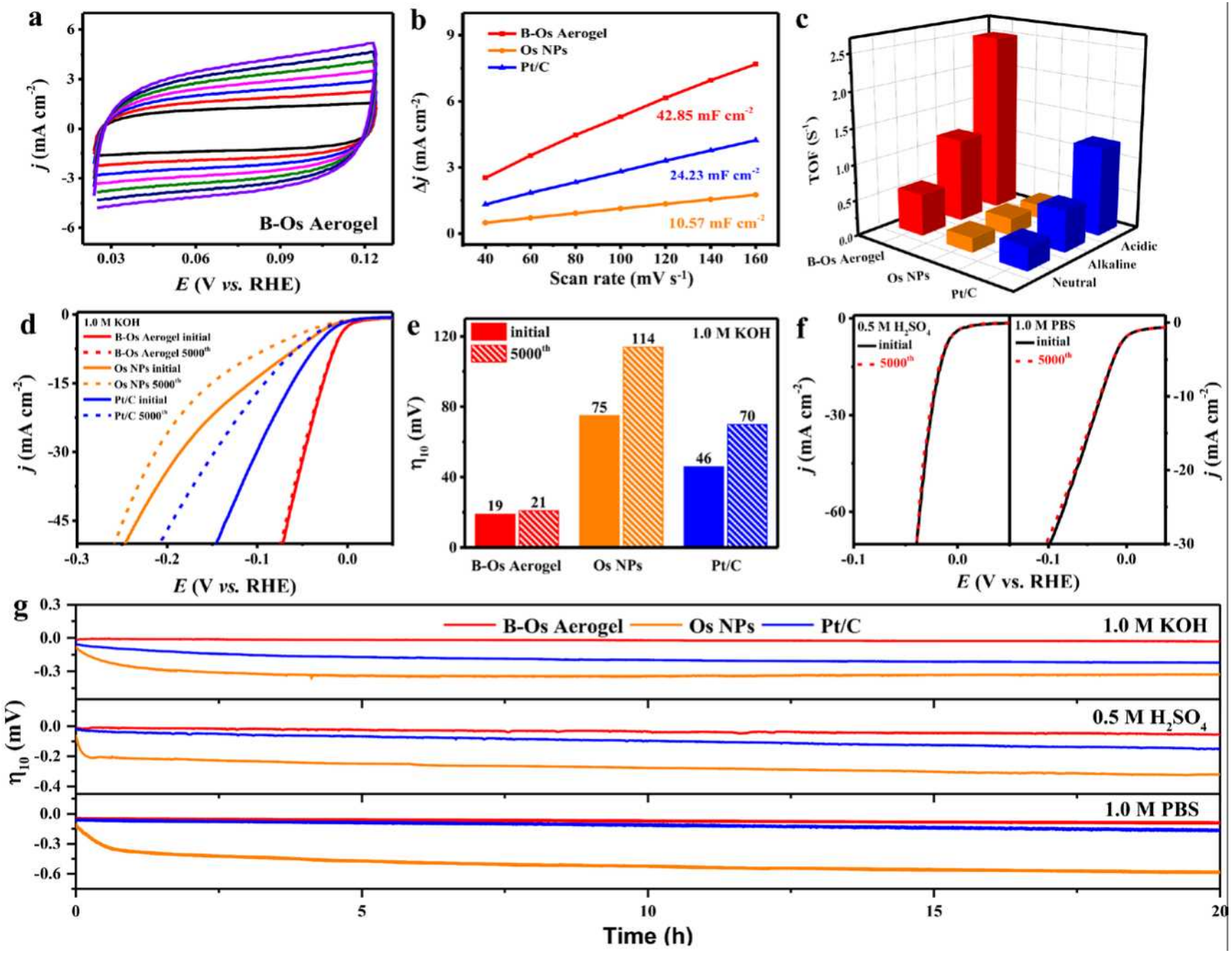
a
B-Os Aerogel
E (V vs. RHE)
b
B-Os Aerogel
Os NPs
Pt/C
42.85 mF cm-2
24.23 mF cm-2
10.57 mF cm-2
Scan rate (mV s-1)
c
TOF (S-1)
B-Os Aerogel
Os NPs
Pt/C
Acidic
Alkaline
Neutral
d
1.0 M KOH
B-Os Aerogel initial
B-Os Aerogel 5000th
Os NPs initial
Os NPs 5000th
Pt/C initial
Pt/C 5000th
E (V vs. RHE)
e
initial
5000th
1.0 M KOH
19
21
75
114
46
70
B-Os Aerogel
Os NPs
Pt/C
f
0.5 M H2SO4
initial
5000th
1.0 M PBS
initial
5000th
E (V vs. RHE)
g
B-Os Aerogel
Os NPs
Pt/C
1.0 M KOH
0.5 M H2SO4
1.0 M PBS
Time (h)

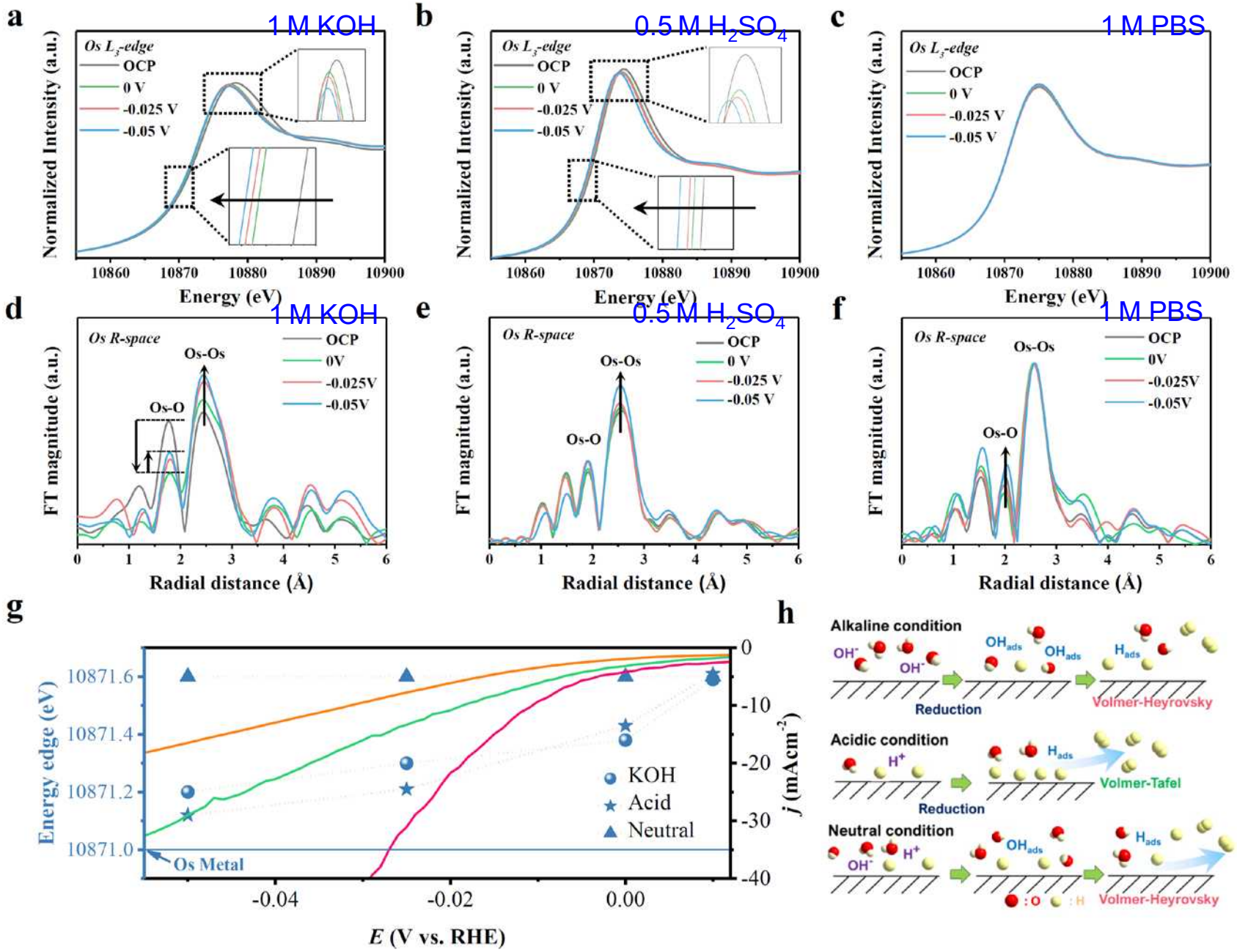

Nat. Commun., **13**, 1143 (2022)

α-CrOOH-modulated Co@CoMoOx for overall water splitting

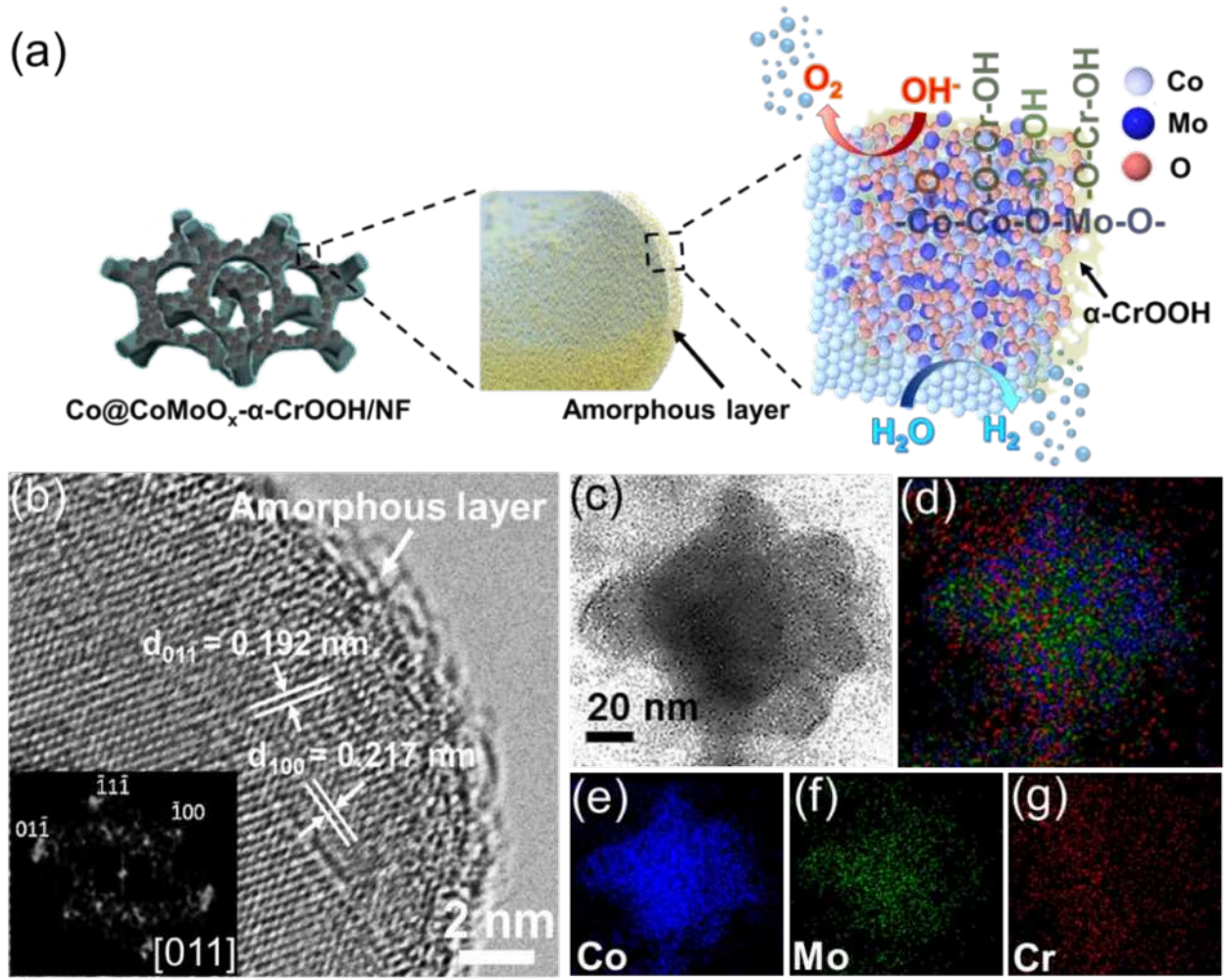

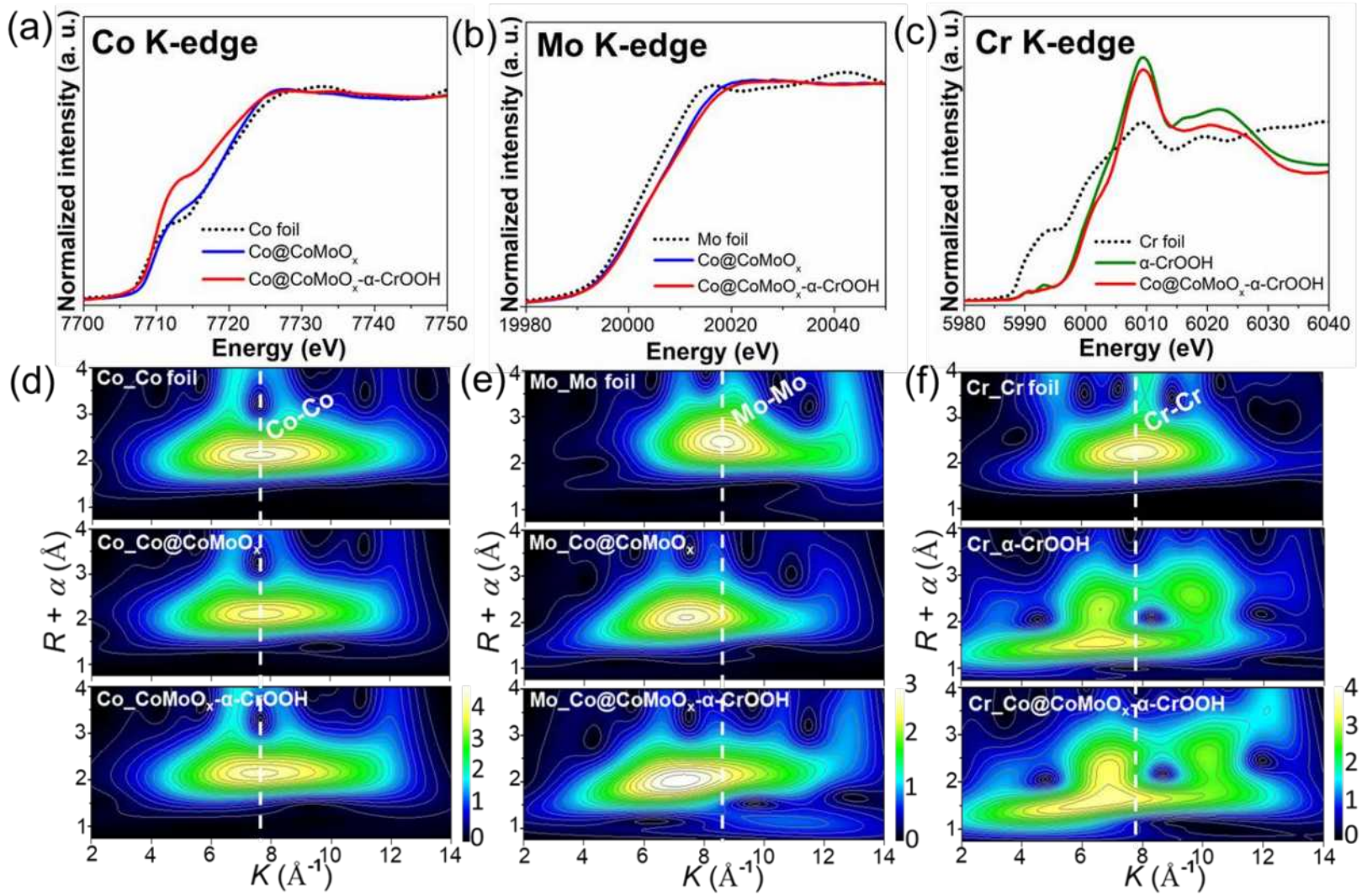

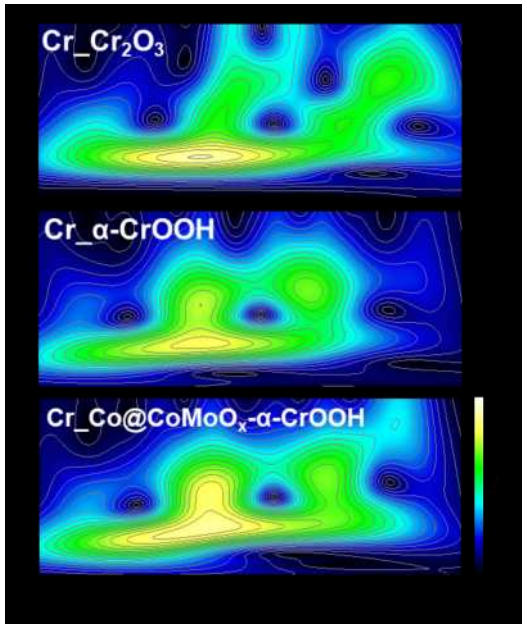

Co : Low oxidation
Mo : High oxidation
Cr : distorted octahedral symmetry

Wavelet transform
Maxi. Intensity : Mo-Co-O interaction

Chem. Eng. J., ***452***, 139715 (2023)

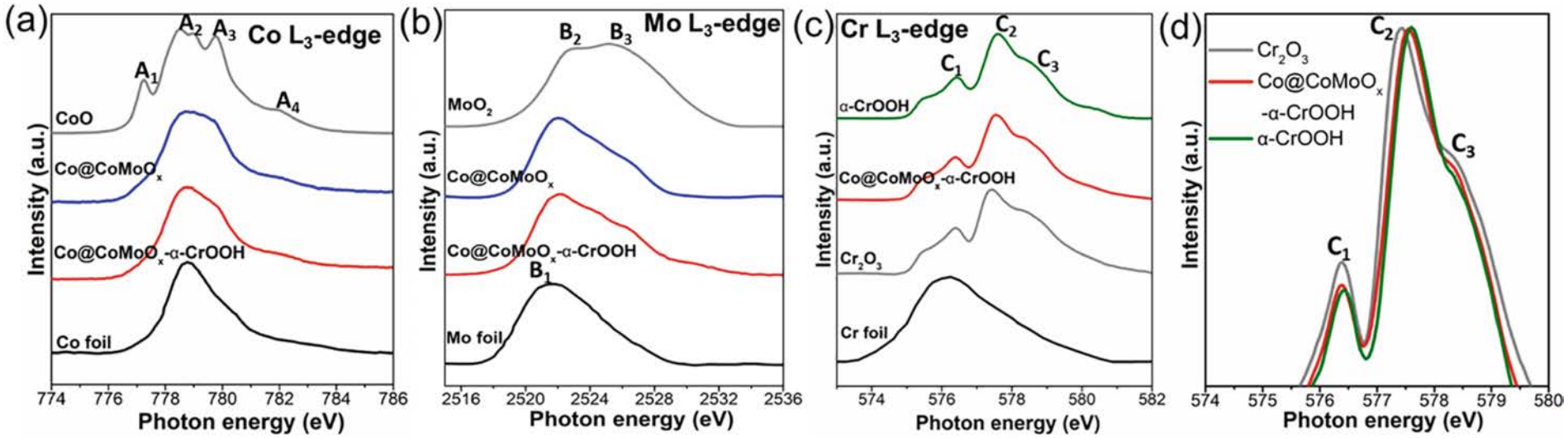

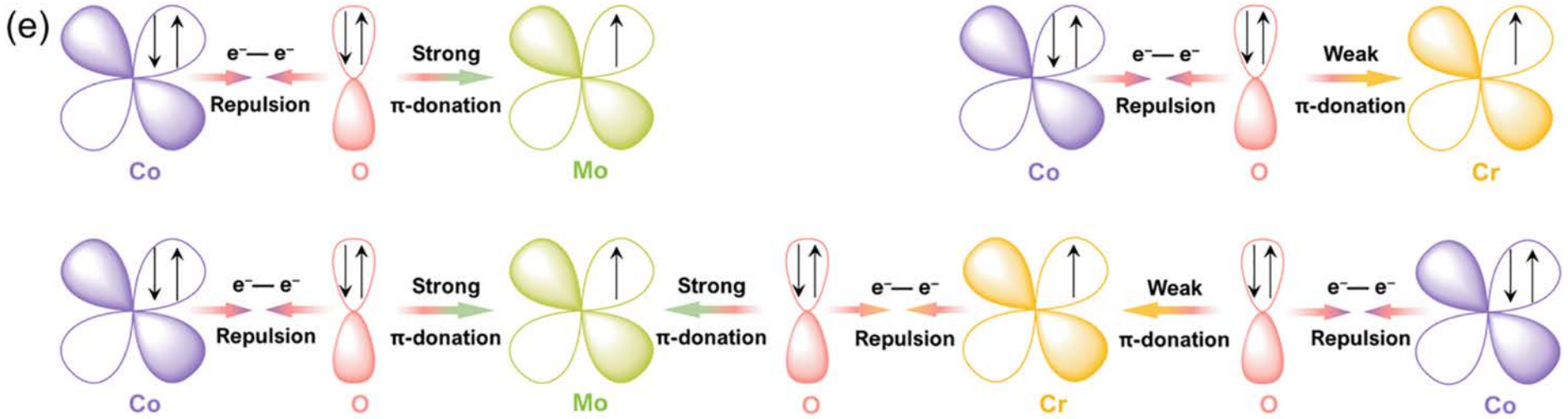

Co : Co^0 + Co^{2+}
Mo : High oxidation
Cr : α-CrOOH

B2 : 2p-4d t_{2g}
B3 : 2p-4d e_g

Electronic coupling /interaction
→ More e^- to Mo
→ redistribution

Co^{2+} : t_{2g} $3d^7$ ($t_{2g}^6 e_g^1$) orbital ; fully occupied
Cr^{3+}, Mo^{4+} and Mo^{6+} : $3d^3$ ($t_{2g}^3 e_g^0$), $4d^2$ ($t_{2g}^2 e_g^0$) and $4d^0$ ($t_{2g}^0 e_g^0$)
Cr & Mo : unpaired e^- in t_{2g}
↑electron donation of π-symmetry → e^- from Co to **Cr and Mo**

Chem. Eng. J., ***452***, 139715 (2023)

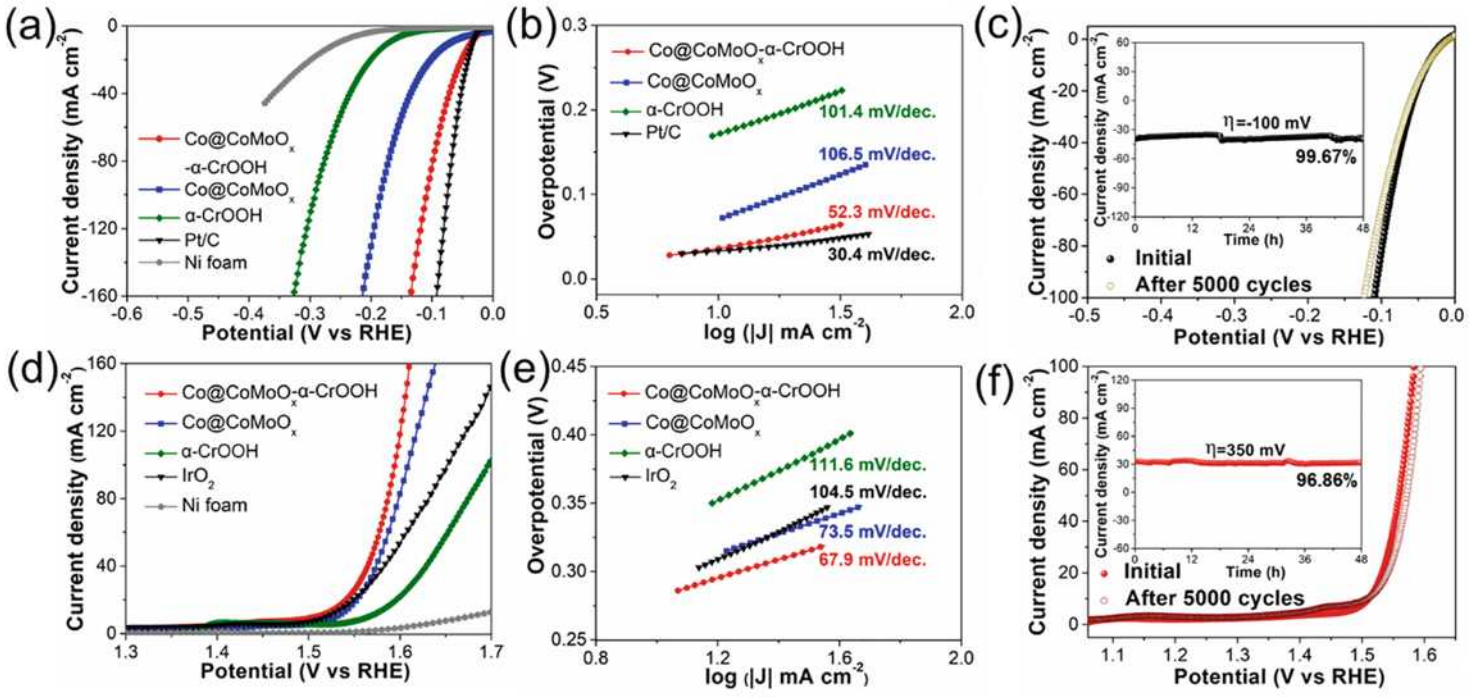

HER : 36 mV@η_{10} vs Pt/C 33 mV@η_{10}
Fixed potential -100 mV for 48 h
OER : 278 mV@η_{10} vs IrO_2 289 mV@η_{10}
Fixed potential 350 mV for 48 h

Two-electrode full cell
1.570 and 1.731 V at current densities 10 and 100 mA cm^{-2}
Pt/C/ NF || IrO_2/NF
1.566 V and 1.738 V at current densities 10 and 100 mA cm^{-2}

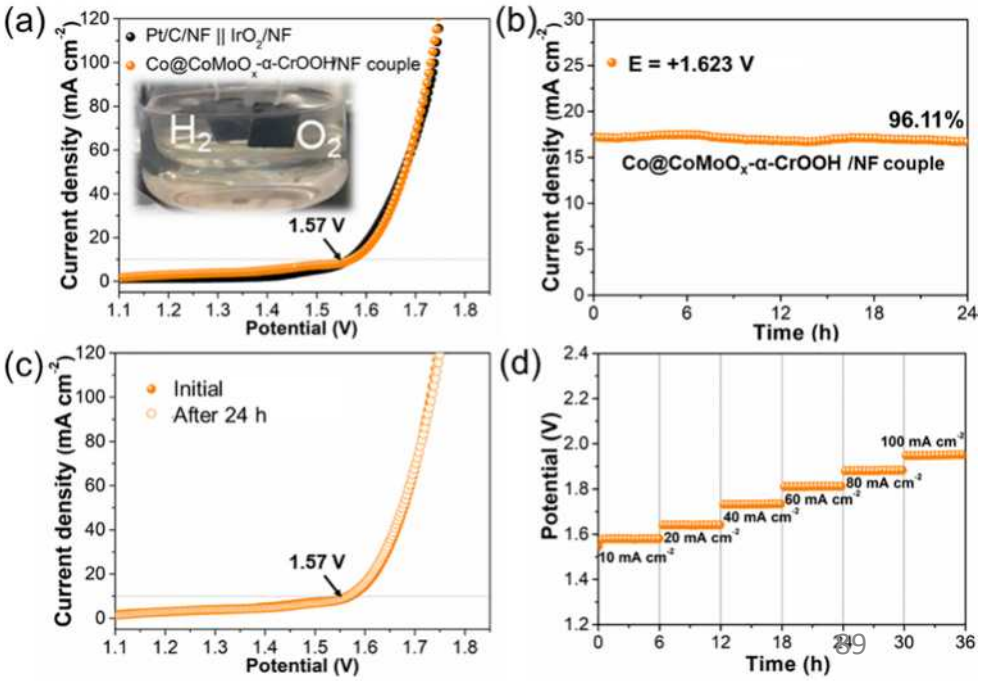

Chem. Eng. J., ***452***, 139715 (2023)

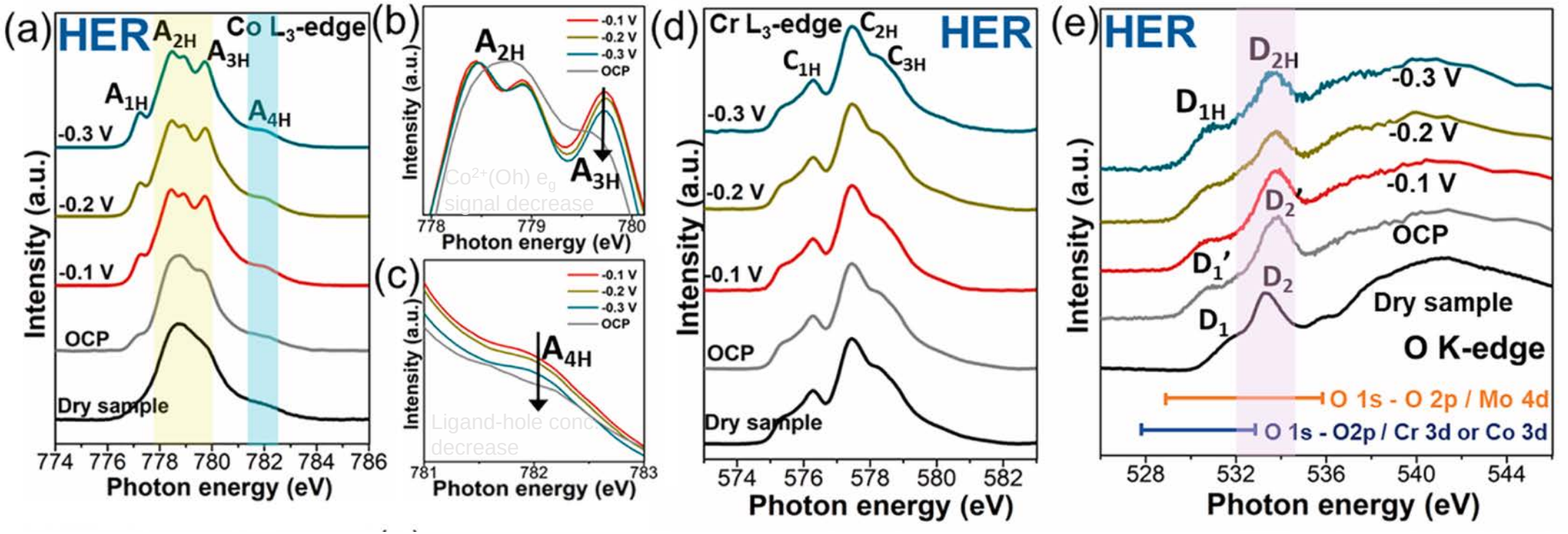

Co : Dry → Co(OH)2 (@OCP) → slight reduction
Mo : Intensified B2H(e_g) , B3H(t_{2g}) → Increased valence
→ adsorption of H* intermediates
Cr : No obvious change
O : D2-D2' ↑ → Co(OH)2 (@OCP)
D2' ↓ → -OH bond breaking

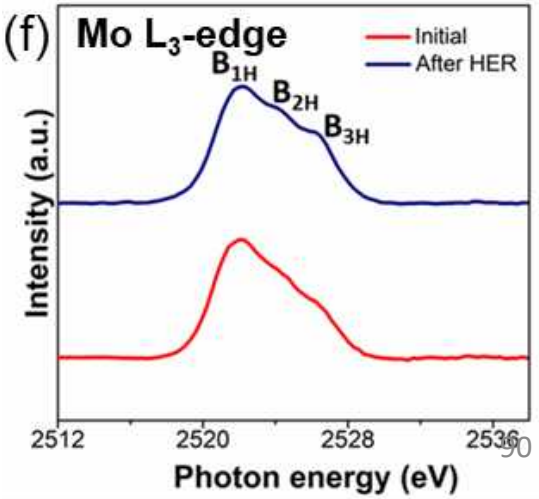

Chem. Eng. J., ***452***, 139715 (2023)

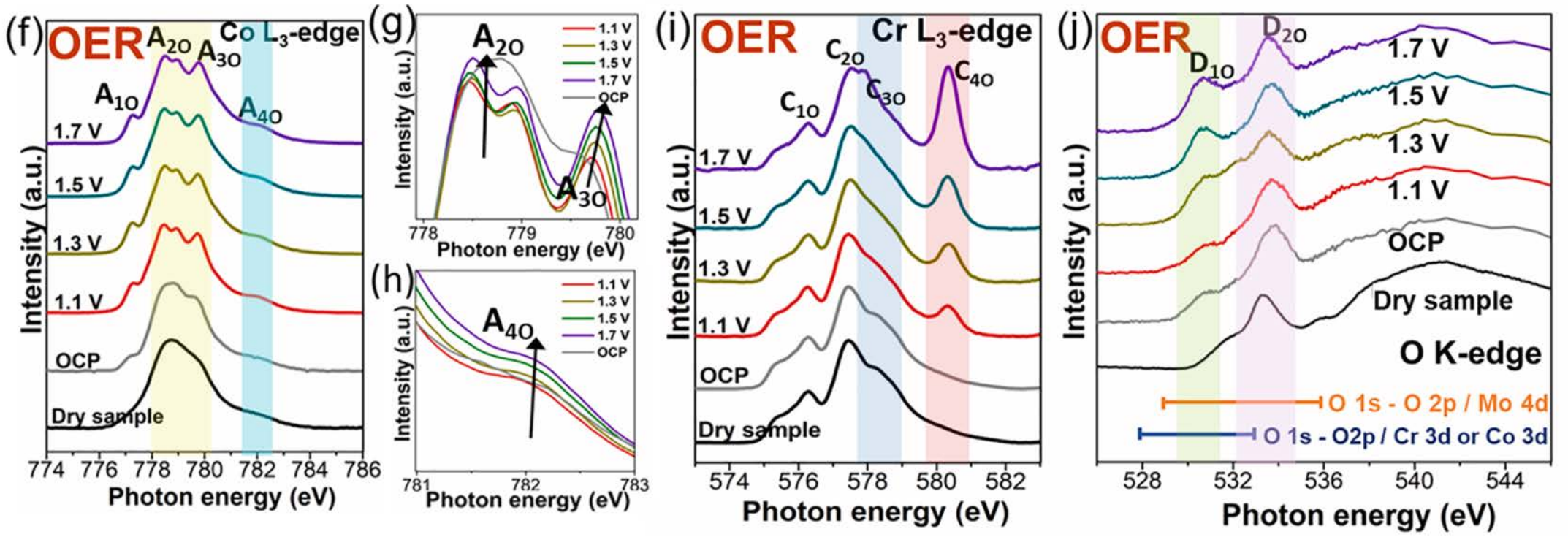

Co : Intensified and edge-shifted for A_{3O} & A_{4O} → Co^{3+} (CoOOH)
Mo : Intensified B_{2O} and B_{3O} → Increased valence (Mo^{4+} and Mo^{6+})
→ e_g^0 orbitals can form stronger binding with oxygen species
Cr : Cr^{3+} → Cr^{6+}
O : signal D_{1O} ↑ → Cr^{6+}/Co^{3+}/Mo^{4+}/Mo^{6+} ↑

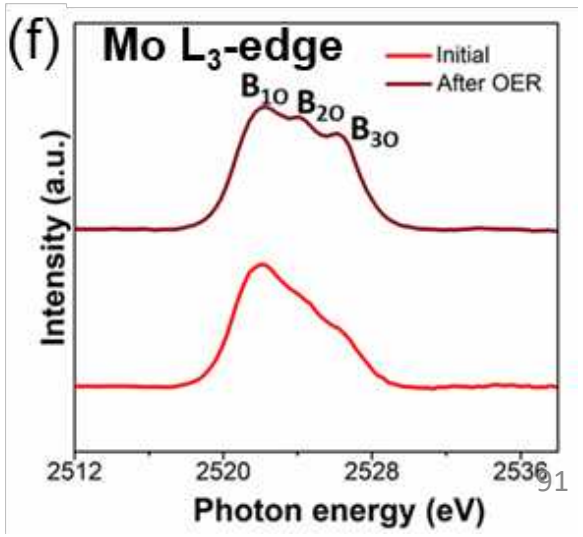

Chem. Eng. J., ***452***, 139715 (2023)

Energy Storage Device

Reliable Electrochemical Energy Storage for Alternative Energy

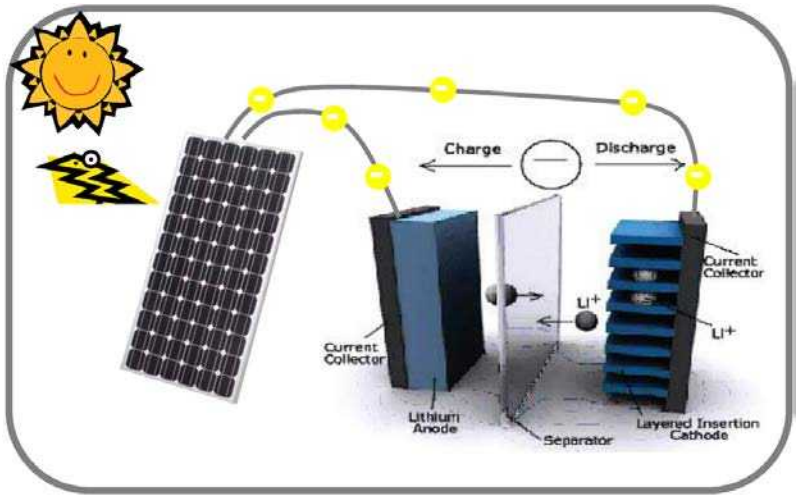

Energy storage devices are “charged” when they absorb energy, either directly from renewable generation devices or indirectly from the electricity grid.
They “discharge” when they deliver the stored energy back into the grid.
Charge and discharge normally require power conversion devices, to transform electrical energy (AC or DC) into a different form of electrical, thermal, mechanical or chemical energy.

Automobile engine start-up assist

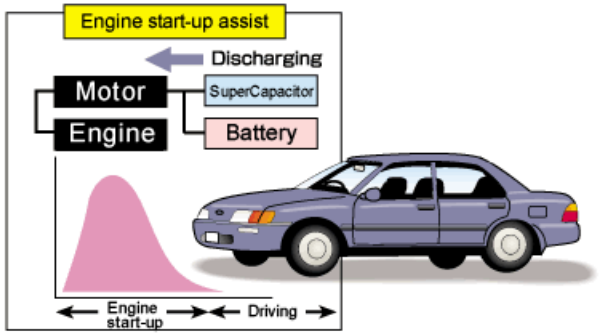

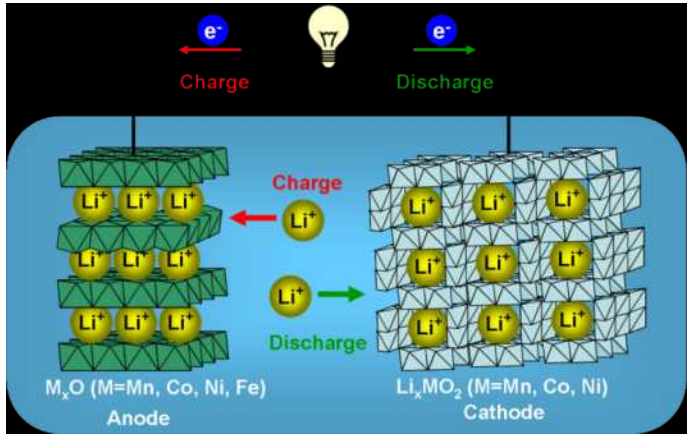

Electron storage device
- **Supercapacitor**
- **Lithium battery**

Energy storage is one of the key challenges we face in the 21st century

Energy Storage

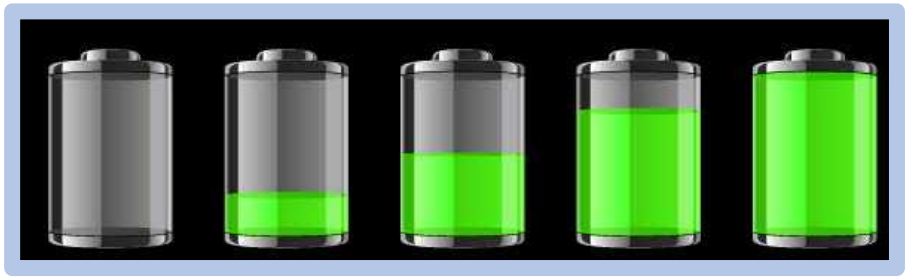

Battery

Capacitor

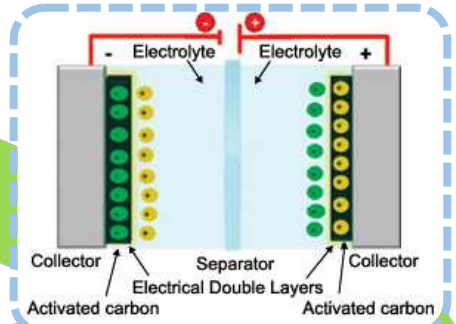

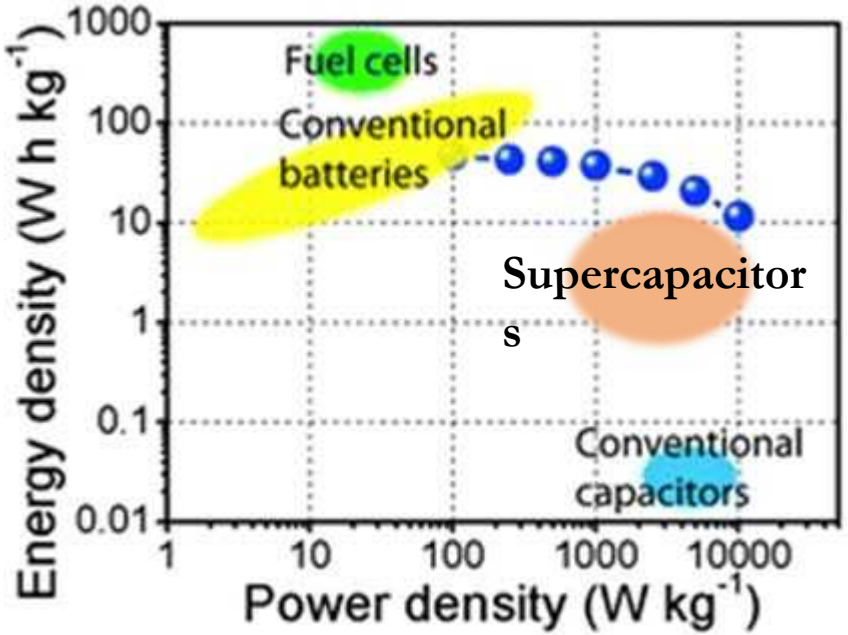

Ragone plots

Supercapacitors bridge between batteries and conventional capacitors

Energy – the capacity to do work

Power – how fast the energy is delivered

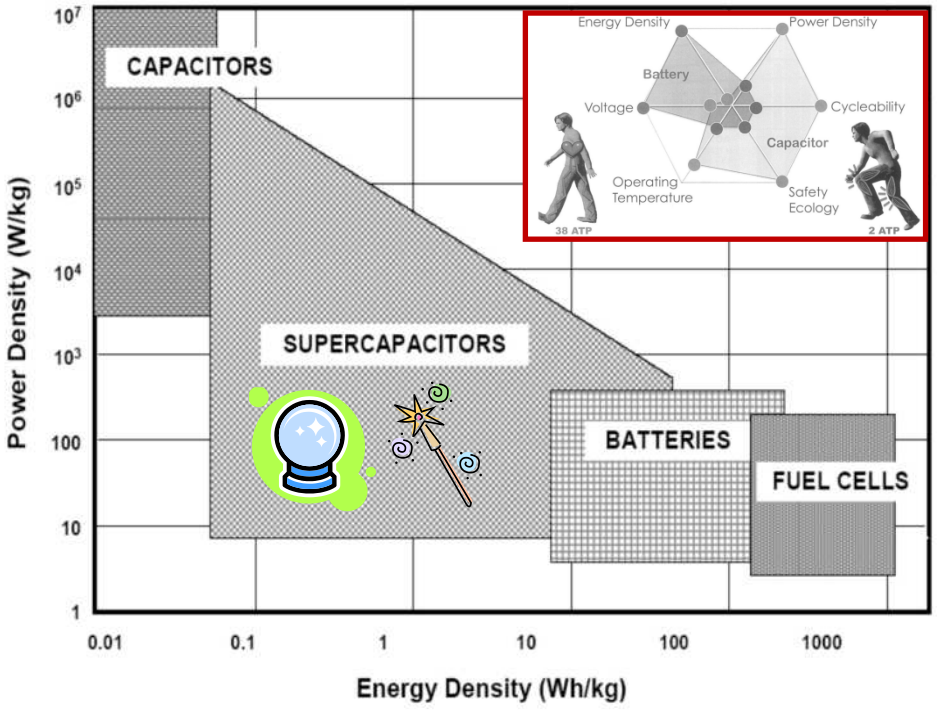

Supercapacitors are able to attain greater energy densities while still maintaining the high power density of conventional capacitors.

Supercapacitors are a potentially versatile solution to a variety of emerging energy applications based on their ability to achieve a wide range of energy and power density.

Obviously We can't invent a giant energy storage device to solve the storage problem

But we can make tradeoffs to optimize performance for a given application and we can continue to make innovative breakthroughs

Capacitor vs. Supercapacitor vs. Battery

Capacitor

- Low Energy Density
- Very High Power Density

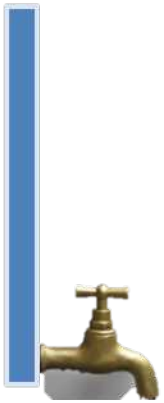

- Small Volume
- High Pressure
- Large Tap

Supercapacitor

- Moderate Energy Density
- High Power Density

- Moderate Volume
- Moderate Pressure
- Moderate Tap

Battery

- High Energy Density
- Low Power Density

- Large Volume
- Small Pressure
- Small Tap

Capacitor vs. Supercapacitor vs. Battery

	BATTERY	SUPERCAPACITOR	CAPACITOR
Charge Time	1 – 5 h	0.3 – 30 s	10^{-3} – 10^{-6} s
Discharge Time	0.3 – 3 h	0.3 – 30 s	10^{-3} – 10^{-6} s
Energy (Wh/kg)	10 – 100	1 – 10	< 0.1
Cycle Life	1000	> 500,000	> 500,000
Specific Power (W/kg)	< 1000	< 10,000	< 100,000
Charge/discharge Efficiency	0.7 – 0.85	0.85 – 0.98	> 0.95

http://www.altenergymag.com/article/2005/02/ultracapacitors-and-the-hybrid-electric-vehicle/159/

Capacitor vs. Supercapacitor vs. Battery

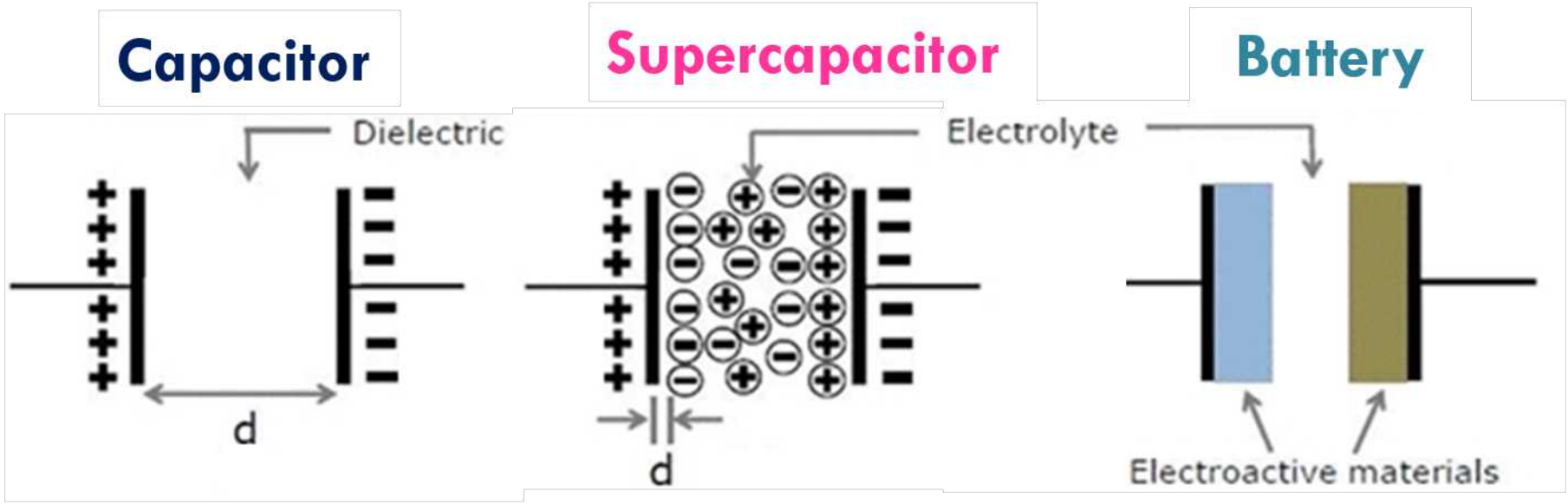

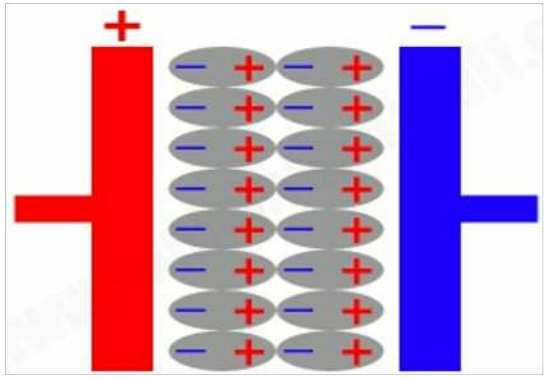

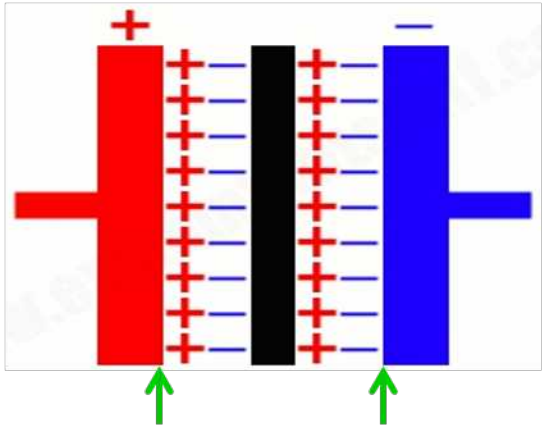

Faradic reactions occur at the surface of active materials

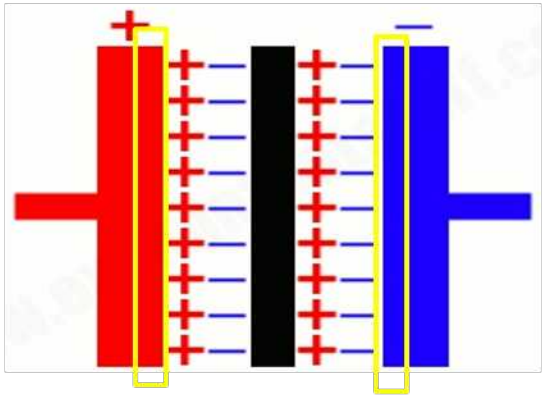

Faradic reactions occur in the whole active material

Nanostructured electrode materials: MnO_2

Accomplishments: MnO_2 nanosheet/carbon cloth

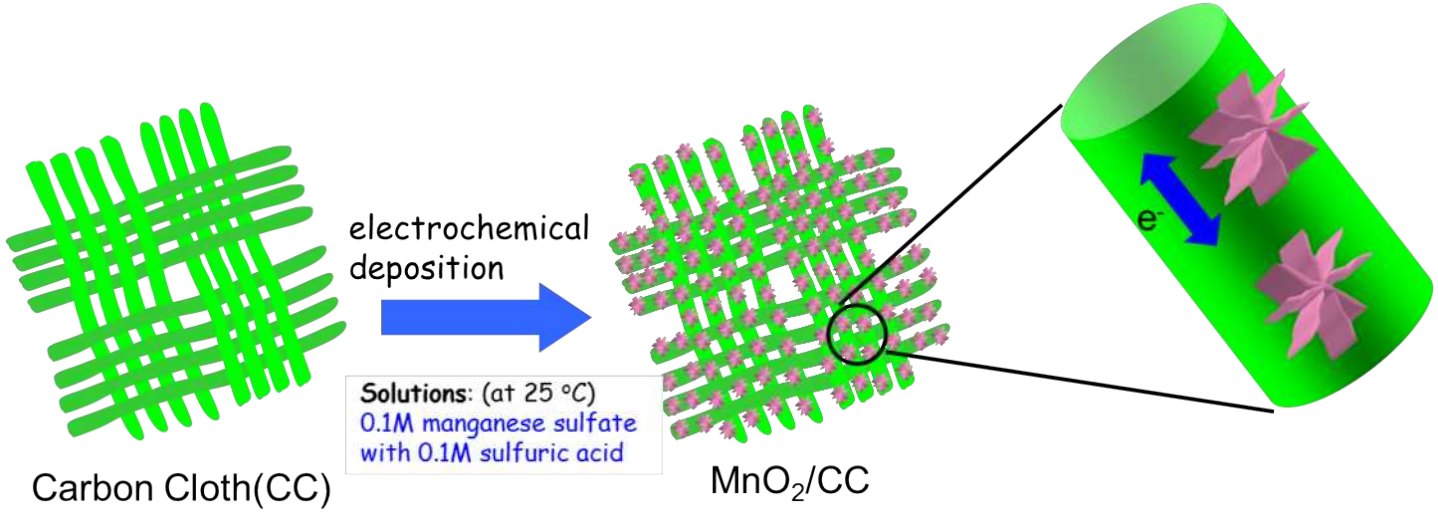

Morphology & Structure of MnO_2

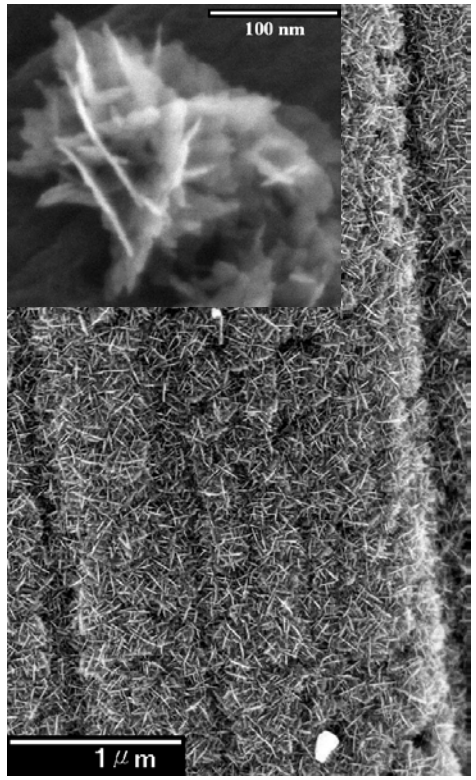

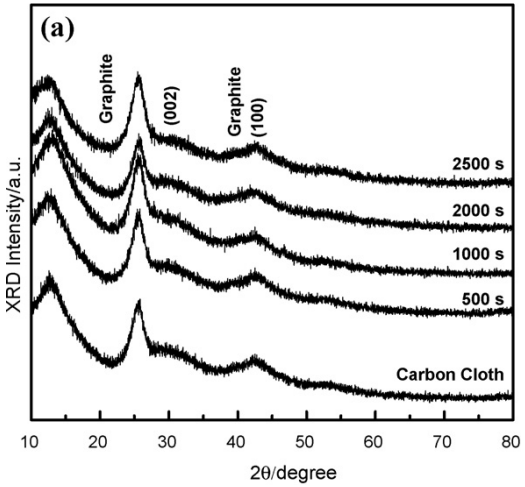

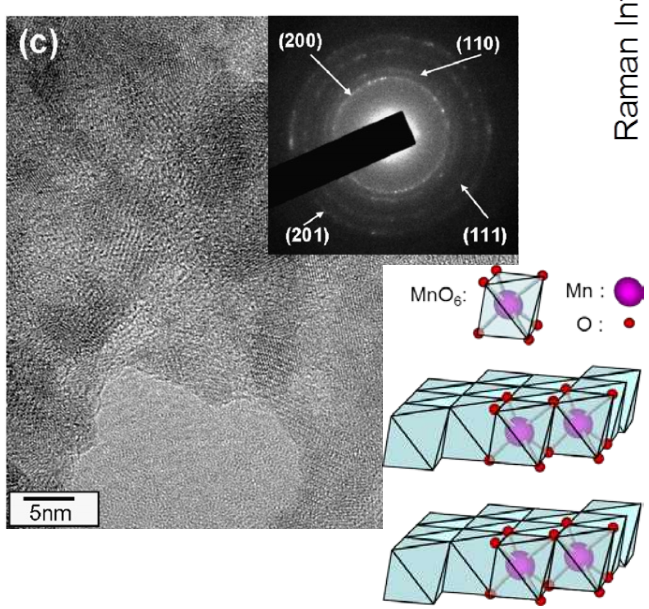

640 cm^{-1}: the symmetric stretching vibration (Mn–O) of the MnO_6 groups.

575 cm^{-1}: (Mn–O) stretching vibration in the basal plane of MnO_6 sheet.

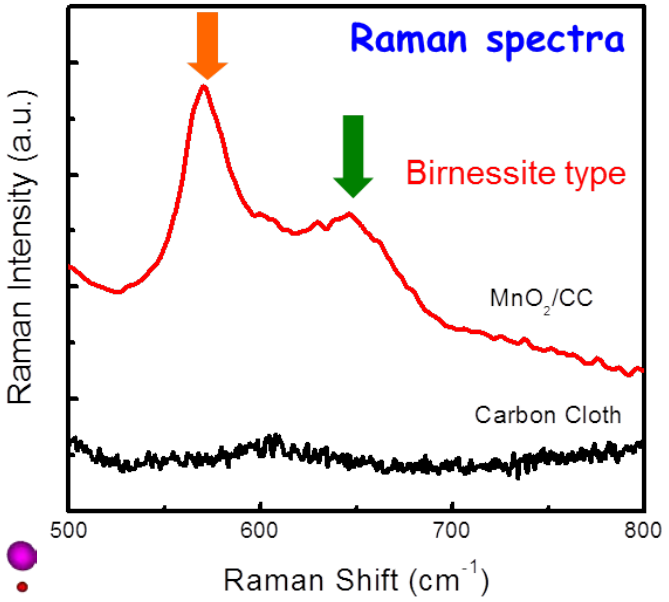

In-situ X-ray Absorption Fine Structure Studies

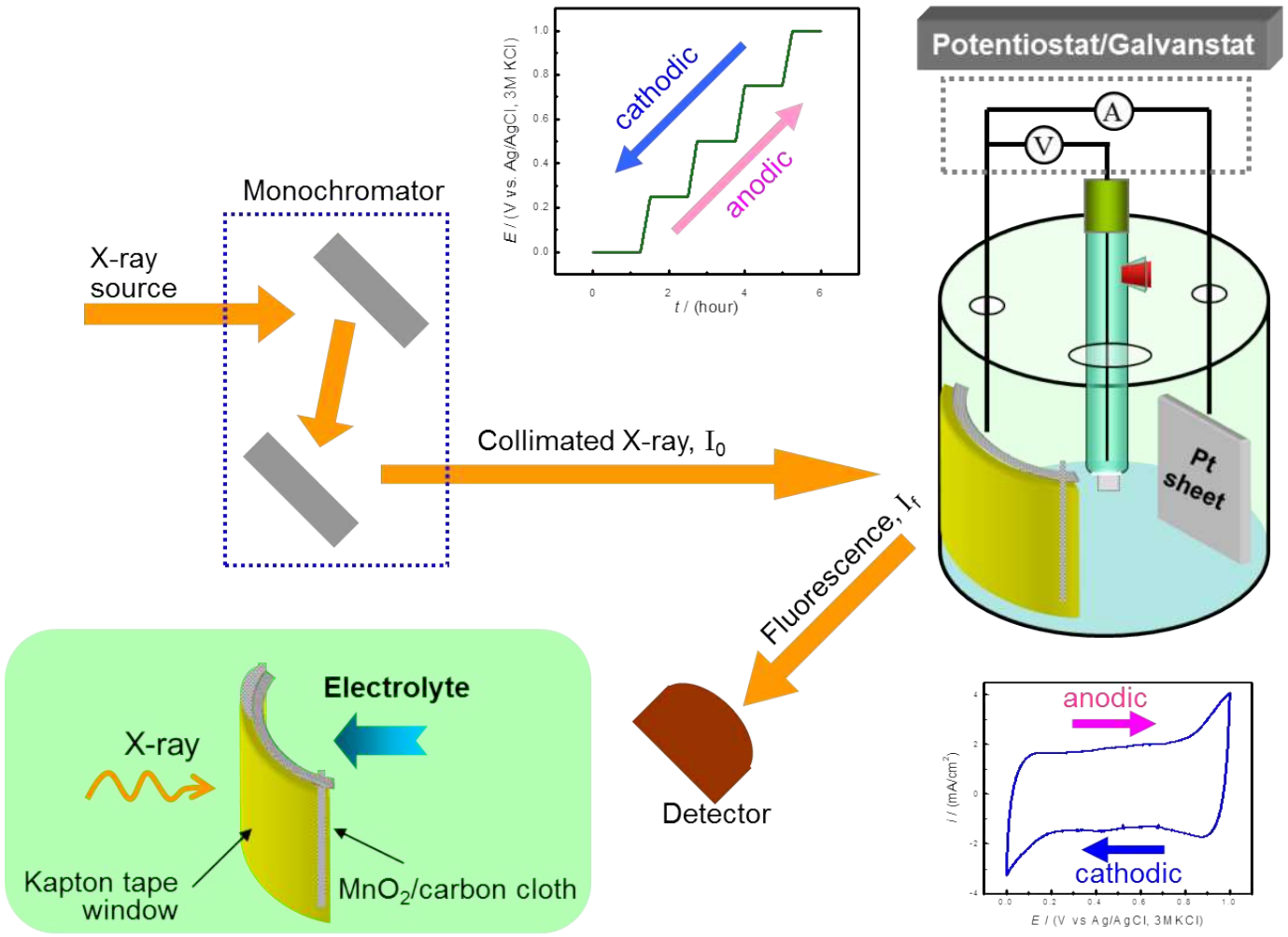

In-situ Mn K-edge XANES Spectra

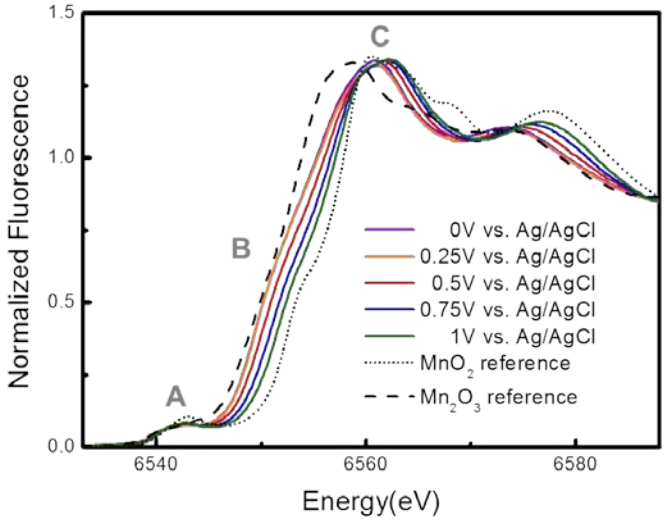

A: pre-edge region
electronic excitation from 1s core state to unoccupied 3d orbital

B: main edge region
C: peak region
electric dipole-allowed transition of 1s core electron to unoccupied 4p bound state with and without a shakedown process, which originated from ligand-to-metal charge transfer.

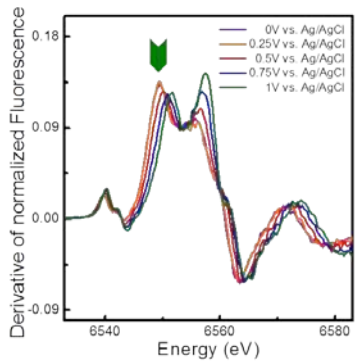

Valence state of Mn can be determined from the first inflection point on the main absorption edge.

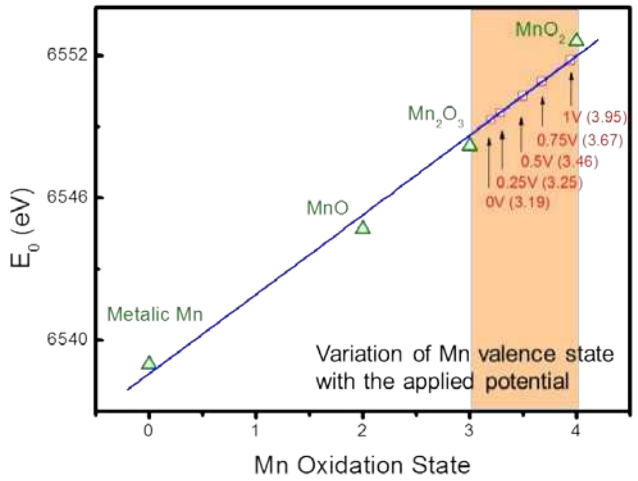

In-situ Mn K-edge XANES Spectra

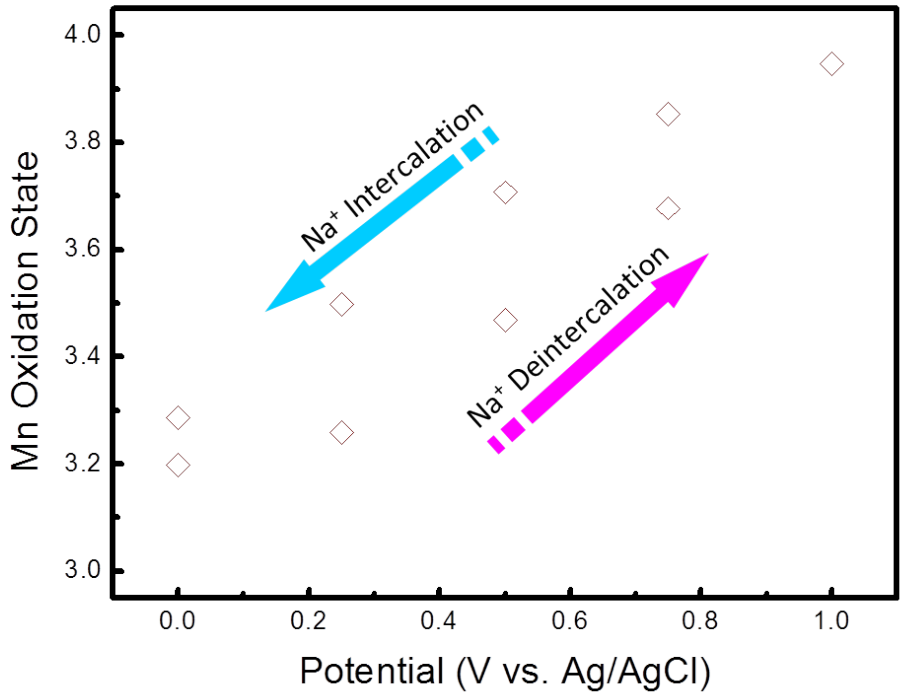

$$Mn(IV)O_2 + x \cdot Na^+ + x \cdot e^- \leftrightarrow Na_x[Mn(III)]_x\,[Mn(IV)]_{1-x}O_2$$

- **Reversible faradic redox transition**
  → superior capacity performance

In-situ Mn K-edge EXAFS Spectra

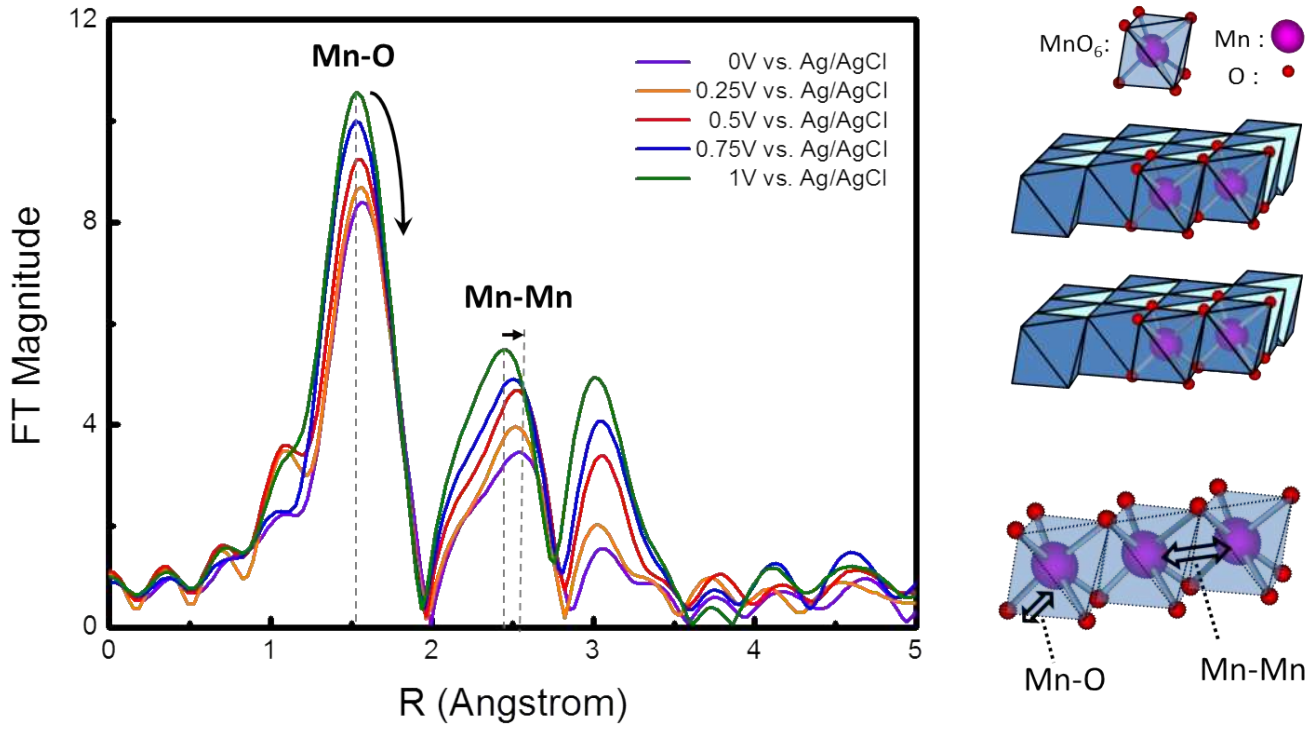

- The increase of Mn-O & Mn-Mn bond length resulted in expansion of MnO_6 layer.
- The decrease in FT magnitude was ascribed to local structure distortion.

Nanostructured electrode materials: FeOOH

Accomplishments: γ-FeOOH nanosheet/carbon cloth

Potentialstatic method

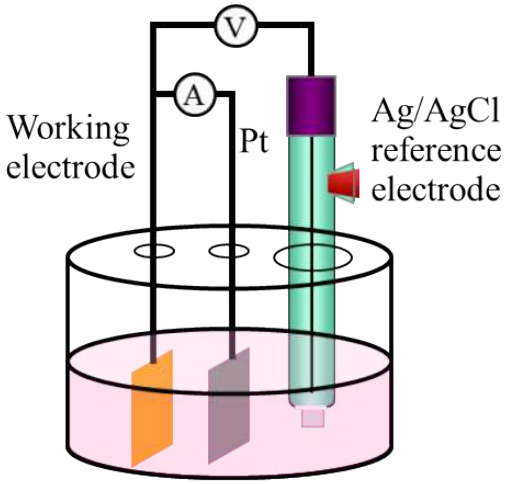

Solutions:
Ammonium iron sulfate $(NH_4)_2Fe(SO_4)_2$
Sodium Acetate (CH_3COONa)
Ammonium Fluoride (NH_4F)

Substrate: Carbon Cloth

Deposit Potential: 0.5-1 V

Deposit time: 0.5-1.5 hr

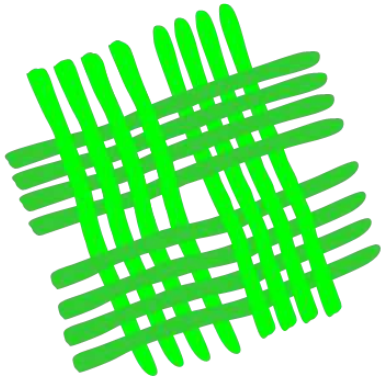

electrochemical deposition

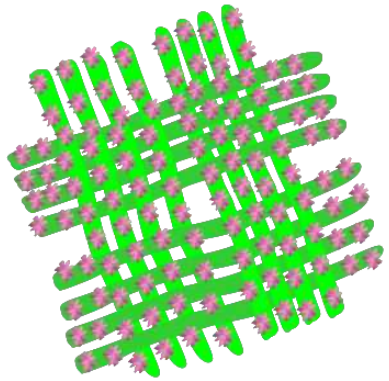

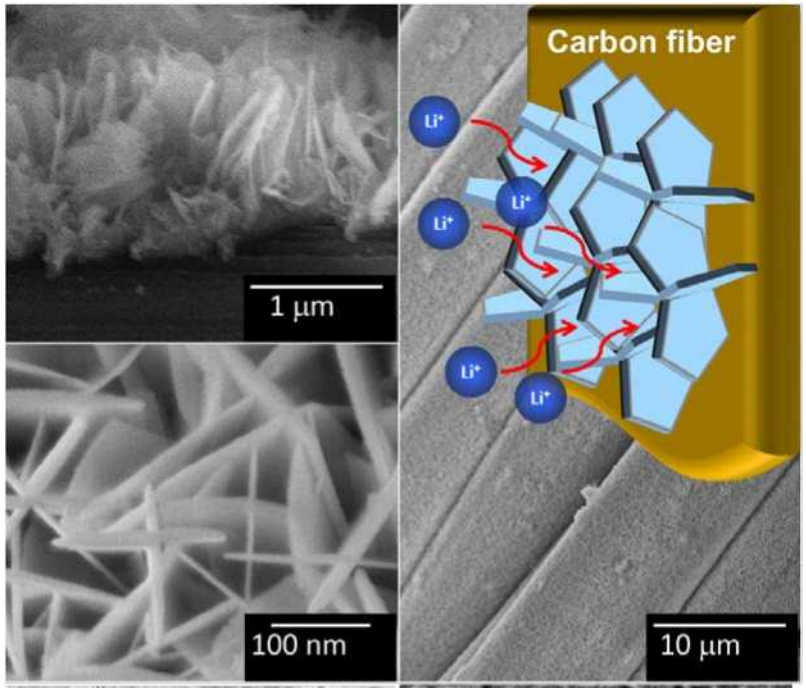

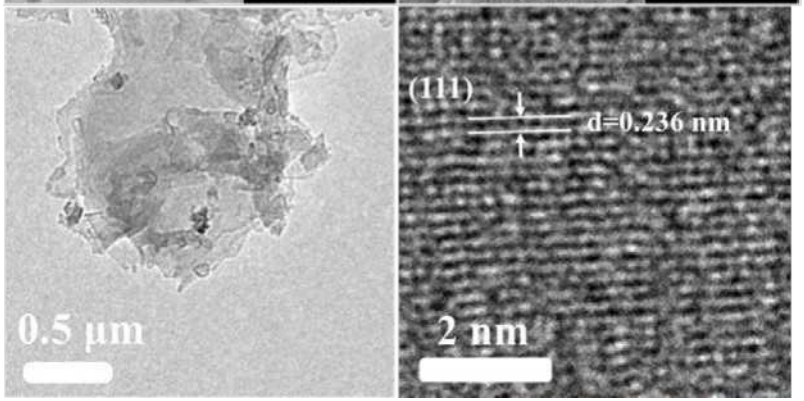

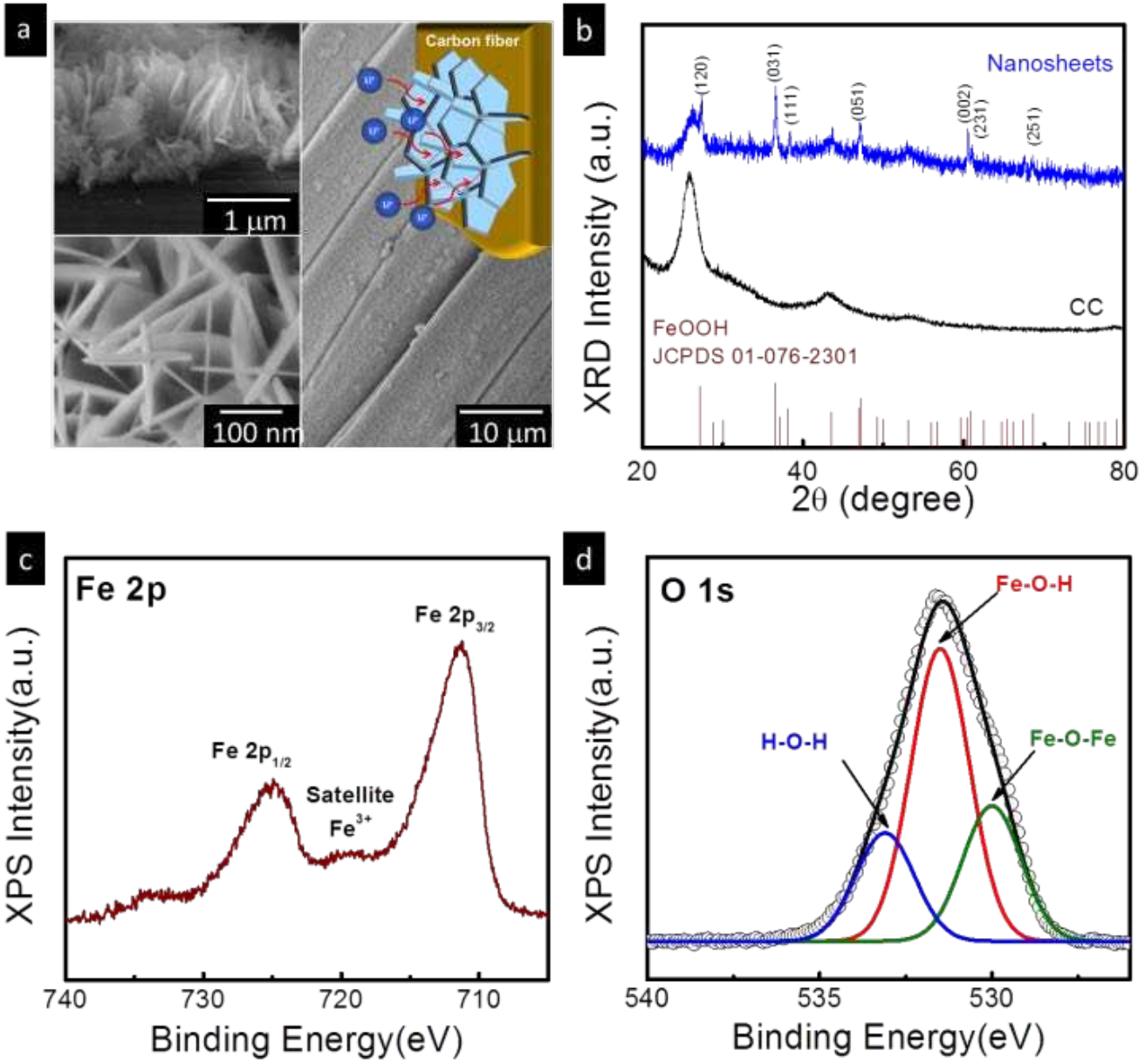

γ-FeOOH

Fe^{3+} in FeOOH

H–O–H
→H_2O molecule
→hydrated form

In-situ Fe K-edge XAS Spectra

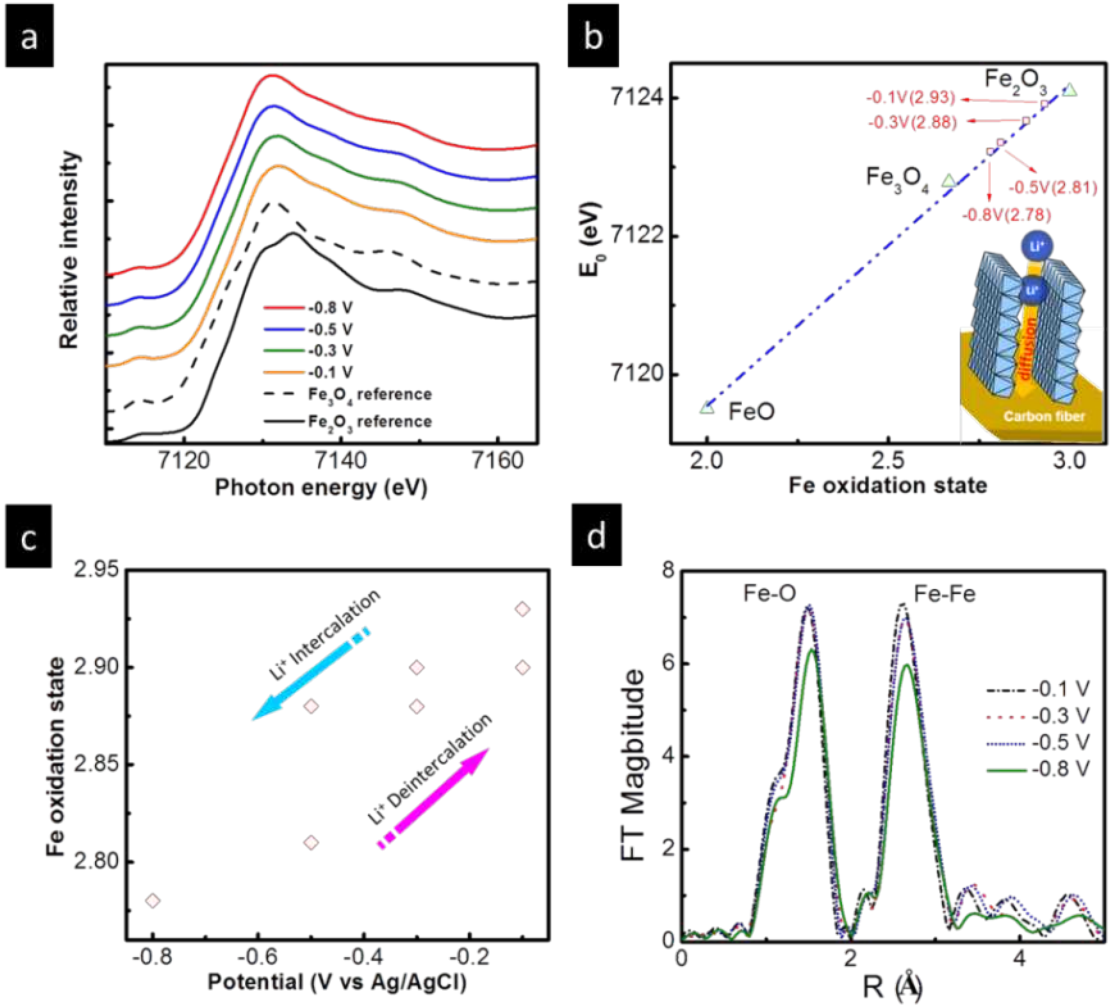

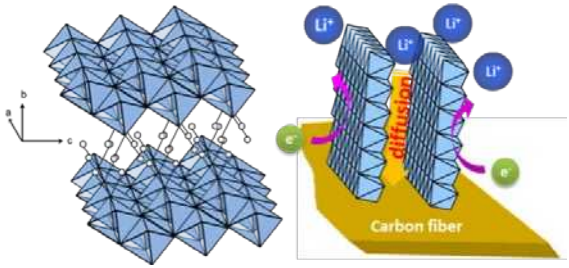

Orthorhombic crystal structure
Infinite layer of [FeO_6] octahedra

- **Reversible faradic redox transition → superior capacity performance**
- **The increase of Fe-O bond length → expansion of FeO_6 layer**
- **The decrease in FT magnitude → local structure distortion**
- **Pseudocapacitive mechanism: Fe(III)OOH + Li^+ ↔ LiFe(II)OOH**

Small, **10**, 3803 (2014)

Nanostructured electrode materials

Accomplishments: $Bi_2Mo_3O_{12}$ Anode Composited with Ti_3C_2

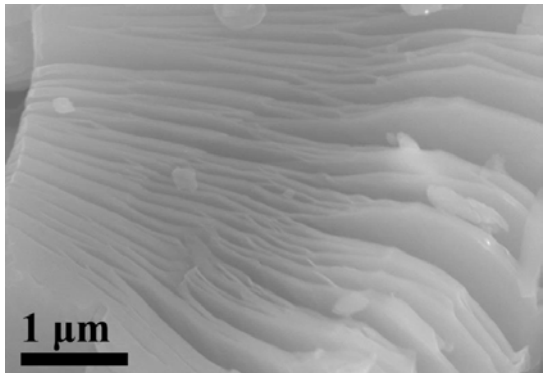

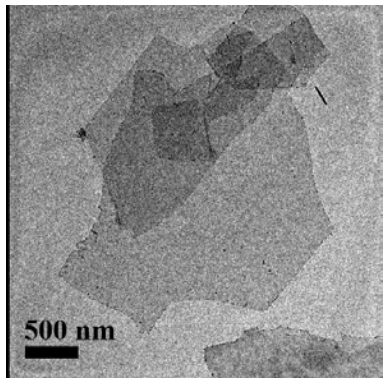

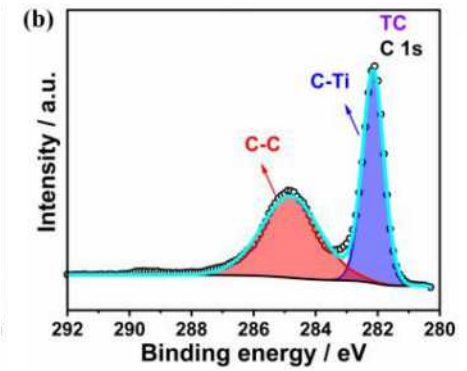

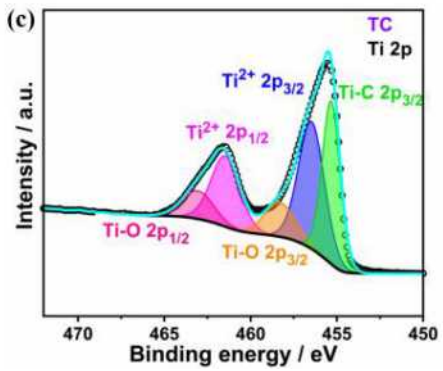

Battery Supercap., **3**, 1296 (2020)

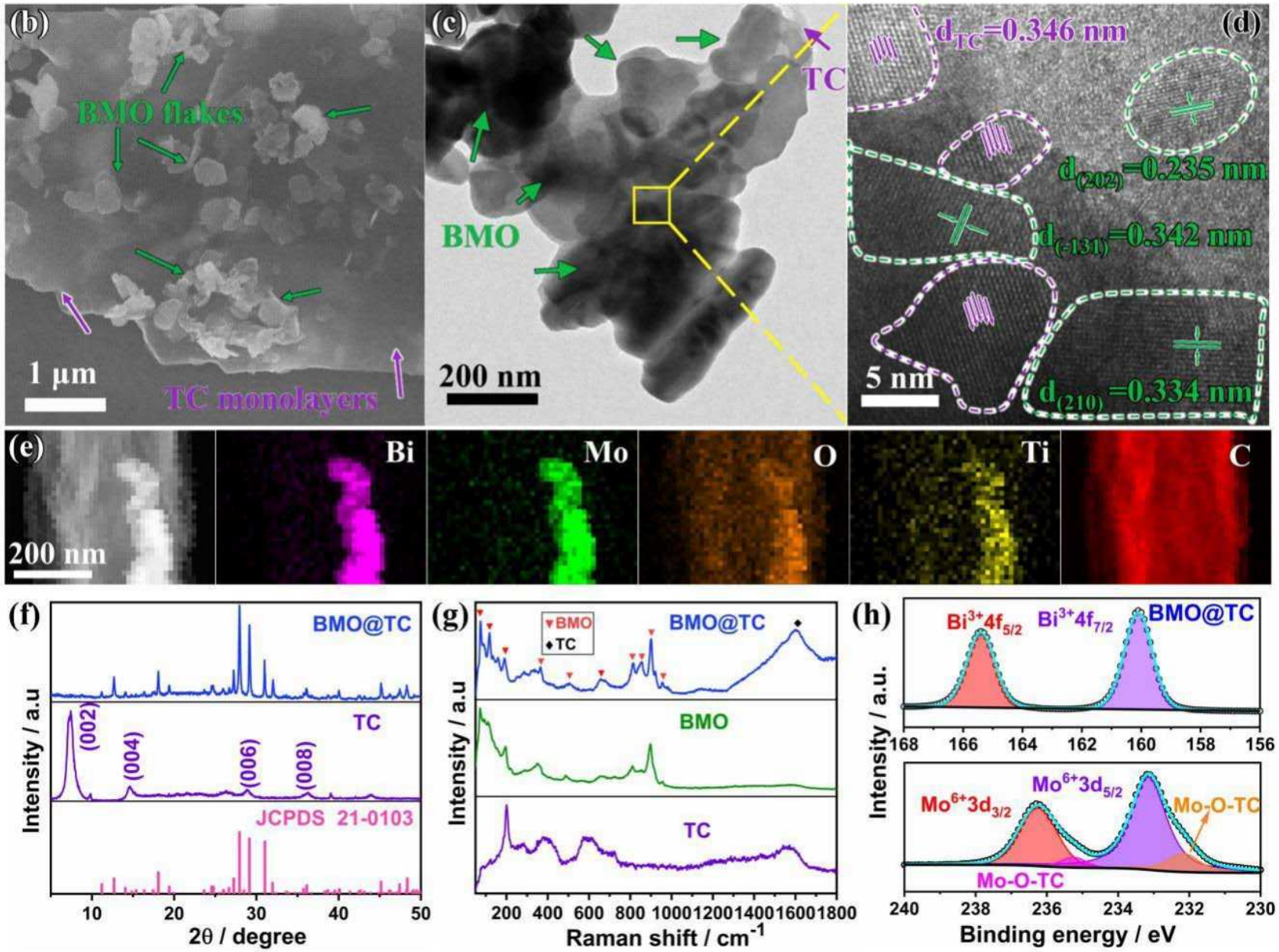

monoclinic α-$Bi_2Mo_3O_{12}$ phase

BMO@TC : 846 mAh/g (1st charge capacity)

High rate performance

After 1000 cycles at high charge/discharge current : 227 mAh/g

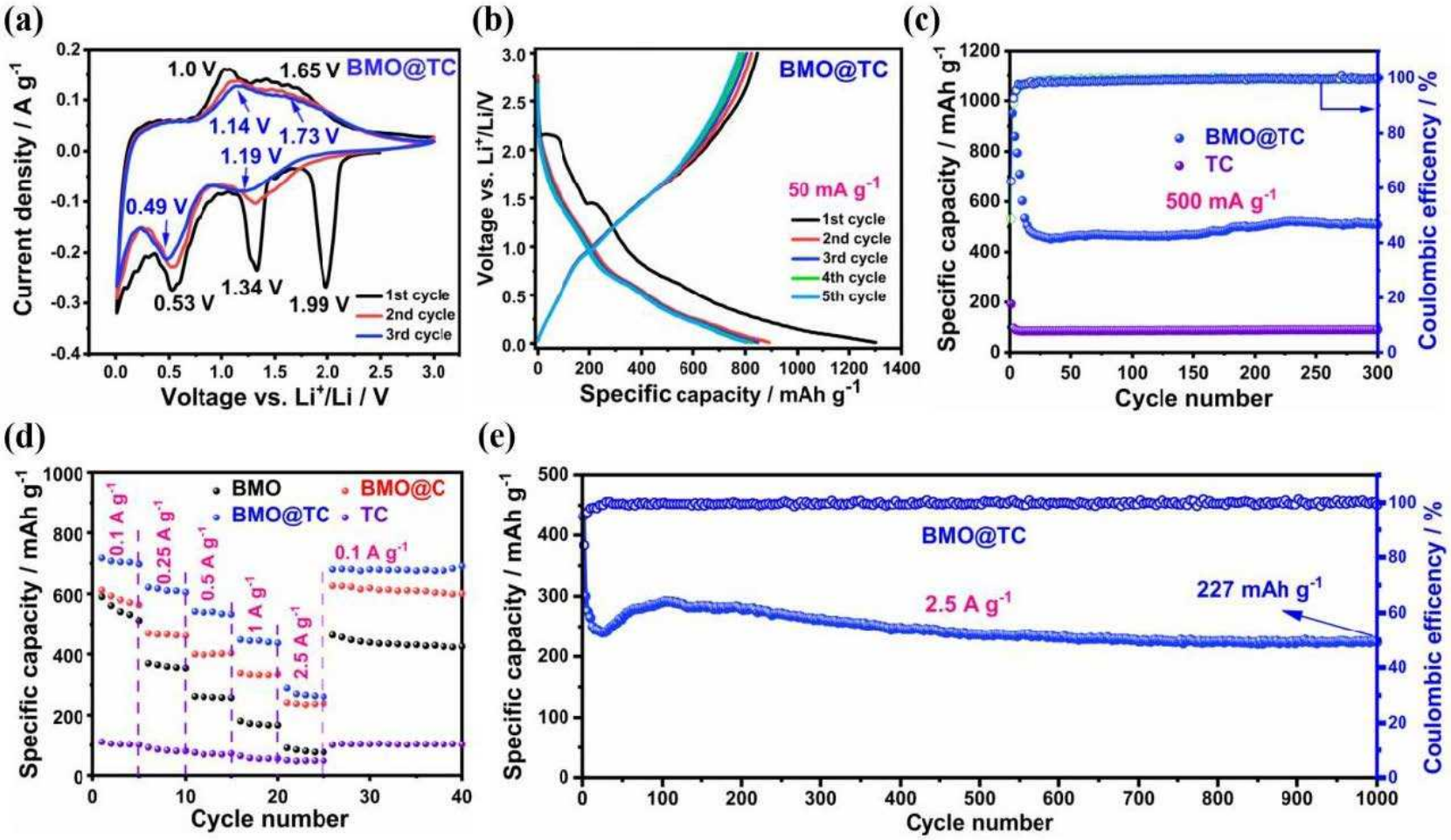

Battery Supercap., **3**, 1296 (2020)

$$Bi_2Mo_3O_{12} + 6Li^+ + 6e^- \rightarrow 3Li_2MoO_4 + 2Bi$$

$$Li_2MoO_4 + xLi^+ + xe^- \leftrightarrow Li_{2+x}MoO_4$$

$$Bi + 3Li^+ + 3e^- \leftrightarrow Li_3Bi$$

Operando XRD at 100 mA/g
BMO : $Bi_2Mo_3O_{12}$
OCP → 3 V → 0 V
1.82 V : complete conversion of BMO
After 1.82 V : new peak $(012)_B$ → Bi
1.05 V : $(221)_{LMO}$ → Li_2MoO_4
Below 0.5 V : $(111)_{BL}$ → Li_3Bi
Shift of $(221)_{LMO}$: Li_2MoO_4 → $Li_{2+x}MoO_4$
0 V → 3 V
After 1.5 V : $(111)_{BL}$ ⇓ & $(012)_B$ ⇑ ⇒ Li_3Bi → Bi
Recovery of $(221)_{LMO}$
$Li_{2+x}MoO_4$ → Li_2MoO_4

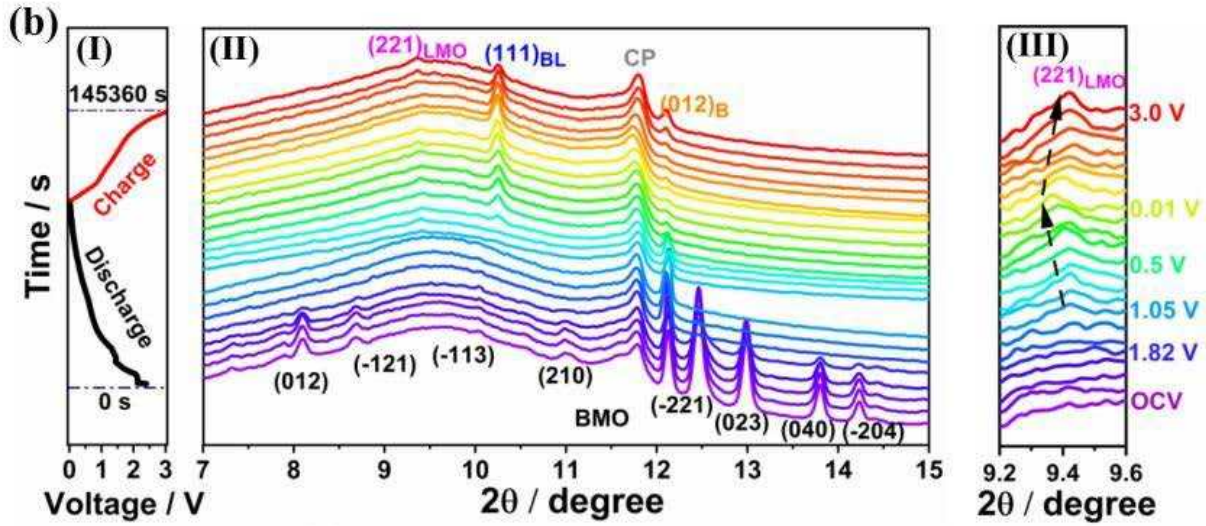

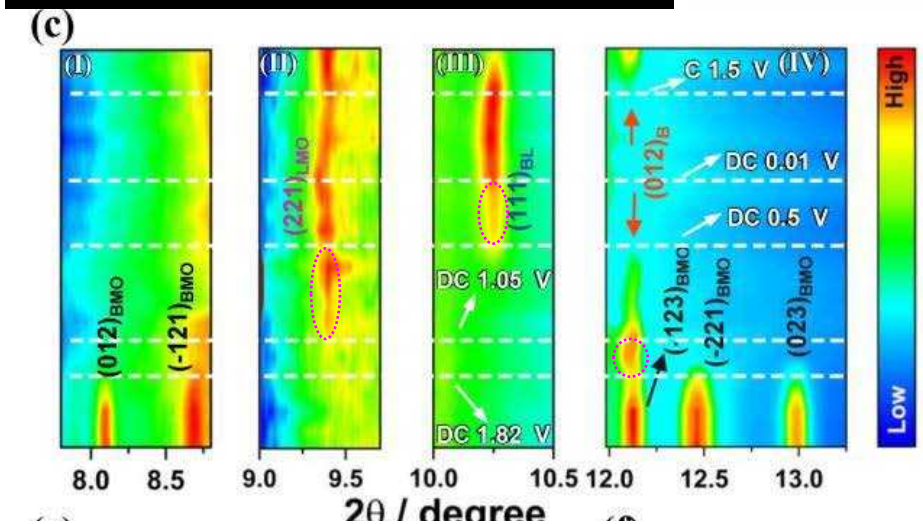

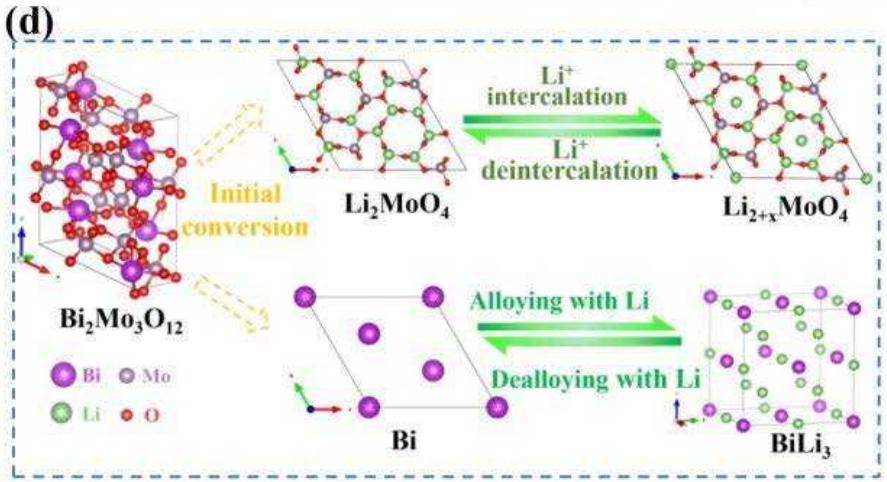

Battery Supercap., **3**, 1296 (2020)

NbN Monocrystals for Supercapacitor

FE-SEM, TEM, HR-TEM & HAADF images

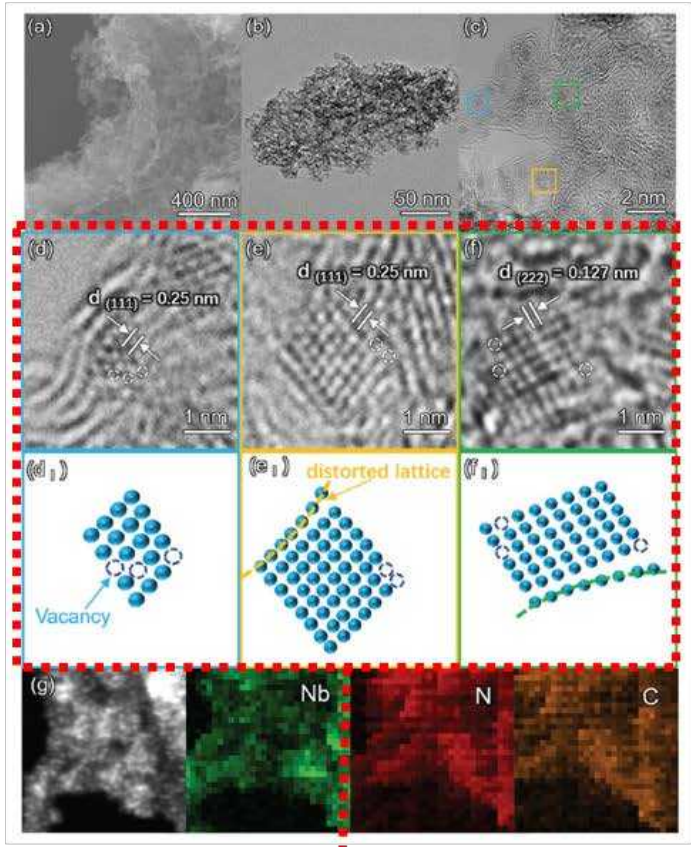

Vacancy & Distortion

Fabrication of NbN@C material for Li-ion storage

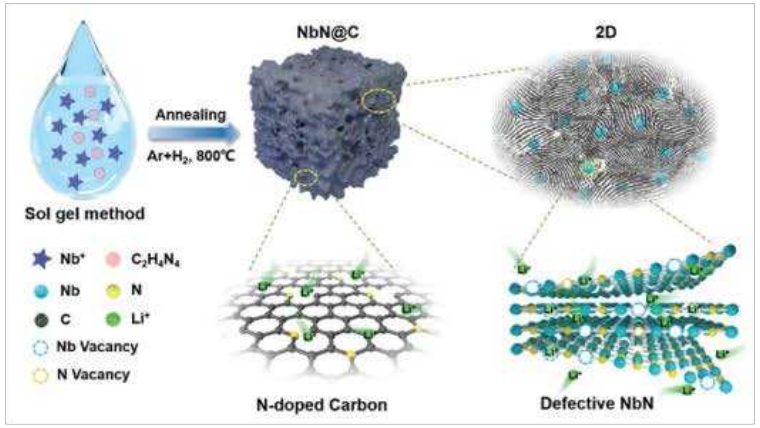

Sol-gel method + Annealing = NbN@C

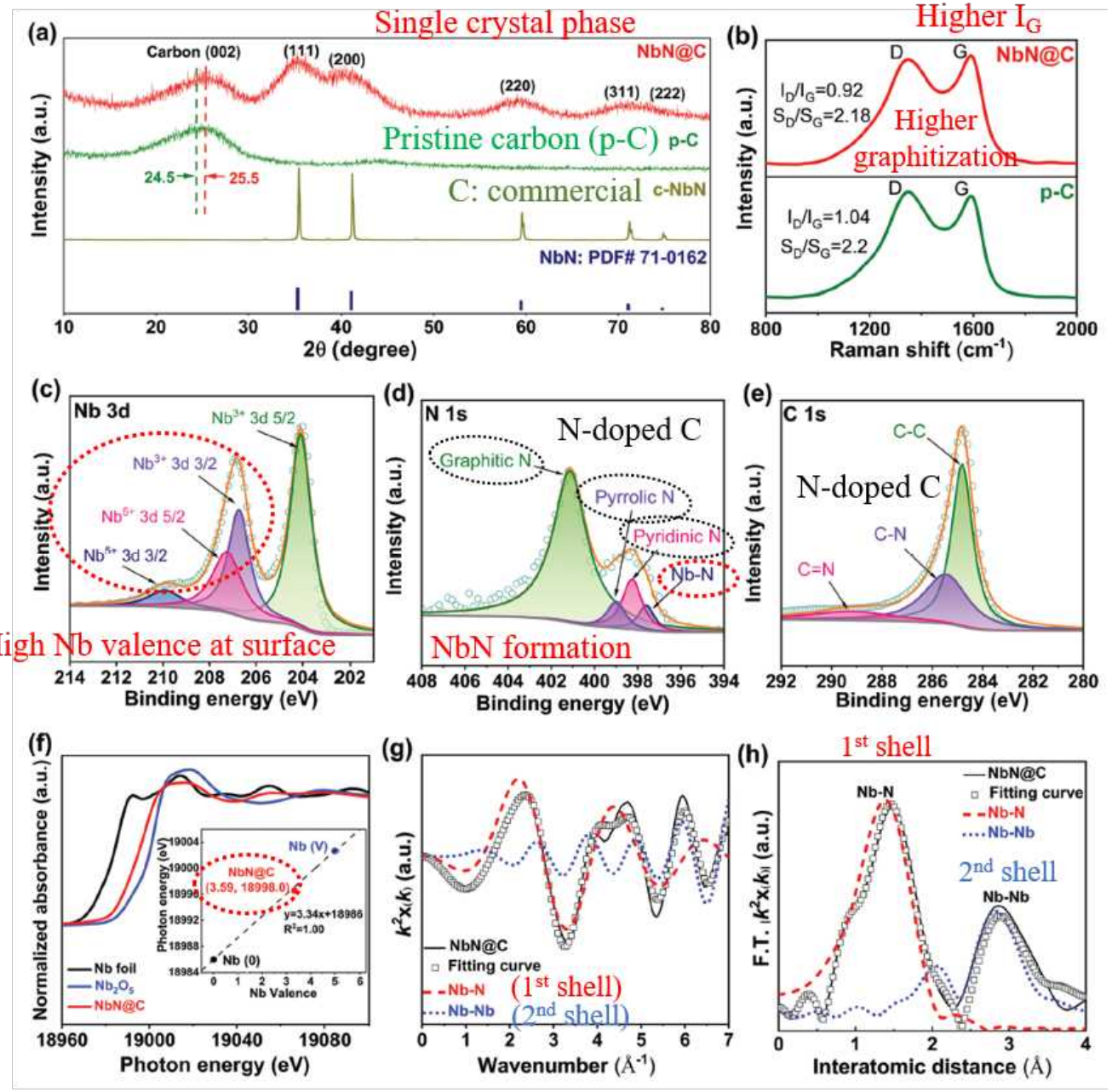

Average Nb valence=3.59

Nb-N & Nb-Nb bonds were identified with high accuracy.

Electrochemical Performances: Half NbN@C cell

Li-storage performances of half NbN@C cell

Anodic peaks

Cathodic peaks@1.55V, 0.84V in 1st cycle (Solid-electrolyte interface, SEI film)

Cathodic peak@0.01V (C component)

→ Multistep Li-ion intercalations/deintercalations

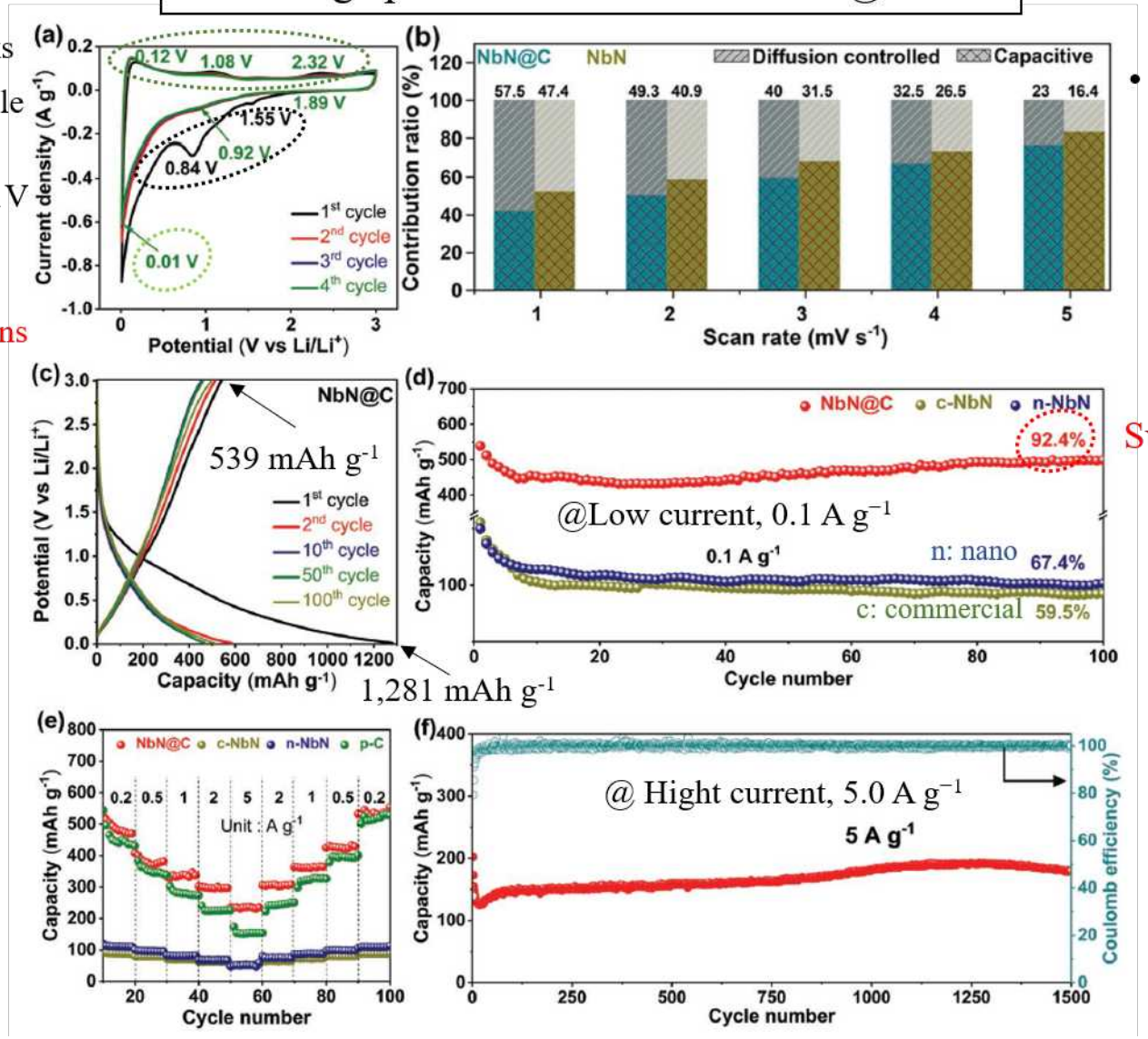

- Surface-controlled (capacitive behavior)
- Diffusion-controlled (battery behavior)

Structural defect favors the Li-ion diffusion into NbN lattice at various scan rates.

Superior capacity retention

Why the NbN@C has better Li-ion storage performances compared with other references?

1. Structural defects at Nb-site vacancy
2. Lattice distortion in NbN monocrystals
3. Additional surface and lattice space

for accommodating alkaline ions.

The electrolyte was 1 M $LiPF_6$ dissolved in ethylene carbonate (EC) and dimethyl carbonate (DMC)

Electrochemical Performances: Full NbN@C//AC Cell

Full cell NbN@C//AC performance

Attractive energy/power density at different potential

LHSC Cell

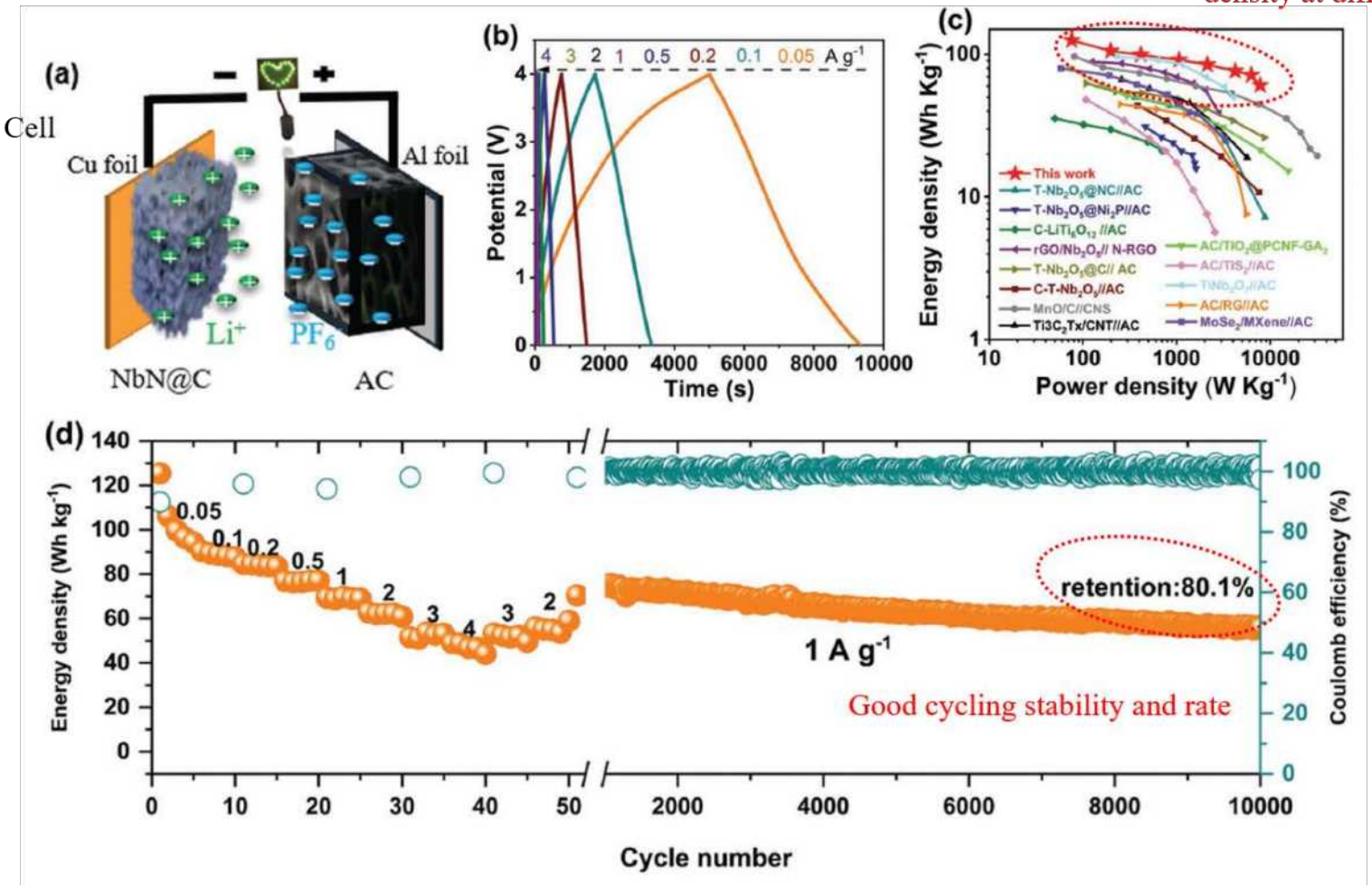

Adv. Funct. Mater., **32**, 2112592 (2022)

Table S1. Fitting results for the NbN component within the NbN@C composite material based on FT-EXAFS spectrum and a perfect *Fm-3m* crystal model.

Model	Path	Coordination number	Bond distance (Å)	Debye-Waller factor (Å^2)	R-factor
Fm-3m	Nb-N	4.95	2.15	0.02051	0.04385
	Nb-Nb	9.90	3.12	0.00036	

- CNs are less than standard values.
- Defects exist at Nb sites.

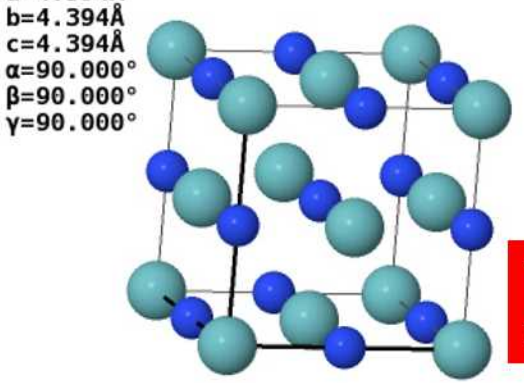

Standard CN:
Nb-N: 6.0
Nb-Nb: 12.0

DFT

What is the actual chemical formula of NbN@C?

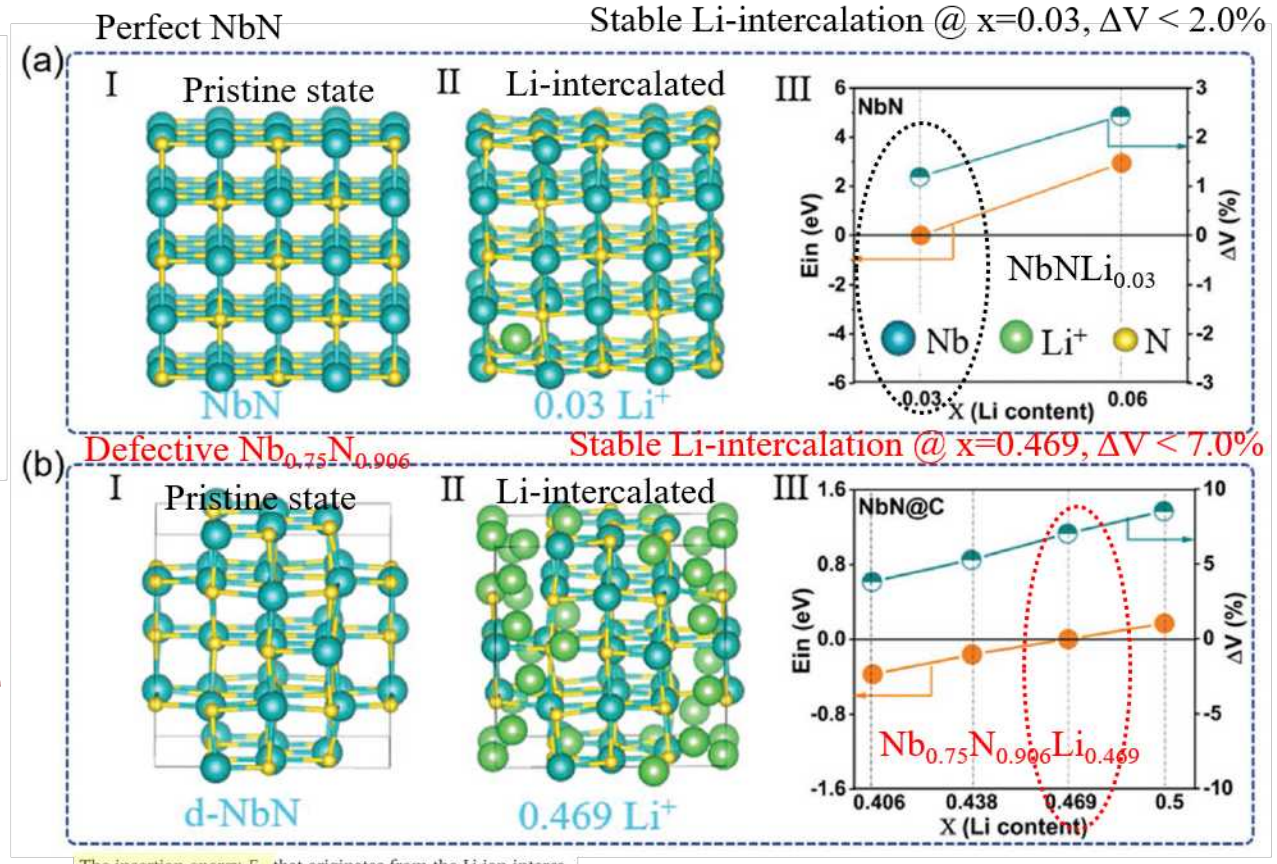

The insertion energy E_{in} that originates from the Li-ion intercalation is defined as follows:

$$E_{in} = (E_2 - E_1 - x\mu_{Li})/x \quad (3)$$

where E_1 and E_2 are the total energies in original and Li-ion intercalated materials, respectively; μ_{Li} is the chemical potential of a Li-ion, and x is the number of Li-ion stabilized in the active material.[41] A positive E_{in} value indicates an endothermic reac-

ΔE_{in} >0, endothermic reaction (Li **unstable** intercalation)
ΔE_{in} <0, exothermic reaction (Li **stable** intercalation)

Adv. Funct. Mater., **32**, 2112592 (2022)